

**MODELING AND NUMERICAL INVESTIGATION OF A
FALLING FILM LIQUID DESICCANT DEHUMIDIFIER
WITH NANOPARTICLES**

BY

QAZI TALAL

A Thesis Presented to the
DEANSHIP OF GRADUATE STUDIES

KING FAHD UNIVERSITY OF PETROLEUM & MINERALS
DHAHRAN, SAUDI ARABIA

In Partial Fulfillment of the
Requirements for the Degree of

MASTER OF SCIENCE

In

MECHANICAL ENGINEERING

MAY 2018

KING FAHD UNIVERSITY OF PETROLEUM & MINERALS

DHAHRAN- 31261, SAUDI ARABIA

DEANSHIP OF GRADUATE STUDIES

This thesis, written by **QAZI TALAL** under the direction of his thesis advisor and approved by his thesis committee, has been presented and accepted by the Dean of Graduate Studies, in partial fulfillment of the requirements for the degree of **MASTER OF SCIENCE IN MECHANICAL ENGINEERING**



Dr. Shahzada Z. Shuja
(Advisor)



Dr. Haitham M.S. Bahaidarah
(Co-Advisor)



Dr. Zuhair M. Gasem
Department Chairman



Dr. Salam A. Zummo
Dean of Graduate Studies



Dr. Syed M. Zubair
(Member)



Dr. Fahad A. Al-Sulaiman
(Member)

24/12/17

Date



Dr. Mohamed A. Antar
(Member)

© Qazi Talal

2018

Dedicated to

*My Father, Mother and Siblings for their continuous prayers, support and inspiration,
which helped me achieve success in life.*

ACKNOWLEDGMENTS

All praises and thanks to Almighty ALLAH (s.w.t) for giving me the determination, understanding and resolve to carry out and complete my M.S. from King Fahd University of Petroleum and Minerals.

First and foremost I would like to express my sincere gratitude to my advisor Dr. Shahzada Z. Shuja for his continuous guidance and support at every stage of my thesis work. I would also like to thank my co-advisor Dr. Haitham M.S. Bahaidarah and my previous advisor Dr. Palanichamy Gandhidasan for their help, encouragement and valuable insight at various stages of my thesis.

I would also like to thank all my committee members Dr. Syed M. Zubair, Dr. Fahad A. Al-Sulaiman and Dr. Mohamed A. Antar for their valuable suggestions regarding my thesis. I would like to express my deepest gratitude to all the Faculty members and fellow peers with whom I have interacted and gained valuable lessons during the duration of my M.S. in KFUPM.

Finally, I would like to thank my parents and siblings for their unconditional love, emotional support and continuous prayers for my success.

TABLE OF CONTENTS

ACKNOWLEDGMENTS	V
TABLE OF CONTENTS	VI
LIST OF TABLES	IX
LIST OF FIGURES	X
LIST OF ABBREVIATIONS	XV
ABSTRACT	XX
ملخص الرسالة	XXII
CHAPTER 1 INTRODUCTION	1
1.1 Hybrid Desiccant Cooling Systems	1
1.2 Advantage of using Desiccant Materials	3
1.3 Types of Desiccant materials	3
1.4 Potential of nanofluids in heat transfer applications	4
1.5 Problem Statement	5
1.6 Specific objectives of this Research	5
CHAPTER 2 LITERATURE REVIEW	7
2.1 Liquid Desiccant Systems	7
2.2 Mass and Heat transfer in liquid desiccant system	9
2.2.1 Mass and heat transfer in counter and parallel flow channel	9
2.2.2 Mass and heat transfer in cross flow channel	11
2.3 Impact of nanoparticles on thermophysical properties of fluids	12

CHAPTER 3 METHODOLOGY AND MATHEMATICAL FORMULATION.....	17
3.1 Governing Equations for parallel and counter flow configuration	19
3.2 Reduced governing equations for parallel and counter flow configuration	20
3.3 Analytical solutions for counter and parallel flow configuration	23
3.4 Finite volume method and method of approach for the numerical analysis	25
3.5 Models to determine the thermophysical property of nanofluids	27
3.5.1 Thermal conductivity models	27
3.5.2 Models for viscosity, density and specific heat	29
 CHAPTER 4 ANALYSIS OF THERMAL CONDUCTIVITY AND VISCOSITY OF LIQUID DESICCANT DUE TO ADDITION OF NANOPARTICLES.....	 32
4.1 Variation of thermal conductivity of liquid desiccant with nanoparticles	34
4.2 Variation of viscosity of liquid desiccant with nanoparticles	42
 CHAPTER 5 NUMERICAL ANALYSIS OF FALLING FILM DEHUMIDIFIER WITH NANOPARTICLES	 47
5.1 Validation of the results for parallel flow channel	48
5.2 Effect of varying various parameters on outlet conditions and heat and mass transfer characteristics.....	52
5.2.1 Effect of varying air Reynolds number	53
5.2.2 Effect of varying desiccant mass flow rate	54
5.2.3 Effect of varying height of the channel.....	55
5.2.4 Effect of varying desiccant concentration	56
5.2.5 Effect of varying desiccant temperature	57
5.2.6 Effect of varying temperature of air	58
5.2.7 Effect of varying nanoparticles volume fraction.....	59
5.2.8 Effect of varying humidity ratio of air.....	60
5.3 Sensitivity Analysis.....	62
5.3.1 Sensitivity analysis for average Nusselt number	63
5.3.2 Sensitivity analysis for average Sherwood number.....	65
5.3.3 Sensitivity analysis for outlet Air temperature.....	65
5.3.4 Sensitivity analysis for outlet Humidity ratio.....	68
5.3.5 Sensitivity analysis results by uncertainty propagation method	70

CHAPTER 6 COMPARATIVE NUMERICAL ANALYSIS OF PARALLEL AND COUNTER FLOW FALLING FILM DEHUMIDIFIERS FOR DIFFERENT LIQUID DESICCANTS WITH DIFFERENT NANOPARTICLES	75
6.1 Comparative numerical analysis of parallel flow falling film dehumidifiers for three different liquid desiccants with three different nanoparticles.....	77
6.1.1 Calcium chloride (CaCl ₂) liquid desiccant (PF)	77
6.1.2 Lithium chloride (LiCl) liquid desiccant (PF).....	82
6.1.3 Lithium bromide (LiBr) liquid desiccant (PF).....	86
6.2 Comparative numerical analysis of counter flow falling film dehumidifiers for three different liquid desiccants with three different nanoparticles.....	90
6.2.1 Calcium chloride (CaCl ₂) liquid desiccant (CF)	91
6.2.2 Lithium chloride (LiCl) liquid desiccant (CF).....	95
6.2.3 Lithium bromide (LiBr) liquid desiccant (CF).....	99
6.3 Comparative numerical analysis of parallel and counter flow falling film dehumidifiers for CaCl₂ liquid desiccant with copper nanoparticles	103
CHAPTER 7 CONCLUSIONS AND RECOMMENDATIONS	109
REFERENCES.....	116
VITAE	120

LIST OF TABLES

Table 4.1: Thermophysical properties of liquid desiccants	33
Table 5.1: Design and operating parameters: Basic value and the range of variation of each parameter for air dehumidification.....	53
Table 5.2: Sensitivity Analysis of average Nusselt number by uncertainty propagation .	72
Table 5.3: Sensitivity Analysis of average Sherwood number by uncertainty propagation	72
Table 5.4: Sensitivity Analysis of outlet air temperature by uncertainty propagation	73
Table 5.5: Sensitivity Analysis of outlet air temperature by uncertainty propagation	74

LIST OF FIGURES

Figure 1.1: Liquid Desiccant cooling system	2
Figure 2.1: Schematic diagram of a dehumidification system utilizing liquid desiccant ...	8
Figure 2.2: Cross flow falling film dehumidifier	13
Figure 3.1: Falling film liquid desiccant dehumidifier (a) Parallel flow channel (b) Counter flow channel	18
Figure 4.1: Variation of thermal conductivity of CaCl ₂ liquid desiccant with increasing volume fraction of nanoparticles using different thermal conductivity models at 35°C and 30% concentration	35
Figure 4.2: Variation of thermal conductivity of LiCl liquid desiccant with increasing volume fraction of nanoparticles using different thermal conductivity models at 35°C and 30% concentration.....	36
Figure 4.3: Variation of thermal conductivity of CaCl ₂ with increasing concentration using different thermal conductivity models at 25°C and 5% volume fraction of nanoparticles	37
Figure 4.4: Variation of thermal conductivity of LiCl with increasing concentration using different thermal conductivity models at 25°C and 5% volume fraction of nanoparticles	38
Figure 4.5: Variation of thermal conductivity of CaCl ₂ with increasing temperature using different thermal conductivity models at 30% concentration and 5% volume fraction of nanoparticles	39
Figure 4.6: Variation of thermal conductivity of LiCl with increasing temperature using different thermal conductivity models at 30% concentration and 5% volume fraction of nanoparticles	39
Figure 4.7: Variation of thermal conductivity of LiBr liquid desiccant with increasing volume fraction of nanoparticles using different thermal conductivity models at 35°C and 40% concentration.....	41
Figure 4.8: Variation of thermal conductivity of LiBr with increasing concentration using different thermal conductivity models at 25°C and 5% volume fraction of nanoparticles	41
Figure 4.9: Variation of thermal conductivity of LiBr with increasing temperature	

using different thermal conductivity models at 40% concentration and 5% volume fraction of nanoparticles	42
Figure 4.10: Variation of viscosity of LiCl, LiBr and CaCl ₂ liquid desiccant with increasing volume fraction of nanoparticles using different viscosity models at 35°C and 30% concentration and 45% concentration for LiBr...	43
Figure 4.11: Variation of viscosity of CaCl ₂ and LiCl with increasing concentration using different viscosity models at 25°C and 5% volume fraction of nanoparticles	44
Figure 4.12: Variation of viscosity of LiBr with increasing concentration using different viscosity models at 25°C and 5% volume fraction of nanoparticles	45
Figure 4.13: Variation of viscosity of CaCl ₂ and LiCl with increasing temperature using different viscosity models at 30% concentration and 5% volume fraction of nanoparticles	46
Figure 4.14: Variation of viscosity of LiBr with increasing temperature using different viscosity models at 45% concentration and 5% volume fraction of nanoparticles	46
Figure 5.1: Temperature distribution of liquid desiccant and air along the wall height at T _d =25°C, T _a =35°C and Z=40%	49
Figure 5.2: Humidity ratio of air along the wall height at T _d =25°C, T _a =35°C and Z=40%	50
Figure 5.3: Concentration of water in desiccant solution along the wall height at T _d =25°C, T _a =35°C and Z=40%	51
Figure 5.4: Effect of varying Reynolds number of air	54
Figure 5.5: Effect of varying mass flow rate of desiccant	55
Figure 5.6: Effect of varying height of the channel	56
Figure 5.7: Effect of varying desiccant concentration	57
Figure 5.8: Effect of varying desiccant temperature.....	58
Figure 5.9: Effect of varying air temperature	59
Figure 5.10: Effect of varying volume fraction of nanoparticles.....	60
Figure 5.11: Effect of varying the humidity ratio of air	61

Figure 5.12: Sensitivity analysis of average Nusselt number (a) Volume fraction (b) Air temperature (c) Reynolds number (d) Mass flow rate (e) Channel height (f) Inlet humidity ratio (g) Desiccant temperature (h) Concentration	64
Figure 5.13: Sensitivity analysis of average Sherwood number (a) Volume fraction (b) Air temperature (c) Reynolds number (d) Mass flow rate (e) Channel height (f) Inlet humidity ratio (g) Desiccant temperature (h) Concentration	66
Figure 5.14: Sensitivity analysis of outlet air temperature (a) Volume fraction (b) Air temperature (c) Reynolds number (d) Mass flow rate (e) Channel height (f) Inlet humidity ratio (g) Desiccant temperature (h) Concentration	67
Figure 5.15: Sensitivity analysis of outlet humidity ratio (a) Volume fraction (b) Air temperature (c) Reynolds number (d) Mass flow rate (e) Channel height (f) Inlet humidity ratio (g) Desiccant temperature (h) Concentration	69
Figure 6.1: Effect of different nanoparticles with varying volume fraction in CaCl ₂ liquid desiccant on outlet air temperature (PF).....	78
Figure 6.2: Effect of different nanoparticles with varying volume fraction in CaCl ₂ liquid desiccant on outlet humidity ratio (PF)	79
Figure 6.3: Effect of different nanoparticles with varying volume fraction in CaCl ₂ liquid desiccant on Nusselt number. (PF)	80
Figure 6.4: Effect of different nanoparticles with varying volume fraction in CaCl ₂ liquid desiccant on average Sherwood number at the interface (PF).....	81
Figure 6.5 : Effect of different nanoparticles with varying volume fraction in LiCl liquid desiccant on outlet air temperature (PF).....	82
Figure 6.6: Effect of different nanoparticles with varying volume fraction in LiCl liquid desiccant on outlet humidity ratio (PF)	83
Figure 6.7: Effect of different nanoparticles with varying volume fraction in LiCl liquid desiccant on Nusselt number (PF).....	84
Figure 6.8: Effect of different nanoparticles with varying volume fraction in LiCl	

liquid desiccant on average Sherwood number at the interface (PF).....	85
Figure 6.9: Effect of different nanoparticles with varying volume fraction in LiBr	
liquid desiccant on outlet air temperature (PF).....	86
Figure 6.10: Effect of different nanoparticles with varying volume fraction in LiBr	
liquid desiccant on outlet humidity ratio (PF)	87
Figure 6.11: Effect of different nanoparticles with varying volume fraction in LiBr	
liquid desiccant on Nusselt number. (PF)	88
Figure 6.12: Effect of different nanoparticles with varying volume fraction in LiBr	
liquid desiccant on average Sherwood number at the interface (PF).....	89
Figure 6.13: Effect of different nanoparticles with varying volume fraction in CaCl ₂	
liquid desiccant on outlet air temperature (CF)	91
Figure 6.14: Effect of different nanoparticles with varying volume fraction in CaCl ₂	
liquid desiccant on outlet humidity ratio (CF).....	92
Figure 6.15: Effect of different nanoparticles with varying volume fraction in CaCl ₂	
liquid desiccant on Nusselt number. (CF).....	93
Figure 6.16: Effect of different nanoparticles with varying volume fraction in CaCl ₂	
liquid desiccant on average Sherwood number at the interface (CF)	94
Figure 6.17: Effect of different nanoparticles with varying volume fraction in LiCl	
liquid desiccant on outlet air temperature (CF)	95
Figure 6.18: Effect of different nanoparticles with varying volume fraction in LiCl	
liquid desiccant on outlet humidity ratio (CF).....	96
Figure 6.19: Effect of different nanoparticles with varying volume fraction in LiCl	
liquid desiccant on Nusselt number (CF).....	97
Figure 6.20: Effect of different nanoparticles with varying volume fraction in LiCl	
liquid desiccant on average Sherwood number at the interface (CF)	98
Figure 6.21: Effect of different nanoparticles with varying volume fraction in LiBr	
liquid desiccant on outlet air temperature (CF)	99
Figure 6.22: Effect of different nanoparticles with varying volume fraction in LiBr	
liquid desiccant on outlet humidity ratio (CF).....	100
Figure 6.23: Effect of different nanoparticles with varying volume fraction in LiBr	
liquid desiccant on Nusselt number. (CF).....	101

Figure 6.24: Effect of different nanoparticles with varying volume fraction in LiBr liquid desiccant on average Sherwood number at the interface (CF)	102
Figure 6.25: Effect of increasing volume fraction of copper nanoparticle in CaCl ₂ liquid desiccant on outlet air temperature for both parallel and counter flow.	104
Figure 6.26: Effect of increasing volume fraction of copper nanoparticle in CaCl ₂ liquid desiccant on outlet humidity ratio for both parallel and counter flow.	105
Figure 6.27: Effect of increasing volume fraction of copper nanoparticle in CaCl ₂ liquid desiccant on Nusselt number for both parallel and counter flow	106
Figure 6.28: Effect of increasing volume fraction of copper nanoparticle in CaCl ₂ liquid desiccant on Sherwood number for both parallel and counter flow	107

LIST OF ABBREVIATIONS

a	coefficients in equation (3.45)
B	width of the wall (m)
b	source term independent of Φ
C	concentration of water in desiccant solution ($\text{kg}_w/\text{kg}_{\text{sol}}$)
C_p	specific heat (J/kgK)
CF	counter flow
CFC	chlorofluorocarbon
CNT	carbon nanotubes
D	diffusion coefficient (m^2/s)
d	diameter (m)
EES	engineering equation solver
g	gravitational acceleration (m/s^2)
H	channel height (m)
h	heat transfer coefficient ($\text{W}/\text{m}^2\text{K}$)
h_{fg}	latent heat of water vapor (J/kg)
HCFC	hydrochlorofluorocarbon

k	thermal conductivity (W/mK)
L	length (m)
\dot{m}	mass flow rate (kg/s)
n	empirical factor
N	number of molecules
Nu	Nusselt number
p	pressure (Pa)
PF	parallel flow
Re	Reynolds number
Sh	Sherwood number
T	temperature (°C)
U	uncertainty
u	velocity in x-direction (m/s)
v	velocity in y-direction (m/s)
V	volume (m ³)
W	air humidity ratio (kg _w /kg _{da})
X	independent variable

x	axial direction representing x-axis coordinates
Y	dependent variable
y	transverse direction representing y-axis coordinates
z	z-axis coordinates
Z	Salt concentration in liquid desiccant ($\text{kg}_{\text{salt}}/\text{kg}_{\text{sol}}$)

Greek Symbols

α	thermal diffusivity (m^2/s)
β	ratio of the nano-layer thickness to original particle radius
φ	volume fraction
Φ	output variable represents T_a, T_d, W, C
Ψ	sphericity
ρ	density (kg/m^3)
δ	thickness (m)
Δ	expression illustrated in equation (3.51)
ν	kinematic viscosity (m^2/s)
μ	dynamic viscosity (kg/ms)

Subscripts

a	air
avg	average value
d	desiccant
da	dry air
e	east node
eff	effective value
f	liquid desiccant
i	inlet
int	interface
max	maximum value
n	north node
nf	liquid desiccant containing nanoparticles (nanofluid)
nom	nominal
o	outlet
p	center node
s	nanoparticle

s	south node in equation (3.45)
salt	represents the solutes CaCl_2 , LiCl and LiBr
sol	liquid desiccant solution
t	total pressure
w	wall
w	liquid water in units of concentration
w	west node in equation (3.45)
ws	saturation pressure
z	vapor pressure

ABSTRACT

Full Name : Qazi Talal
Thesis Title : Modeling and Numerical investigation of a falling film liquid desiccant dehumidifier with nanoparticles
Major Field : Mechanical Engineering
Date of Degree : May 2018

In this research, nanoparticles were added to liquid desiccant falling film dehumidifier to enhance the heat and mass transfer characteristics as well as the cooling and the dehumidification process. Different liquid desiccants were investigated by adding different nanoparticles. Both parallel and counter flow configurations were studied in this research. Numerical analysis was implemented to determine the heat and mass transfer characteristics with appropriate boundary conditions. Because of the addition of nanoparticles, the liquid desiccant thermo-physical properties such as specific heat, thermal conductivity, viscosity, density etc. were calculated from different models available in the literature. The results of this study indicate that, at 5% volume fraction of any nanoparticle, parallel flow channel leads to better cooling and dehumidification of air compared to counter flow channel. For both flow configurations, the best liquid desiccant for carrying out cooling and dehumidification is lithium bromide. The best nanoparticle is copper for counter flow channel and aluminum oxide for parallel flow channel. Increasing the volume fraction of nanoparticles from 1% to 5% has a more significant effect on counter flow channel compared to parallel flow channel, because the reduction of air temperature and humidity ratio is greater with increasing volume fraction. The rate of heat and mass transfer also increases with increasing volume fraction for counter flow channel. Therefore, the

addition of nanoparticles to liquid desiccant is recommended for counter flow channel. For parallel flow channel, although the cooling and dehumidification of air are improved, the heat and mass transfer rate decrease with increasing volume fraction; hence, further experimental studies are required to investigate the feasibility of adding nanoparticles.

ملخص الرسالة

الاسم الكامل: قاضي طلال

عنوان الرسالة: النمذجة والتحقق العددي للمجففات السائلة المبنية على أساس التدفق الهابط المقلل للرطوبة مع استخدام الجسيمات النانوية

التخصص: الهندسة الميكانيكية

تاريخ الدرجة العلمية: مايو ، 2018

في هذا البحث تمت دراسة المجففات السائلة المبنية على أساس التدفق الهابط المقلل للرطوبة والمزودة بجسيمات نانوية، لتحسين خصائص نقل الحرارة والكتلة و تحسين عملية التبريد وتقليل الرطوبة. أنواع مختلفة من المجففات السائلة تم دراستها بإضافة أنواع مختلفة من الجسيمات النانوية. في هذا البحث تم دراسة نوعين من تكوينات التدفق ، التدفق المتوازي والعكسي. تم تنفيذ التحليل العددي لتحديد خصائص الكتلة ونقل الحرارة مع إعتبار الشروط الحدودية المناسبة. نتيجة لإضافة الجسيمات النانوية تم حساب الخواص الفيزيائية-الحرارية للمجففات السائلة مثل الحرارة النوعية والتوصيل الحراري واللزوجة والكثافة وما إلى ذلك من النماذج المختلفة والمتاحة في الأبحاث السابقة. النتائج المستخلصة من هذه الدراسة تشير إلى أن في حالة الحجم الجزئي (5% لأي من الجسيمات النانوية)، فإن قنوات التدفق المتوازي تعطي تبريد وإزالة الرطوبة أفضل مقارنةً بقنوات التدفق العكسي. أفضل مادة لإجراء التبريد وإزالة الرطوبة يمكن استخدامها في كلى التكوينين المتوازي والعكسي هي بروميد الليثيوم. إن أفضل جسيمات نانوية يمكن إستخدامها في قنوات التدفق العكسي هي جسيمات النحاس بينما أفضل جسيمات نانوية يمكن إستخدامها في قنوات التدفق المتوازي هي جسيمات أكسيد الألمونيوم. إن زيادة الحجم الجزئي للجسيمات النانوية من 1% إلى 5% له تأثير أكثر أهمية في قنوات التدفق العكسي مقارنة بقنوات التدفق المتوازي، وهذا يرجع إلى إرتفاع معدل انخفاض درجة حرارة الهواء ونسبة الرطوبة مع زيادة الحجم الجزئي. كما أن معدل نقل الحرارة و الكتلة أيضاً يزيد مع زيادة الحجم الجزئي في حالة قنوات التدفق العكسي. وبالتالي ، يوصى بإضافة جسيمات نانوية إلى المجففات السائلة لقنوات التدفق العكسي. بالنسبة لقنوات التدفق المتوازية، بالرغم من تحسن برودة الهواء و إزالة الرطوبة منه، إلا إن معدل نقل الحرارة والكتلة قلّ مع زيادة الحجم الجزئي؛ وبالتالي يحتاج إجراء مزيد من الدراسات التجريبية لفحص مدى جدوى إضافة جسيمات نانوية.

CHAPTER 1

INTRODUCTION

This research will focus primarily on improving the mass and heat transfer characteristics and the dehumidifier performance. Dehumidification has many applications especially industry related, such as metallurgical, chemical, combustion and air conditioning industries. Other systems such as refrigeration, mechanical compression and heat pump systems can be used for dehumidification but all these systems have a very high operating cost. The dehumidification process is carried out by utilization of vapour compression cycles in typical air conditioning systems, which requires a large amount of cost and energy as air needs to be cooled to very low temperatures for the moisture to condense out as water vapour. This is more applicable in case of the coastal areas in Kingdom of Saudi Arabia (KSA). For these regions, the liquid desiccant based dehumidification technology needs to be employed for saving energy and reducing the cost.

1.1 Hybrid Desiccant Cooling Systems

In hybrid air-conditioning systems the dehumidification process is carried out independently and the sensible cooling process can be performed separately by using conventional vapor compression cycle or an indirect evaporative cooling system. For the hybrid desiccant cooling system a schematic diagram proposed by Dai et al. [1] is shown in Figure 1.1, which utilizes a liquid desiccant. In many of these systems the general process that occurs is, the liquid desiccant in the dehumidifier comes in contact with the air that is hot and humid.

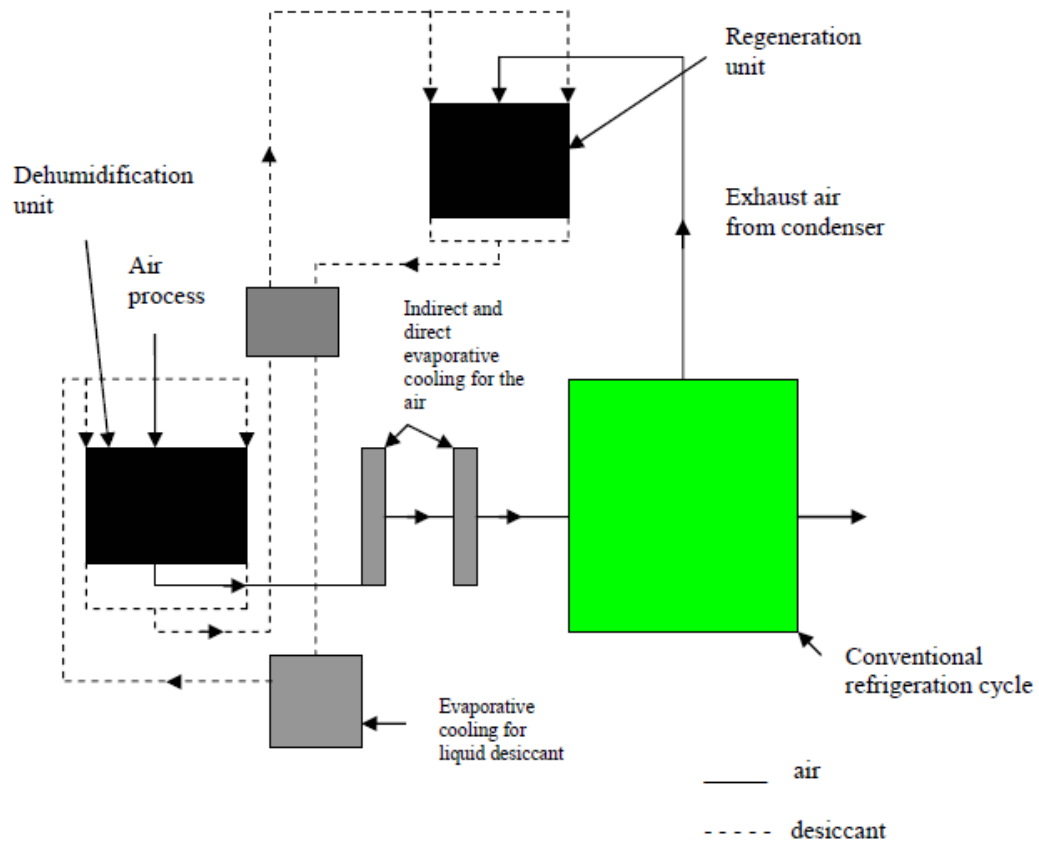


Figure 1.1: Liquid Desiccant cooling system

The liquid desiccant droplets are eliminated and humidity ratio is also maintained at the required level. The air is then sent to the conventional system. Due to absorbing the water vapor molecules from the humid air the concentration of water in liquid desiccant solution increases and the liquid desiccant becomes a weak solution. From the dehumidifier, weak liquid desiccant exits and enters a heat exchanger where the weak desiccant is preheated and the resulting strong desiccant exits from the regenerator. By low-grade energy such as solar energy, the weak desiccant is regenerated and the concentration of water in the desiccant solution is decreased resulting in a strong liquid desiccant solution. This strong liquid desiccant solution can now be re-used in the dehumidifier to carry out the

dehumidification process again. The strong liquid desiccant exiting the regenerator then goes through an evaporative cooler for further cooling before it re-enters the dehumidifier. These cycles will lead to a continuous process where air dehumidification occurs, followed by cooling and consequently the regeneration of liquid desiccant.

1.2 Advantage of using Desiccant Materials

In the early years, Loff [2] used tri-ethylene glycol solution to dehumidify the air. Research was started in the use of desiccant materials along with the conventional system. In the evaporator, microorganisms and bacteria accumulate at tube and fin surfaces, where water vapor condenses [3]. Utilization of desiccant materials removes the need for evaporator for dehumidification. From various studies it is a known fact that Chlorofluorocarbon (CFC) and Hydrochlorofluorocarbon (HCFC) that are used in the conventional system as refrigerant, causes ozone layer depletion. The alternative solution is to use desiccant materials for dehumidification and cooling .Waste heat, solar energy and natural gas are low grade energy that can be used to regenerate desiccant materials. Using this new hybrid system will result in decreased energy consumption, better quality of indoor air and a product that is environmentally friendly. In addition, the adverse effects caused by the emission of greenhouse gases which result in global warming are reduced, as consumption of fossil fuels to provide the energy for conventional air conditioning systems are reduced.

1.3 Types of Desiccant materials

Recently there have been many studies regarding solar driven cooling systems that utilize either liquid or solid desiccants. Most systems utilize solid desiccant which require

regeneration temperature that is comparatively high. Utilization of liquid desiccant systems is the alternative which require lower regeneration temperature. This research will focus on utilizing liquid desiccants instead of solid desiccants. Liquid desiccants are salt concentrations in water such as calcium chloride (CaCl_2), lithium bromide (LiBr), lithium chloride (LiCl) and tri-ethylene glycol.

It is easier to regenerate (between $50\text{-}65^\circ\text{C}$) liquid desiccant compared to solid desiccant which requires high grade energy to regenerate. Liquid desiccants also have low pressure drop across the system.

CaCl_2 is the one with the lowest absorption ability due its high vapor pressure relatively. However, CaCl_2 is common because its availability and low cost. On the other side, LiCl has the highest absorption ability and stability. A comparative study between LiCl and LiBr indicated that in the dehumidification process LiCl performance is better than LiBr due its low vapor pressure while LiBr performance is better in the regeneration process.

1.4 Potential of nanofluids in heat transfer applications

The analysis and research will be performed to improve the liquid desiccant cooling system performance. For this purpose the nanoparticles in fluids will be utilized, that is in the liquid desiccant to enhance its thermo-physical properties, and also to study the various changes in other liquid desiccant parameters due to the utilization of the nanoparticles. Nanoparticles in fluids are a new technology and a significant amount of research has been done in this sector particularly due to its possible improvement in applications of heat transfer. Compared to fluids thermal conductivity of solids is higher at different orders of magnitude. This depends on selection of the particular solid particles. A lot of research

have been performed that shows the superior impact of the nanoparticles in increasing the heat transfer characteristics and also various thermo-physical properties, one example is thermal conductivity. Such fluids with ultrafine particles are referred to as nanofluids and research in this field shows they have significant and promising role in the advancement of many industrial applications. In the literature different kinds of nanoparticles have been utilized for enhancement of heat transfer properties such as copper (Cu), magnesium oxide (MgO), copper oxide (CuO), aluminum oxide (Al₂O₃), carbon nanotubes (CNT), titanium dioxide (TiO₂), and many others.

1.5 Problem Statement

The primary purpose of this research is to model and simulate the impact of nanoparticles in liquid desiccant falling film dehumidifier. Different types of liquid desiccant will be investigated by the addition of different nanoparticles for counter flow and parallel flow falling film dehumidifier. These objectives can be attained by performing a numerical analysis to determine the mass and heat transfer characteristics of the liquid desiccant with nanoparticles. All the above mentioned research would be carried out to optimize the liquid desiccant dehumidifier and provide helpful insight to the researchers and scientists. Until now extensive research has not been carried out for improving liquid desiccants by the utilization of nanoparticles, hence the findings of this research are expected to be a base for the advancement of solar driven desiccant based hybrid cooling systems.

1.6 Specific objectives of this Research

Specific objectives of this research are listed below:

- For liquid desiccant systems, flow configuration, impact of nanoparticles on heat transfer properties, types of nanoparticles and utilization of nanoparticles in liquid desiccants; a comprehensive literature review will be performed.
- To investigate the selection of nanoparticles suitable for liquid desiccants.
- To determine the various thermo-physical properties of different nanoparticles (Cu, Al₂O₃, TiO₂) with different liquid desiccants (CaCl₂, LiCl, LiBr) as the base fluid from suitable models available in literature.
- Modeling and numerical analysis of the liquid desiccant falling film dehumidifier for distinct configurations of flow. Both counter flow and parallel flow will be studied.
- Parametric study of the dehumidifier. This includes the impact of different controlling parameters on heat and mass transfer characteristics and outlet air conditions.

CHAPTER 2

LITERATURE REVIEW

This study will focus on utilizing nanoparticles in liquid desiccant dehumidifying technology to improve the mass and heat transfer characteristics and the dehumidifier performance. Hence some literature review is done on liquid desiccant dehumidification.

2.1 Liquid Desiccant Systems

In hybrid cooling systems dehumidifiers reduce the humidity level in the air and is generally used for cooling purposes. Pesaran et al. [4] reviewed desiccant dehumidifying technologies. Figure 2.1 illustrates a dehumidification system utilizing liquid desiccant. There are two chambers in the system. One chamber is to carry out the dehumidification and the other chamber is used for regenerating the desiccant. The air enters into the required space after the dehumidification is carried out in the dehumidification chamber. The moisture containing liquid desiccant exits the dehumidifier and enters the regenerator. In the regenerator, moisture is removed by adding heat. Hence in this manner dehumidification and regeneration occurs.

Different apparatus such as packed tower, column tower, or in a spray tower with a finned-tubed surface can be used to carry out the dehumidification process. The finned-tubed surface type dehumidifier requires unreasonably high air velocity for certain cases.

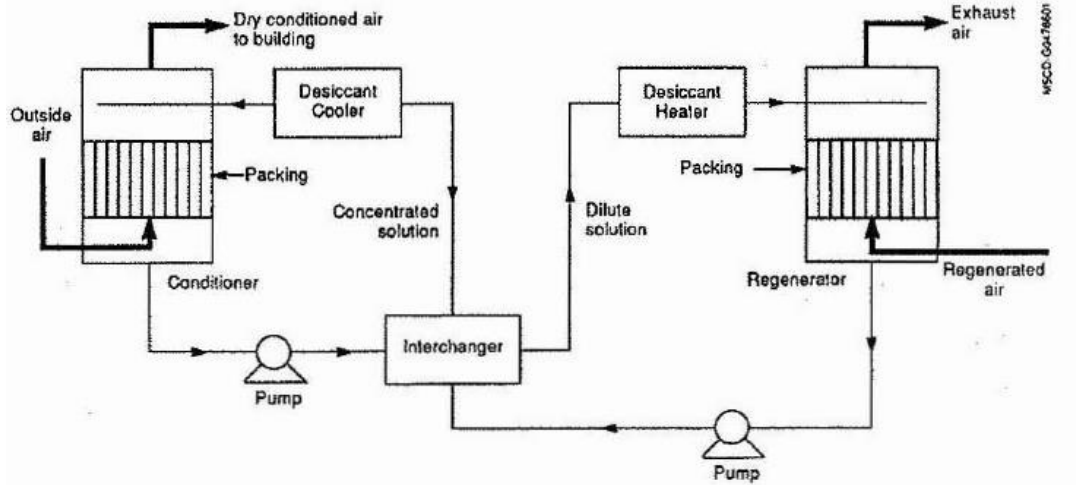


Figure 2.1: Schematic diagram of a dehumidification system utilizing liquid desiccant

It is also difficult to control the liquid film on the fin. In the spray tower, the solution is sprayed into the air stream by means of a nozzle which disperse the solution into a fine spray. This type of dehumidifier has the advantage of low air pressure drop, but is offset by a relatively high pumping cost for the solution. Further, the tendency for entrainment of liquid by the gas leaving is considerable. In packed tower, from the top strong desiccant is distributed and allowed to flow slowly by trickling down in a thin film through the tower. Air to be dehumidified flows in the opposite direction, providing a counter-flow arrangement for mass transfer. Packed tower dehumidifiers have been studied mathematically and experimentally as desiccant-based dehumidifiers, extensively. Another process is utilization of falling film desiccant for carrying out the dehumidification of air [3]. This can occur in either parallel, counter or cross-flow configuration.

2.2 Mass and Heat transfer in liquid desiccant system

The mass and heat transfer between liquid desiccant and air was investigated by Al-Farayedhi et al. [5] for packing tower with gauze-type structure. The study compared liquid desiccant of three different types. A remarkable improvement in the coefficient of mass transfer was detected for the lithium chloride, calcium chloride solution. However, the improvement was less significant for the other solutions used.

For water cooled liquid desiccant system three models of laminar flow was developed by Mesquita et al. [6]. Between the air and liquid desiccant, the coefficients of mass and heat transfer were calculated. The film thickness was calculated for temperature and concentration gradient by the most advanced model.

Sheridan and Mitchell [7] used hybrid desiccant cooling system to examine the energy consumption for hot-dry and hot-humid climates. In hot-dry climate higher energy was saved by hybrid cooling system compared to the climate that was hot-humid. A hybrid air-conditioning unit that used liquid desiccant was investigated by Howell and Peterson [8]. They reached the conclusion, that 25% reduction in consumption of power can be achieved and the condensation and evaporation areas can be reduced by 34%.

2.2.1 Mass and heat transfer in counter and parallel flow channel

Parallel flow channel was investigated by Rahamah et al. [9]. He analyzed the laminar flow of air and falling film liquid desiccant. A decrease in air temperature and humidity ratio at the exit was observed due to increasing the channel height. In desiccant solution a decrease in concentration of water at inlet results in improvement of the dehumidification process.

Numerical study was performed by Ali et al. [10] for falling film desiccant and air in counter and parallel flow channel. The enhancements in mass transfer and heat transfer in the flow was investigated by addition of copper nanoparticle. Superior and improved air dehumidification was observed for the channel with parallel flow compared to the counter flow from the numerical results. The air dehumidification is improved when air has a low Reynolds number. But improvement in the rate of regeneration is observed when air has a high Reynolds number. Improvement in dehumidification and rate of regeneration is observed at greater height of channel. Increase in nanoparticle volume fraction also resulted in improved cooling and dehumidification.

Research was carried out analyzing the coefficients of mass and heat transfer between liquid desiccant and air and for inclined counter and parallel flow with addition of copper nanoparticles by Ali and Vafai [11]. By adding copper nanoparticles, in one section of the research they investigated the impact of increased thermal conductivity in dehumidifier and regenerator. The thermal conductivity was determined using the Hamilton and Crosser model.

The transfer of heat between desiccant film and air is increased due to higher thermal conductivity as the copper nanoparticles volume fraction is increased and this results in decrease in temperature of air at exit by approximately 5 % due to thickness of the desiccant film being very small.

Also another observation that was made was that although the nanoparticle volume fraction was increased the exit concentration remained approximately constant. From these observations the research concluded that addition of copper nanoparticles resulted in

significant improvement for only the air cooling process. In case of the dehumidification and regeneration processes, there is some enhancement but it is minimal due to the desiccant film thickness being much less compared to the air thickness. Enhancement was observed in the regeneration and dehumidification process when the inclination angle was increased.

2.2.2 Mass and heat transfer in cross flow channel

Cross flow dehumidifiers are easier to build for practical applications than parallel and counter flow dehumidifiers. Many studies have been made on adiabatic and internally cooled counter flow dehumidifier with respect to their mass and heat transfer models but less research have been made on cross flow dehumidifiers. Park et al. [12] investigated between air and liquid desiccant flowing in cross flow configuration. He investigated the transfer of mass and heat that occurs between them, experimentally and also by numerical analysis. Based on finite differencing the numerical model was created. By central differencing, diffusion terms are expressed and by upstream differencing the convection terms are expressed. The results concluded that when the air mass flow rate decreases, air temperature decreases and humidity ratio regulation is improved. The numerical results followed a similar trend as the experimental results.

Saman and Alizadah [13] investigated the dehumidification and cooling process and suggested a cross-flow configuration for the plate. Liquid desiccant dehumidified the main air stream and water was sprayed to cool the following air stream. For each flow chamber, the numerical model was constructed on the basis of control volume, and boundary conditions were satisfied by an iterative method. It was not possible to obtain comfort level

conditions for the parameters i.e. the humidity and the air temperature. Therefore, further operations were carried out to obtain the necessary cooling and dehumidification.

For liquid desiccant system with cross flow configuration mass and heat transfer model was developed by Liu et al. [14]. For cross flow configuration between falling film liquid desiccant and air, Ali et al. [15] investigated the heat and mass transfer by adding copper nanoparticles for cooling and dehumidification. The conclusions reached were that the mass transfer and heat transfer between falling film liquid desiccant and air were improved due to higher thermal conductivity. Higher thermal conductivity was obtained due to increasing copper nanoparticles. Hence, it results in improved dehumidification and cooling as well as a more dynamically stable solution. In addition, the increase in channel length and decreasing width of the channel results in improved cooling and dehumidification process for the exit air conditions. Figure 2.2 illustrates the cross flow falling film dehumidifier [15].

2.3 Impact of nanoparticles on thermophysical properties of fluids

The concept of utilizing nanoparticles in fluids have been extensively investigated by researchers. Fluids containing suspended nano-sized solid particles are called nanofluids. The nanoparticles may be metallic or non-metallic. When introduced into a fluid, nanoparticles show significant enhancement of the various properties of the fluid and higher heat transfer characteristics. Nanofluids are used for various industrial, automotive and other applications. Escher et al. [16] researched cooling electronics and studied the utilization of nanofluids in this sector. The various applications of nanofluids in solar technology was reviewed by Mahian et al. [17].

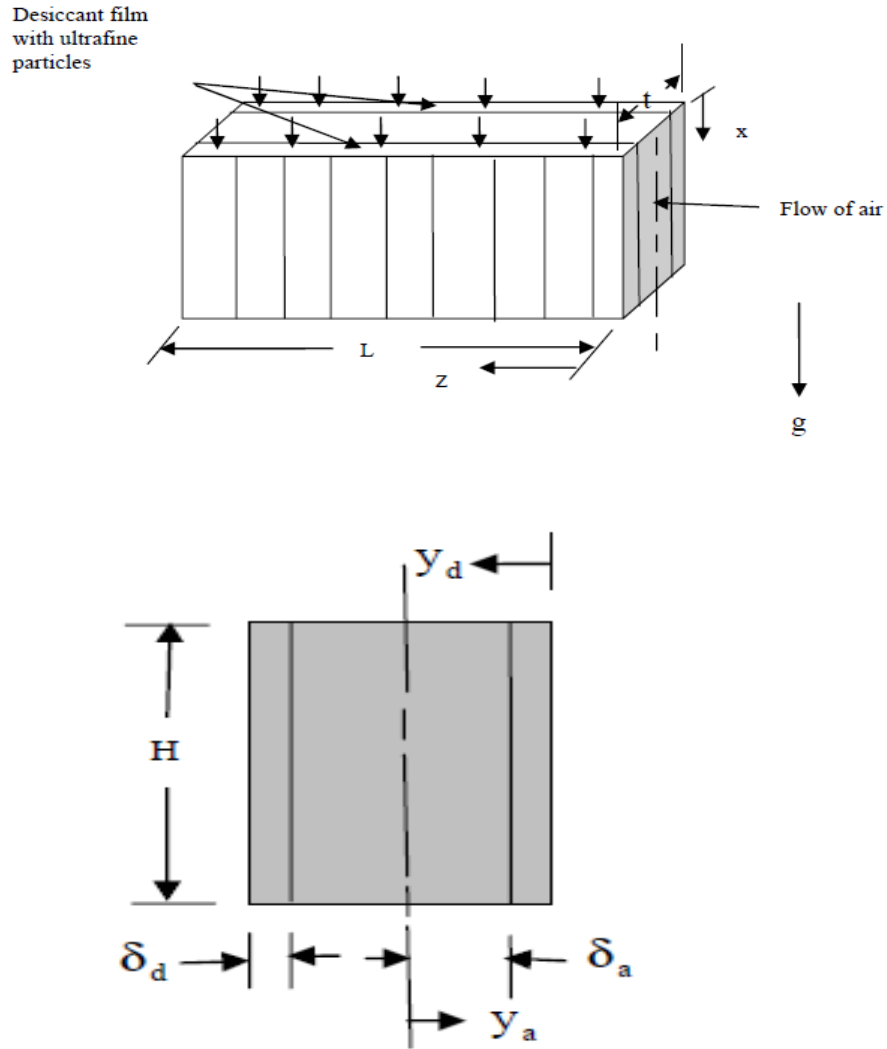


Figure 2.2: Cross flow falling film dehumidifier

Application of nanofluids in solar water heaters and collectors were initially conducted by researchers. In the past few decades, there have been many researches both theoretical and experimental to study the impact of nanoparticles on the increase and improvement of heat transfer characteristics in different kinds of thermal appliances. One such example is in the solar water heater where the role of nanofluids are discussed by researchers Natarajan and Satish [18].

Researchers have also used various preparation methods, different models and characteristics in order to calculate wide range of thermo-physical properties of fluids containing nanoparticles (i.e., density, specific heat capacity, viscosity, thermal conductivity, vapor pressure) [19][20]. The heat transfer field was improved due to the positive effect of nanoparticles on thermal characteristics, and this had a major impact on a number of industrial applications including heating and cooling, power generation, air-conditioning, transportation, metallurgical applications, ventilation, chemical applications etc. [21][22]. The impact on the thermo-physical properties of fluids due to addition of nanoparticles such as specific heat, viscosity, thermal conductivity is a very significant field of study due to effect of these properties on the heat and mass transfer potential of nanofluids. Inclusion of nanoparticles results in higher thermal conductivity resulting in improved heat transfer but viscosity also increases adversely affecting the heat transfer characteristics. Hence, it is necessary that increase in thermal conductivity should be significant enough to overcome the adverse effects of increased viscosity.

Many researchers have performed extensive studies on the variation of thermo-physical properties. Some studies on viscosity and thermal conductivity are mentioned below. Choi et al. [23] carried out research to determine the increase of fluid thermal conductivity when nanoparticles are present in it. Lee et al. [24] researched the various techniques to determine the nanofluid thermal conductivity. Xuan and Li [25] investigated a process in order to concoct a nanofluid. The nanofluid thermal conductivity was determined by utilizing a hot wire equipment. The results suggested that as the volume fraction was increased, thermal conductivity increased significantly. In another study conducted by Xuan and Roetzel [26] researched the calculation of nanofluid thermal conductivity and proposed two methods.

In one method, the assumption was made that nanofluids are conventional single-phase fluids and the dispersion factor was considered in the second method. Thomas and Sobhan [27] researched and experimented on nanofluids, and calculated the nanofluid thermal conductivity.

Ethylene glycol was experimented by Eastman et al. [28] to determine the effective thermal conductivity by adding copper nanoparticles to it. For 0.3% copper nanoparticles volume fraction having less than 10 nm mean diameter, there was a rise in thermal conductivity of approximately 40%. The theoretical models prediction were much lower than the results. It was concluded that theoretical models were anomalous and the models should consider the particle thermal conductivity effect and particle diameter.

Garg et al. [29] experimentally investigated the enhancement of thermal conductivity and viscosity of ethylene glycol fluid by addition of copper nanoparticles. The results indicated that the experimental value of thermal conductivity was double the value obtained by Maxwell model. By performing analytical calculations, it was concluded that the nanofluid would have an adverse effect as coolant in heat exchangers. This is because compared to the thermal conductivity increase; the increment in viscosity was more significant. However, if the tube diameter is increased better thermal performance can be obtained due to increment in thermal conductivity becoming more significant.

Murshed et al. [30] investigated the enhancement in water thermal conductivity due to inclusion of TiO₂ nanoparticles. Two different shapes was considered: One was spherical nanoparticles with 15 nm and other was rod-shaped with dimensions (10nm diameter 40 nm length). The thermal conductivity was measured by hot wire apparatus. The values

obtained from the following theoretical models: Hamilton and Crosser, Wasp and Bruggeman model, were compared with the experimental values. The results indicated that increasing volume fraction resulted in increased thermal conductivity and the increment was much greater than values obtained from theoretical models. Another observation made was that the size and shape of the nanoparticle has a considerable effect on the thermal conductivity value. While there have been many studies related to thermal conductivity improvement, the effect on viscosity due to nanoparticles has received much less attention but it is a crucial thermo-physical property that influences the heat transfer and flow characteristics. This is because the pumping power due to the pressure drop depend on this property. The viscosity data was measured by Murshed et al. [31] for Al_2O_3 and TiO_2 /water-based nanofluids at 5% volume fraction and the highest increment obtained was about 80%. Experimental studies were performed by Nguyen et al. [32] to study the impact on viscosity in Al_2O_3 /water nanofluid due to the variation of temperature and volume fraction. The results indicated that increasing the temperature resulted in a decrease in the viscosity but volume fraction increase resulted in a notable increase in viscosity.

Hence for this study the mass and heat transfer enhancement of the liquid desiccant dehumidifier with nanoparticles will be investigated and the effect on dehumidifier performance due to the nanoparticles. The governing equations of mass, momentum, energy and concentration will be solved with appropriate boundary conditions numerically for different flow configurations. The required properties of thermal conductivity, viscosity etc. of liquid desiccant with nanoparticles will be obtained from various models cited in the literature.

CHAPTER 3

METHODOLOGY AND MATHEMATICAL FORMULATION

By investigating the impact of the relevant parameters, the falling film dehumidifier performance with different nanoparticles in different liquid desiccants will be evaluated. This will be carried out by detailed modeling and numerical analysis of the dehumidifier and will incorporate mass and heat transfer modeling, geometric modeling. Based on the research carried out the optimum parameters for designing falling film dehumidifier with nanoparticles will be determined.

Mass and heat transfer occurs during the dehumidification process. The dehumidification occurs due to the difference in partial pressure of water vapor between the air and desiccant. Various parameters for investigating the falling film dehumidifier performance include inlet conditions of the air (humidity ratio, temperature), inlet desiccant condition (concentration and temperature), desiccant and air Reynolds number, height of the channel and the nanoparticle volume fraction etc. The effect of these parameters on the mass and heat transfer characteristics i.e. the Sherwood number and the Nusselt number and the outlet air conditions (humidity ratio and temperature) will be investigated.

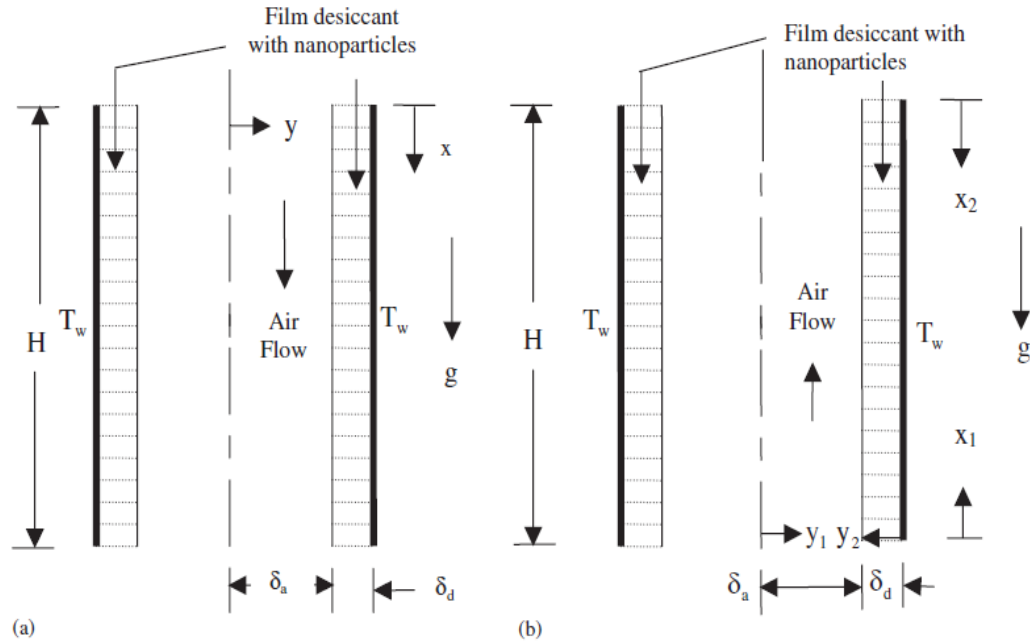


Figure 3.1: Falling film liquid desiccant dehumidifier (a) Parallel flow channel (b) Counter flow channel

Two flow configurations for falling film dehumidifier was investigated in this study. Figure 3.1 illustrates the two flow configurations i.e. parallel flow configuration and counter flow configuration. The figure illustrates a falling film of desiccant solution with the air flowing upwards in the counter flow channel and downwards in the parallel flow channel. Several assumptions are made for the purpose of this research. The flow in both channels for desiccant and air is steady and laminar. The temperature of the wall is constant at 10°C . At the interface between liquid desiccant solution and air, there is thermodynamic equilibrium. At the entrance of the channel, fully developed velocity profile exists. The gravitational force of air is neglected. The thermal properties of air and liquid desiccant is constant throughout the height of the channel. The thickness of the desiccant film is constant.

3.1 Governing Equations for parallel and counter flow configuration

The governing equations for counter flow and parallel flow channel are the same and they are mentioned below.

The governing mass and momentum equation for the desiccant are:

$$\frac{\partial u_d}{\partial x} + \frac{\partial v_d}{\partial y_d} = 0 \quad (3.1)$$

$$\rho_d \left(u_d \frac{\partial u_d}{\partial x} + v_d \frac{\partial u_d}{\partial y_d} \right) = \rho_d g_x - \frac{\partial p}{\partial x} + \mu_d \left(\frac{\partial^2 u_d}{\partial x^2} + \frac{\partial^2 u_d}{\partial y_d^2} \right) \quad (3.2)$$

$$\rho_d \left(u_d \frac{\partial v_d}{\partial x} + v_d \frac{\partial v_d}{\partial y_d} \right) = \rho_d g_{y_d} - \frac{\partial p}{\partial y_d} + \mu_d \left(\frac{\partial^2 v_d}{\partial x^2} + \frac{\partial^2 v_d}{\partial y_d^2} \right) \quad (3.3)$$

The energy equation for desiccant film is:

$$\rho_d c_p \left(u_d \frac{\partial T_d}{\partial x} + v_d \frac{\partial T_d}{\partial y_d} \right) = \mu_d \left(\frac{\partial^2 T_d}{\partial x^2} + \frac{\partial^2 T_d}{\partial y_d^2} \right) \quad (3.4)$$

The concentration equation for the desiccant film is:

$$u_d \frac{\partial c}{\partial x} + v_d \frac{\partial c}{\partial y_d} = D_d \left(\frac{\partial^2 c}{\partial x^2} + \frac{\partial^2 c}{\partial y_d^2} \right) \quad (3.5)$$

Similarly for air the governing mass and momentum equation are:

$$\frac{\partial u_a}{\partial x} + \frac{\partial v_a}{\partial y_a} = 0 \quad (3.6)$$

$$\rho_a \left(u_a \frac{\partial u_a}{\partial x} + v_a \frac{\partial u_a}{\partial y_a} \right) = -\frac{\partial p}{\partial x} + \mu_a \left(\frac{\partial^2 u_a}{\partial y_a^2} + \frac{\partial^2 u_a}{\partial x^2} \right) \quad (3.7)$$

$$\rho_a \left(v_a \frac{\partial v_a}{\partial y_a} + u_a \frac{\partial v_a}{\partial x} \right) = -\frac{\partial p}{\partial y_a} + \mu_a \left(\frac{\partial^2 v_a}{\partial y_a^2} + \frac{\partial^2 v_a}{\partial x^2} \right) \quad (3.8)$$

The energy equation for air is:

$$\rho_a c_p \left(v_a \frac{\partial T_a}{\partial y_a} + u_a \frac{\partial T_a}{\partial x} \right) = \frac{\partial}{\partial y_a} \left(k_a \frac{\partial T_a}{\partial y_a} \right) + \frac{\partial}{\partial x} \left(k_a \frac{\partial T_a}{\partial x} \right) \quad (3.9)$$

The diffusion equation for air is:

$$v_a \frac{\partial W}{\partial y_a} + u_a \frac{\partial W}{\partial x} = D_a \left(\frac{\partial^2 W}{\partial y_a^2} + \frac{\partial^2 W}{\partial x^2} \right) \quad (3.10)$$

3.2 Reduced governing equations for parallel and counter flow configuration

Based on the assumptions mentioned above the governing equations for counter flow and parallel flow channel are reduced to:

$$\frac{\partial u_d}{\partial x} = 0 \quad (3.11)$$

$$\rho_d g_x + \mu_d \left(\frac{\partial^2 u_d}{\partial x^2} + \frac{\partial^2 u_d}{\partial y_d^2} \right) = 0 \quad (3.12)$$

The energy equation for desiccant film is:

$$\rho_d c_p \left(u_d \frac{\partial T_d}{\partial x} \right) = \mu_d \left(\frac{\partial^2 T_d}{\partial x^2} + \frac{\partial^2 T_d}{\partial y_d^2} \right) \quad (3.13)$$

The concentration equation for the desiccant film is:

$$u_d \frac{\partial C}{\partial x} = D_d \left(\frac{\partial^2 C}{\partial x^2} + \frac{\partial^2 C}{\partial y_d^2} \right) \quad (3.14)$$

Similarly for air the reduced governing mass and momentum equation are:

$$\frac{\partial u_a}{\partial x} = 0 \quad (3.15)$$

$$\frac{\partial p}{\partial x} = \mu_a \left(\frac{\partial^2 u_a}{\partial y_a^2} + \frac{\partial^2 u_a}{\partial x^2} \right) \quad (3.16)$$

The energy equation for air is:

$$\rho_a c_p \left(u_a \frac{\partial T_a}{\partial x} \right) = \frac{\partial}{\partial y_a} \left(k_a \frac{\partial T_a}{\partial y_a} \right) + \frac{\partial}{\partial x} \left(k_a \frac{\partial T_a}{\partial x} \right) \quad (3.17)$$

The diffusion equation for air is:

$$u_a \frac{\partial W}{\partial x} = D_a \left(\frac{\partial^2 W}{\partial y_a^2} + \frac{\partial^2 W}{\partial x^2} \right) \quad (3.18)$$

The interface conditions and boundary conditions for parallel and counter flow channel utilized in our study are illustrated below.

For the parallel flow channel the interfacial conditions and boundary conditions are:

$$C=C_i \quad T_d=T_{di} \quad v_d=0 \quad u_d=u_{di} \quad \text{at } x=0 \text{ and } \delta_a < y < \delta_a + \delta_d \quad (3.19)$$

$$W=W_i \quad T_a=T_{ai} \quad v_a=0 \quad u_a=u_{ai} \quad \text{at } x=0 \text{ and } 0 < y < \delta_a \quad (3.20)$$

$$\frac{\partial C}{\partial x} = 0 \quad \frac{\partial T_d}{\partial x} = 0 \quad v_d = 0 \quad \frac{\partial u_d}{\partial x} = 0 \quad \text{at } x=H \text{ and } \delta_a < y < \delta_a + \delta_d \quad (3.21)$$

$$\frac{\partial W}{\partial x} = 0 \quad \frac{\partial T_a}{\partial x} = 0 \quad v_a = 0 \quad \frac{\partial u_a}{\partial x} = 0 \quad \text{at } x=H \text{ and } 0 < y < \delta_a \quad (3.22)$$

$$\frac{\partial W}{\partial y} = 0 \quad \frac{\partial T_a}{\partial y} = 0 \quad v_a = 0 \quad \frac{\partial u_a}{\partial y} = 0 \quad \text{at } y=0 \text{ and } 0 < x < H \quad (3.23)$$

$$\frac{\partial u_d}{\partial y} = 0 \quad W=W_{int} \quad T_a=T_d \quad u_a=u_d \quad \text{at } y=\delta_a \text{ and } 0 < x < H \quad (3.24)$$

$$\frac{\partial C}{\partial y} = 0 \quad T_d = T_w \quad u_d = 0 \quad \text{at } y = \delta_a + \delta_d \text{ and } 0 < x < H \quad (3.25)$$

For the counter flow channel the interfacial conditions and boundary conditions are:

$$C = C_i \quad T_d = T_{di} \quad v_d = 0 \quad u_d = u_{di} \quad \text{at } x = 0 \text{ and } \delta_a < y < \delta_a + \delta_d \quad (3.26)$$

$$W = W_i \quad T_a = T_{ai} \quad v_a = 0 \quad u_a = u_{ai} \quad \text{at } x = H \text{ and } 0 < y < \delta_a \quad (3.27)$$

$$\frac{\partial C}{\partial x} = 0 \quad \frac{\partial T_d}{\partial x} = 0 \quad v_d = 0 \quad \frac{\partial u_d}{\partial x} = 0 \quad \text{at } x = H \text{ and } \delta_a < y < \delta_a + \delta_d \quad (3.28)$$

$$\frac{\partial W}{\partial x} = 0 \quad \frac{\partial T_a}{\partial x} = 0 \quad v_a = 0 \quad \frac{\partial u_a}{\partial x} = 0 \quad \text{at } x = 0 \text{ and } 0 < y < \delta_a \quad (3.29)$$

$$\frac{\partial W}{\partial y} = 0 \quad \frac{\partial T_a}{\partial y} = 0 \quad v_a = 0 \quad \frac{\partial u_a}{\partial y} = 0 \quad \text{at } y = 0 \text{ and } 0 < x < H \quad (3.30)$$

$$\frac{\partial u_d}{\partial y} = 0 \quad W = W_{int} \quad T_a = T_d \quad u_a = u_d \quad \text{at } y = \delta_a \text{ and } 0 < x < H \quad (3.31)$$

$$\frac{\partial C}{\partial y} = 0 \quad T_d = T_w \quad u_d = 0 \quad \text{at } y = \delta_a + \delta_d \text{ and } 0 < x < H \quad (3.32)$$

By applying appropriate boundary conditions to the energy concentration and diffusion equations, the energy balance and mass balance at the interface can be obtained. At the interface for both counter flow and parallel flow channel the mass balance and heat balance results in:

$$-k_a \frac{\partial T_a}{\partial y_a} - \rho_a D_a h_{fg} \frac{\partial W}{\partial y_a} = k_d \frac{\partial T_d}{\partial y_d} \quad (3.33)$$

$$\rho_a D_a \frac{\partial W}{\partial y_a} = -\rho_d D_d \frac{\partial C}{\partial y_d} \quad (3.34)$$

3.3 Analytical solutions for counter and parallel flow configuration

By integrating the mass and momentum equations of both air and desiccant film the velocity profiles are obtained.

The velocity profile of air for parallel flow channel is given by:

$$u_a = u_{int} - (u_{int} - u_{max})\left(1 - \frac{y^2}{\delta_a^2}\right) \quad (3.35)$$

The velocity profile of air for counter flow channel is given by:

$$u_a = -(u_{int} - (u_{int} - u_{max})\left(1 - \frac{y^2}{\delta_a^2}\right)) \quad (3.36)$$

The velocity profile for desiccant film is the same for both parallel and counter flow channel and is given by:

$$u_d = \frac{\rho g}{\mu} \left(\delta_a y + \frac{(\delta_a + \delta_d)^2}{2} - \delta_a^2 - \delta_a \delta_d - \frac{y^2}{2} \right) \quad (3.37)$$

The thickness of the desiccant film is dependent on mass flow rate of desiccant and is given by:

$$\delta_d = \left(\frac{3\dot{m}_d \mu_d}{\rho_d^2 g} \right)^{\frac{1}{3}} \quad (3.38)$$

At the interface of the channel, the humidity ratio is given by:

$$W_{int} = 0.62185 \frac{p_z}{(p_t - p_z)} \quad (3.39)$$

p_z is the vapor pressure of the desiccant solution and is expressed by:

$$p_z = p_{ws} \left(1 - 0.828Z - 1.496Z^2 + \frac{Z(T_{int}-40)}{350} \right) \quad (3.40)$$

Heat and mass transfer correlations can be investigated by average Nusselt number and average Sherwood number.

The average Nusselt number at the interface is given by:

$$Nu_{avg} = \frac{4\delta_a}{H} \int_0^H \frac{\partial T_a / \partial y_a}{T_a - T_{int}} \quad (3.41)$$

The average Sherwood number at the interface is given by:

$$Sh_{avg} = \frac{4\delta_a}{H} \int_0^H \frac{\partial W / \partial y_a}{W_i - W_{int}} \quad (3.42)$$

The Reynolds numbers for desiccant and air are given by:

$$Re_a = \frac{4\rho_a u_a \delta_a}{\mu_a} \quad (3.43)$$

$$Re_d = \frac{4\rho_d u_d \delta_d}{\mu_d} \quad (3.44)$$

In order to carry out the numerical analysis of the falling film dehumidifier the finite volume method is utilized. The finite volume method and the procedure to carry out the numerical analysis is discussed in detail in the next section.

3.4 Finite volume method and method of approach for the numerical analysis

In order to carry out the numerical analysis of the falling film dehumidifier the finite volume method is utilized. In this analysis the discretization is done where the governing partial differential equations are converted into discrete algebraic equations.

The first step is the discretization of the geometry using mesh generation. The domain is divided into cells to solve the conservation equations at each cell. The geometry in this study is rectangular channel with two layers for desiccant flow and air flow. For the desiccant flow channel, the domain is divided into 100 cells in the axial direction and 10 cells in the transverse direction. For the air flow channel the domain is divided into 30 cells in the transverse direction and 100 cells in the axial direction.

The domain is divided into control volumes and the computational node lies at the center of the control volume. The integral form of the partial differential equations are discretized into linear algebraic equations for each control volume. These equations are then solved simultaneously and iteratively to obtain the temperature, humidity and concentration distributions.

In the conservation equations the convection term, diffusion term and source terms are discretized to form an algebraic equation. The general form of the algebraic equation is:

$$a_p \Phi_p = a_e \Phi_e + a_w \Phi_w + a_n \Phi_n + a_s \Phi_s + b_p \quad (3.45)$$

The convection terms in the above equation is discretized by the upwind differencing scheme to preserve the directional nature of the convection process. Based on the heat and

mass balance equations at the interface the discretized equations for the interface specifically are determined by the finite volume method separately.

After the discretized equations are derived, they are solved simultaneously and iteratively at each node of the control volume mesh grid. The procedure of the numerical analysis is described briefly below:

- The inlet conditions for both desiccant and air solutions needs to be specified.
- The boundary conditions at the exit of the channel and the centerline needs to be assigned
- The temperature of the wall and height of the channel needs to be fixed.
- The size of channel for both air and desiccant film needs to be specified.
- The thickness of the desiccant film is obtained from equation (3.38) based on the desiccant mass flow rate.
- The thickness of air channel can then be obtained by subtracting desiccant film thickness from size of the channel.
- The velocity profiles of both air and desiccant channel are obtained from equations (3.35) (3.36) and equation (3.37) respectively.
- The maximum velocity of the air channel is obtained from the Reynolds number of air which is determined from mass flow rate of air.
- The air and desiccant properties are obtained from relevant expressions and databases and are used to calculate the diffusion and convection terms in the discretized equations.

- The discretized equations are then solved iteratively and simultaneously at each node of the control volume to obtain the temperature, humidity ratio and concentration distributions.
- Based on the temperature distribution at the interface the average Nusselt number at the interface is determined from equation (3.41)
- Based on the humidity ratio distribution at the interface the average Sherwood number at the interface is determined from equation (3.42)

3.5 Models to determine the thermophysical property of nanofluids

Various models are available in the literature to determine the thermophysical property of nanofluids. These models are discussed in detail especially for thermal conductivity and viscosity as many studies to determine these properties have been carried out previously.

3.5.1 Thermal conductivity models

The solving of energy equation requires the thermal conductivity and the velocity profile requires the viscosity and these can be obtained from the following models. In order to determine the thermal conductivity of the liquid desiccant solutions containing nanoparticles, conventional models were used as there were no models available in the literature specific to liquid desiccant solutions. The conventional models are discussed below.

Two methods to calculate the thermal conductivity of the nanofluids were described by Xuan and Roetzel [26]. One of them was the conventional method and the other was the

modified conventional method taking into account the thermal dispersion. The nanofluids thermal conductivity according to the modified approach is given by:

$$(\rho C_p)_{eff} = (1 - \phi)(\rho C_p)_f + \phi(\rho C_p)_s \quad (3.46)$$

In the above equation the nanoparticles volume fraction is ϕ , (15):

$$\phi = \frac{V_s}{V_f + V_s} = N \frac{\pi}{6} d_s^3 \quad (3.47)$$

An expression to calculate the thermal conductivity of mixtures of solid-liquid composition was developed by Hamilton and Crosser [33]:

$$\frac{k_{eff}}{k_f} = \frac{k_s + (n-1)k_f - (n-1)\phi(k_f - k_s)}{k_s + (n-1)k_f + \phi(k_f - k_s)} \quad (3.48)$$

In the above equation k_{eff} denotes the effective thermal conductivity of the nanofluid. Empirical factor n is given by $n = 3/\psi$ and has different values and varies with the shape of the nanoparticle. The sphericity is given by ψ , which for a porous medium is the dispersed thermal conductivity.

An alternative model was proposed by Wasp for thermal conductivity calculation. The Wasp model was used by Xuan and Li [25]. This model is not valid for cylindrical particles. For spherical particles the Wasp model agrees with Hamilton & Crosser model.

$$\frac{k_{eff}}{k_f} = \frac{k_s + 2k_f - 2\phi(k_f - k_s)}{k_s + 2k_f + \phi(k_f - k_s)} \quad (3.49)$$

One of the more recent models is the Bruggeman model and it is proposed by Hui et al. [34] and also utilized in Murshed et al. [30]. This model is applicable for a mixture of randomly dispersed and homogeneous spherical nanoparticles. The particle interactions

has been taken into account in these models. In addition, there is no limitation on particle volume fraction.

$$\frac{k_{eff}}{k_f} = \frac{1}{4} [(3\phi - 1) \frac{k_s}{k_f} + (2 - 3\phi)k_f] + \frac{k_f}{4} \sqrt{\Delta} \quad (3.50)$$

$$\Delta = [(3\phi - 1)^2 \left(\frac{k_s}{k_f}\right)^2 + (2 - 3\phi)^2 + 2(2 + 9\phi - 9\phi^2) \left(\frac{k_s}{k_f}\right)] \quad (3.51)$$

Yu and Choi [35] proposed a thermal conductivity model based on the inclusion of an interfacial layer. They expressed the thermal conductivity of the nanoparticle as an equivalent value by integrating the value of β into the expression.

$$\frac{k_{eff}}{k_f} = \frac{k_s + 2k_f + 2\phi(k_s - k_f)(1 + \beta)^3}{k_s + 2k_f - \phi(k_s - k_f)(1 + \beta)^3} \quad (3.52)$$

In the above expression β is the ratio of nanolayer thickness to original particle radius, and the value of $\beta=0.1$ is usually taken for calculating the thermal conductivity.

3.5.2 Models for viscosity, density and specific heat

In order to model the viscosity of nanofluids many different models have been suggested by researchers. One of the earliest models was suggested by Einstein [36] for determining the viscosity as a function of volume fraction for volume concentration of 5% and lower. Einstein's equation is expressed by:

$$\mu_{eff} = (1 + 2.5\phi)\mu_f \quad (3.53)$$

In the above expression μ_{eff} is the nanofluid viscosity, μ_f is the base fluid viscosity and ϕ is the nanoparticle volume fraction. Another researcher Brinkman [37] proposed an

expression that was an extension of Einstein's equation of viscosity for concentrated mixtures and is given by:

$$\mu_{eff} = \frac{1}{(1-\phi)^{2.5}} \mu_f \quad (3.54)$$

Batchelor [38] studied the effect of Brownian motion on viscosity for spherical particles and proposed an expression given by:

$$\mu_{eff} = (1 + 2.5\phi + 6.2\phi^2)\mu_f \quad (3.55)$$

This expression gives the effective viscosity for suspensions having isotropic structures.

In order to obtain the density of nanofluids the mixture rule principle can be utilized. The density of nanofluids can be expressed as:

$$\rho_{eff} = (1 - \phi)\rho_f + \phi\rho_s \quad (3.56)$$

In the above expression ρ_{eff} is the density of the nanofluid, ρ_s is the nanoparticle density and ρ_f is the density of the liquid desiccant.

The specific heat of the nanofluids can be similarly defined as:

$$Cp_{eff} = (1 - \phi)Cp_f + \phi Cp_s \quad (3.57)$$

In the above expression Cp_{eff} is the specific heat of the nanofluid, Cp_s is the nanoparticle specific heat and Cp_f is the specific heat of the liquid desiccant.

These correlations will be revised to take into account the effect of liquid desiccant with nanoparticles. The nanoparticles are generally spherical in shape hence all calculations will be made for spherical nanoparticles. CNT (carbon nanotubes) which are cylindrical in

shape will not be considered as desiccant film thickness is very low and agglomeration of CNT may cause obstruction in the flow of liquid desiccant.

CHAPTER 4

ANALYSIS OF THERMAL CONDUCTIVITY AND VISCOSITY OF LIQUID DESICCANT DUE TO ADDITION OF NANOPARTICLES

Based on these models mentioned above respectively the variation in thermal conductivity and viscosity will be determined. Several parameters will be considered in order to carry out this investigation. Three nanoparticles will be added to the liquid desiccant: Copper, Aluminium oxide and Titanium oxide. Three different liquid desiccants will be utilized as base fluid namely (Lithium Bromide) LiBr, (Lithium Chloride) LiCl and (Calcium Chloride) CaCl₂. The volume fractions of these nanoparticles will be varied from 0.5% to 5%. The temperature range will be varied from 15°C to 35°C for CaCl₂ and LiCl. This is the temperature range required to carry out the dehumidification and cooling process. In case of LiBr calculations due to limitations, a custom range of 17-35°C for thermal conductivity will be utilized and 25-35°C in case of viscosity of nanofluid calculations. The concentration of CaCl₂ and LiCl in water will be varied from 30% to 40% and in case of LiBr will be varied from 40% to 53% for thermal conductivity and 45%-55% for viscosity. The temperature range and concentration range for CaCl₂ was specified in the analysis carried out by Rahamah et al. [9]. Hence for LiCl similar values for the range were assigned. Similar range of values would have been assigned for LiBr but due to limitations in the software to determine these properties the custom range specified for LiBr in the software Engineering Equation Solver (EES) was used. The range of nanoparticle volume fraction was assigned from the studies made by Murshed et al. [31]. Four models will be

used to calculate the thermal conductivity of the liquid desiccant with nanoparticles: Hamilton & Crosser model, Wasp model, Yu and Choi model, Bruggeman model. The three models suggested by Batchelor, Brinkman and Einstein models will be used to determine the viscosity of nanofluids. The thermal conductivities and viscosities were calculated by the above mentioned models according to the parameters mentioned previously. In the thermal conductivity models, one of the variables is thermal conductivity of the liquid desiccant (k_f). Also similarly, in the viscosity models there is a term (μ_f) which is the viscosity of the liquid desiccant.

Table 4.1: Thermophysical properties of liquid desiccants

Liquid Desiccants	Concentration	Thermal Conductivity (W/mK)	Specific Heat (J/kgK)	Density (kg/m³)	Viscosity (kg/ms)
Calcium chloride	30%	0.5725	2766	1283	0.004238
Lithium chloride	30%	0.5334	2962	1180	0.005334
Lithium bromide	50%	0.4481	2140	1530	0.003255

Table 4.1 illustrates the various thermophysical properties of all three liquid desiccants. These properties were calculated by using the correlations derived by Conde [39]. Conde performed a study on the various properties of lithium and calcium chloride. The other values required were obtained from the property values given by EES. For all models, Wasp model, Hamilton & Crosser model, Yu and Choi model and the Bruggeman model the spherical nanoparticle was considered. The Wasp model and Hamilton & Crosser model gave identical values of thermal conductivity. The Bruggeman model gives values that are slightly higher and the Yu & Choi model gives the highest values for thermal conductivity.

4.1 Variation of thermal conductivity of liquid desiccant with nanoparticles

Figures 4.1 and 4.2 illustrates the variation of thermal conductivity with increasing volume fraction using different thermal conductivity models at 35°C temperature and 30% concentration for CaCl₂ and LiCl liquid desiccant respectively using different kinds of nanoparticles. In the case when copper nanoparticles with CaCl₂ are considered the Yu and Choi model results in the highest increase in thermal conductivity approximately 19% with Wasp model showing an increase of about 14% as the volume fraction is varied from 0.5% to 5%. The Bruggeman model indicates an increase of about 17%; it gives results that is almost the average of the other two models.

When Al₂O₃ nanoparticle is used with CaCl₂ liquid desiccant in case of Yu and Choi model the thermal conductivity shows an increase of approximately 18%. For the other two models the increase is similar but slightly lower than (about 1%) when copper nanoparticles are used. With TiO₂ nanoparticles and CaCl₂ liquid desiccant the results indicate an increase in thermal conductivity approximately 3% lower than when copper nanoparticles are used for all models. The results for variation in thermal conductivity in the cases when LiCl is used, is similar to the variation observed with CaCl₂ for all models and all nanoparticles. But the thermal conductivity values of LiCl are approximately 4% lower than values of CaCl₂.

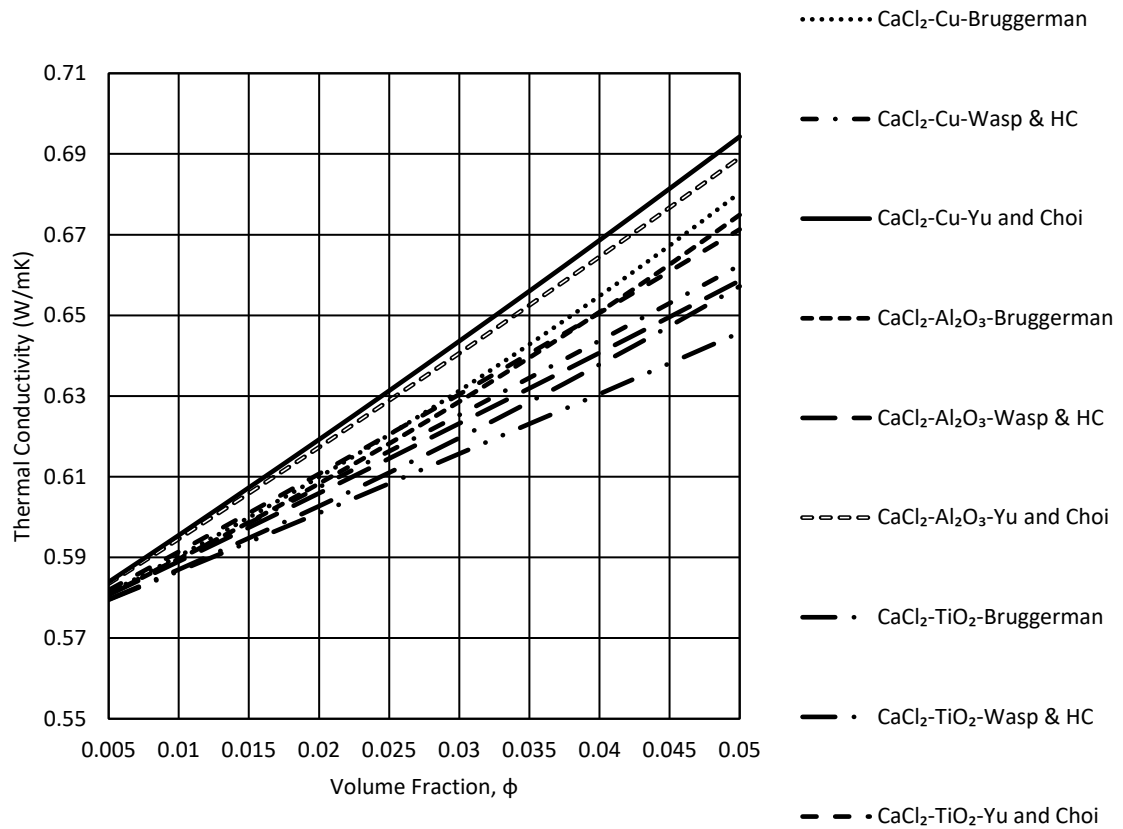


Figure 4.1: Variation of thermal conductivity of CaCl₂ liquid desiccant with increasing volume fraction of nanoparticles using different thermal conductivity models at 35°C and 30% concentration

This is because the base fluid LiCl has lower thermal conductivity. From the above mentioned results it is clear that different models indicate different increases in thermal conductivity. Also the utilization of different nanoparticles have a significant impact on the values of thermal conductivity. The results indicate that if the nanoparticle thermal conductivity is higher it will give higher values for the nanofluid.

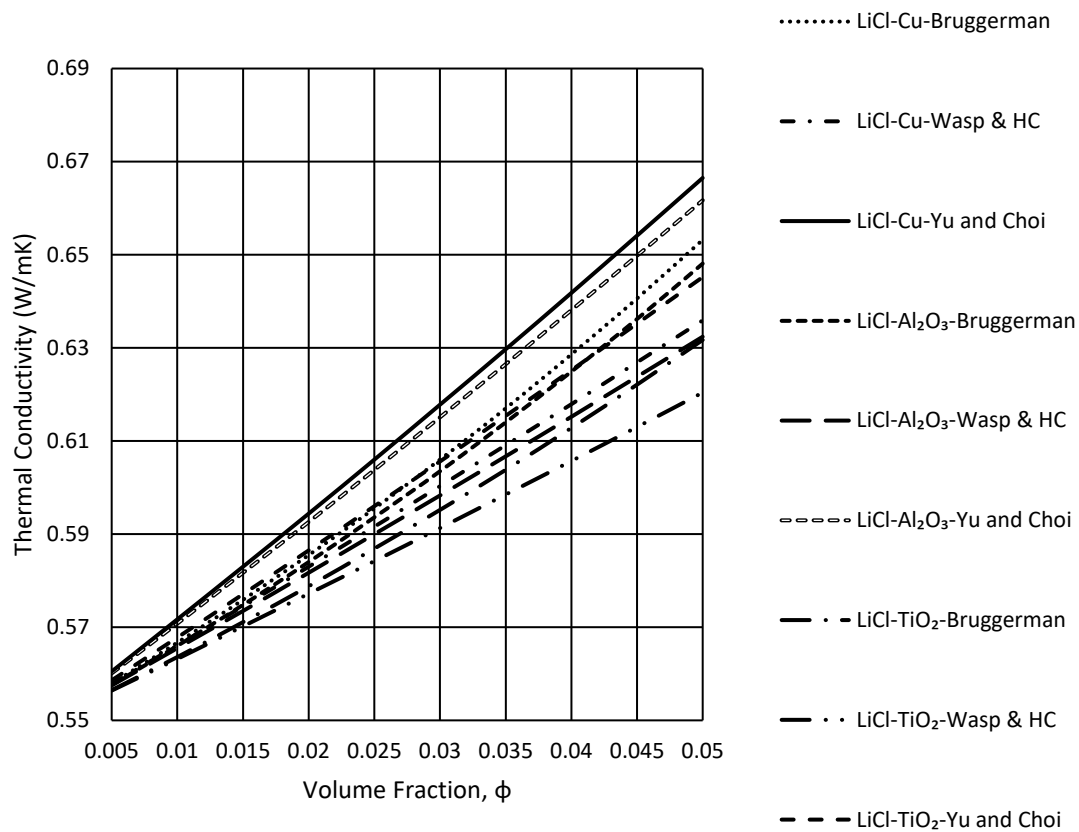


Figure 4.2: Variation of thermal conductivity of LiCl liquid desiccant with increasing volume fraction of nanoparticles using different thermal conductivity models at 35°C and 30% concentration

Figures 4.3 and 4.4 illustrates the variation of thermal conductivity using different models as the concentration of CaCl₂ and LiCl solution i.e. liquid desiccant was increased from 30% to 40%. The comparison was made at 25°C temperature and 5% volume fraction of nanoparticles.

The results indicated that for all models with different nanoparticles indicated the same decrease in thermal conductivity approximately 2.8% for CaCl₂ and 2.1% for LiCl respectively as the concentration of liquid desiccant was increased from 30% to 40%. The conclusion reached was that in this scenario increasing the concentration affects all the

solution in the same manner i.e. as the concentration is varied the other factors do not have any impact on the value of thermal conductivity.

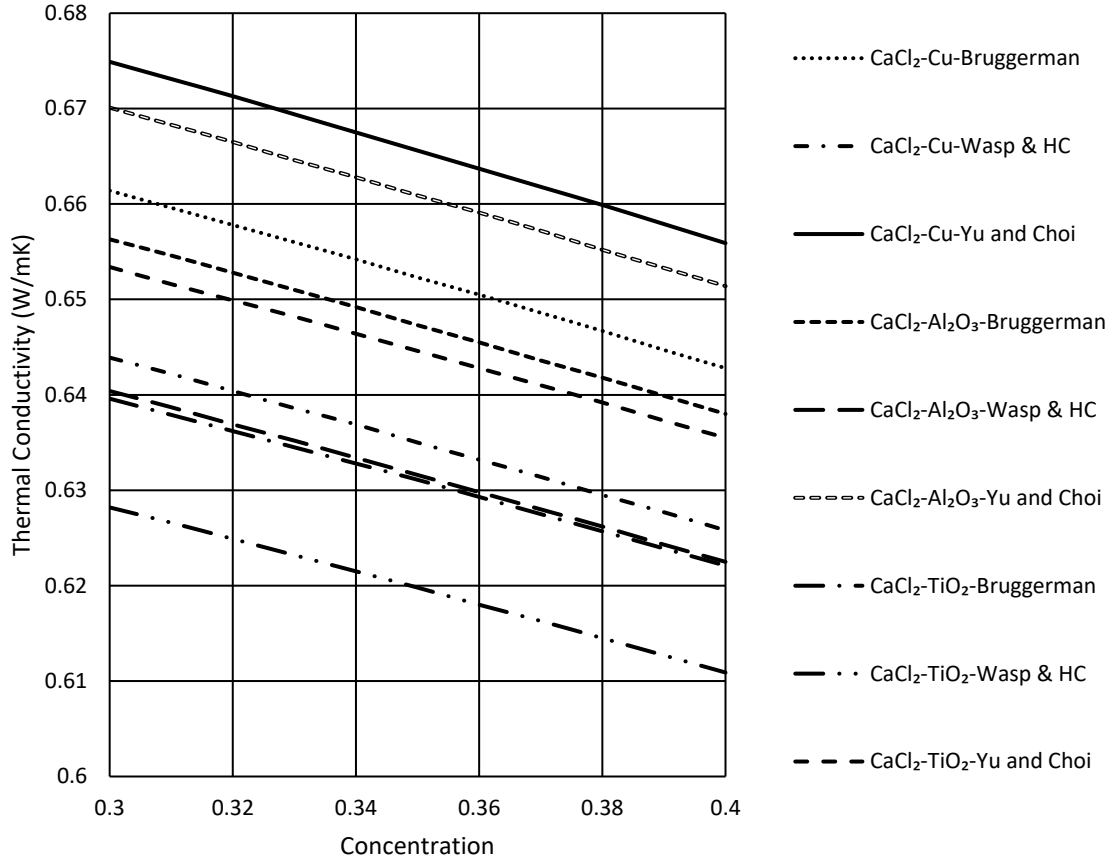


Figure 4.3: Variation of thermal conductivity of CaCl₂ with increasing concentration using different thermal conductivity models at 25°C and 5% volume fraction of nanoparticles

The reason for decrease in thermal conductivity is that CaCl₂ and LiCl concentration in water increases. This increase results in lower thermal conductivity of the solution as the water component has higher thermal conductivity than CaCl₂ and LiCl.

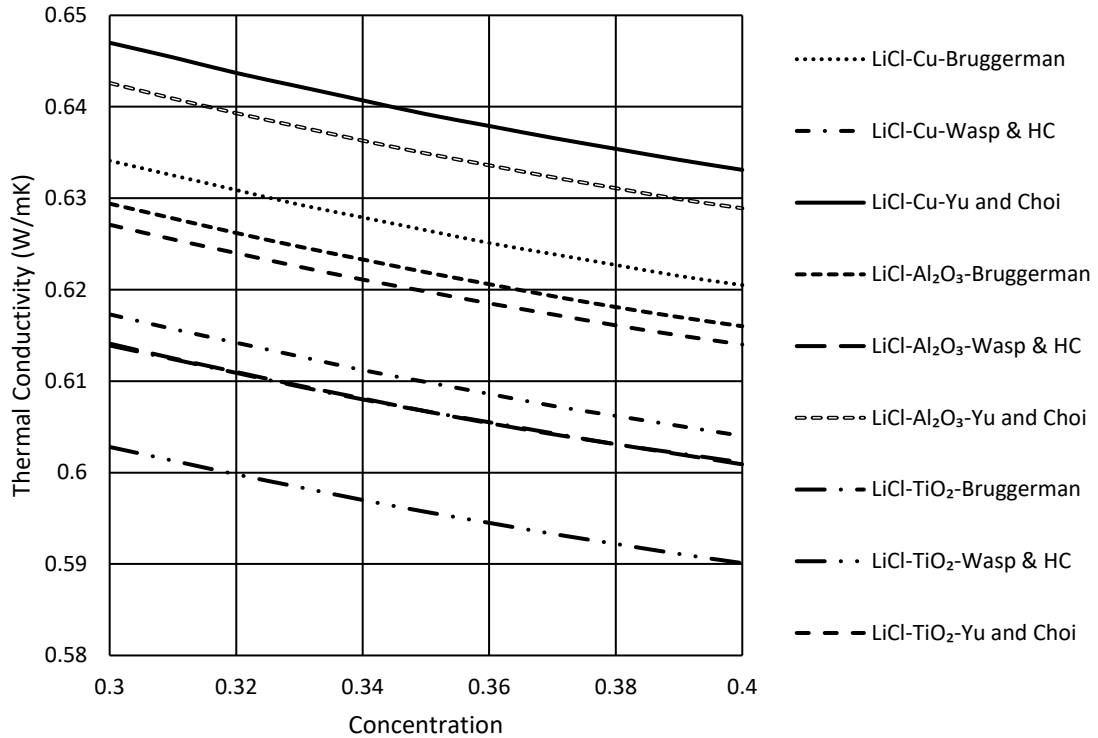


Figure 4.4: Variation of thermal conductivity of LiCl with increasing concentration using different thermal conductivity models at 25°C and 5% volume fraction of nanoparticles

Figure 4.5 and 4.6 illustrates the variation of thermal conductivity of CaCl₂ and LiCl respectively using different models as the temperature of liquid desiccant was increased from 15°C to 35°C. The comparison was made at 30% concentration and 5% volume fraction of nanoparticles. The results for CaCl₂ liquid desiccant indicate for all models with copper nanoparticle show an increase in thermal conductivity by approximately 6.3% as temperature increases from 15°C to 35°C. Utilizing Al₂O₃ and TiO₂ nanoparticles show an increase of approximately 6.2% and 6.1% respectively. Utilization of LiCl liquid desiccant also results in a similar increase in thermal conductivity of approximately 6.2-6.5 % for all models and nanoparticles. Hence, the increase in values due to increasing temperature is approximately similar for all three nanoparticles.

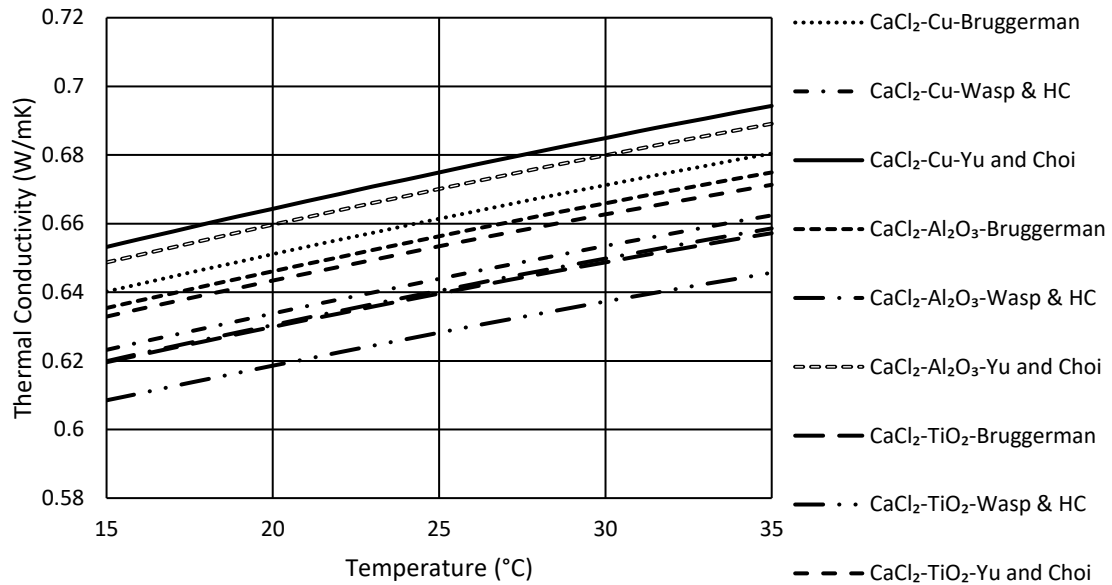


Figure 4.5: Variation of thermal conductivity of CaCl₂ with increasing temperature using different thermal conductivity models at 30% concentration and 5% volume fraction of nanoparticles

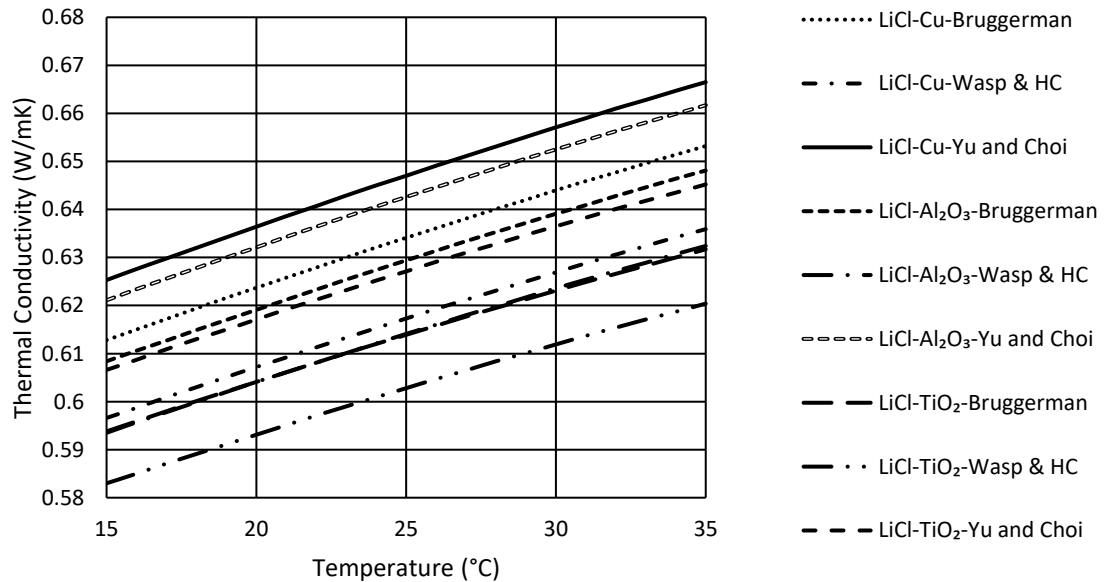


Figure 4.6: Variation of thermal conductivity of LiCl with increasing temperature using different thermal conductivity models at 30% concentration and 5% volume fraction of nanoparticles

The slight variation is due to the type of nanoparticle but its impact in this scenario is very minor. Thermal conductivity is function of temperature and as the temperature is increased the thermal conductivity increases as illustrated by the results. As liquid desiccant solution concentration remains the same, hence the range of increase is also similar. The results also indicated that Yu and Choi model gives the highest values with the Wasp/ Hamilton & Crosser model giving the lowest values and the Bruggeman model giving average values of the two.

Similarly, the variation of thermal conductivity for LiBr by varying the volume fraction, concentration and temperature are also obtained but are illustrated in separate figures due to the difference in range of concentration and temperature. Figure 4.7 illustrates the variation of thermal conductivity with increasing volume fraction from 0.5% to 5% using different thermal conductivity models at 35°C temperature and 30% concentration for LiBr liquid desiccant using different kinds of nanoparticles. The results for variation in thermal conductivity in the cases when LiBr is used, is similar to the variation observed with CaCl₂ and LiBr for all models and all nanoparticles. However, the thermal conductivity values obtained by utilizing LiBr are much lower than both CaCl₂ and LiCl liquid desiccants. In some comparisons made from the results obtained it was found to be approximately 8-12% lower than the values obtained for CaCl₂.

Figure 4.8 illustrates the variation of thermal conductivity using different models as the concentration of LiBr solution i.e. liquid desiccant was increased from 40% to 53%.

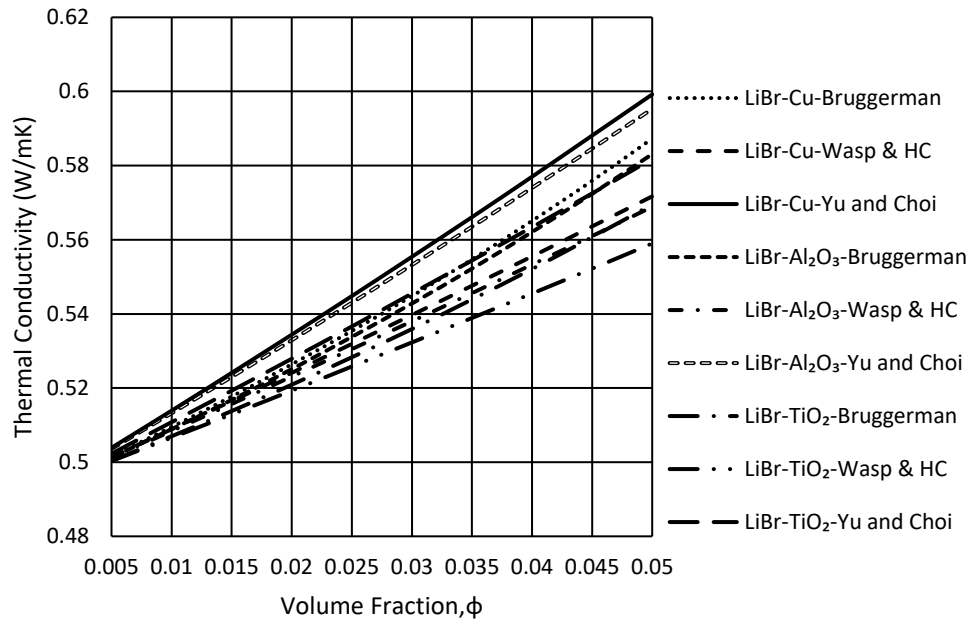


Figure 4.7: Variation of thermal conductivity of LiBr liquid desiccant with increasing volume fraction of nanoparticles using different thermal conductivity models at 35°C and 40% concentration

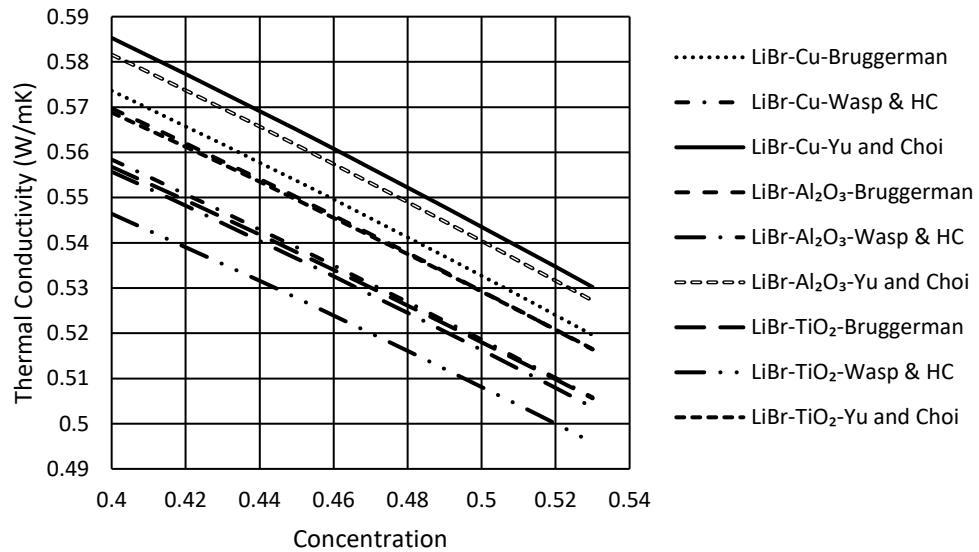


Figure 4.8: Variation of thermal conductivity of LiBr with increasing concentration using different thermal conductivity models at 25°C and 5% volume fraction of nanoparticles

The comparison was made at 25°C temperature and 5% volume fraction of nanoparticles. For all models an approximate decrease of 9.2-9.4% was observed as the concentration was increased. Hence, increasing concentration caused a very significant decrease in LiBr liquid desiccant.

An approximate increase of 4.3-4.6% is observed in LiBr desiccant at 5% volume fraction of nanoparticles, as the temperature is increased from 17-35°C for all cases in Figure 4.9.

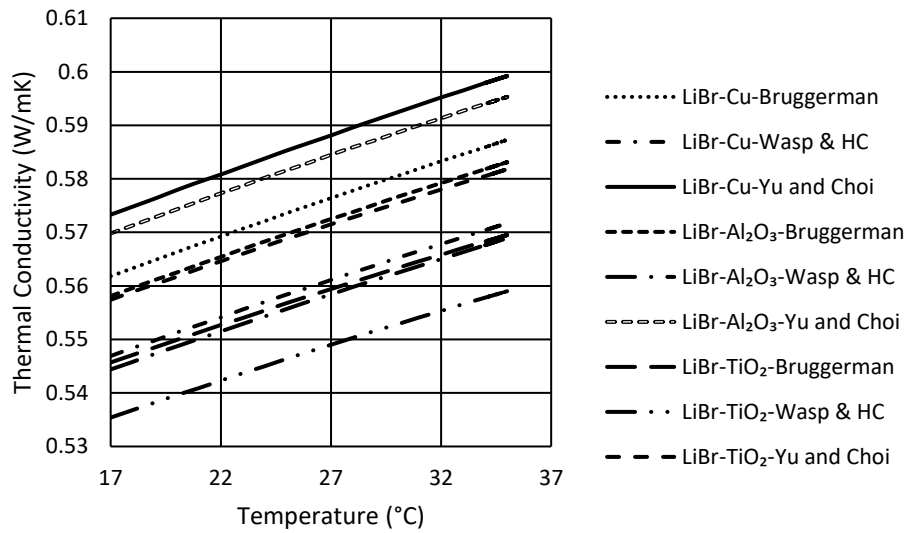


Figure 4.9: Variation of thermal conductivity of LiBr with increasing temperature using different thermal conductivity models at 40% concentration and 5% volume fraction of nanoparticles

4.2 Variation of viscosity of liquid desiccant with nanoparticles

The variation in viscosity of liquid desiccant due to the increase in volume fraction of nanoparticles from 0.5% to 5% is investigated at temperature of 30°C. The results suggested that for all models the viscosity of the nanofluid is independent of the type of

nanoparticle used. Figure 4.10 shows the variation in viscosity in LiCl, LiBr and CaCl₂ liquid desiccants.

Three model equations are used to determine the variation in viscosity: Batchelor [38], Brinkman [37] and Einstein [36]. For all three desiccants, it can be observed that the Batchelor model provides the highest value and the Einstein model provides the lowest value with the Brinkman model providing values closer to the Batchelor model.

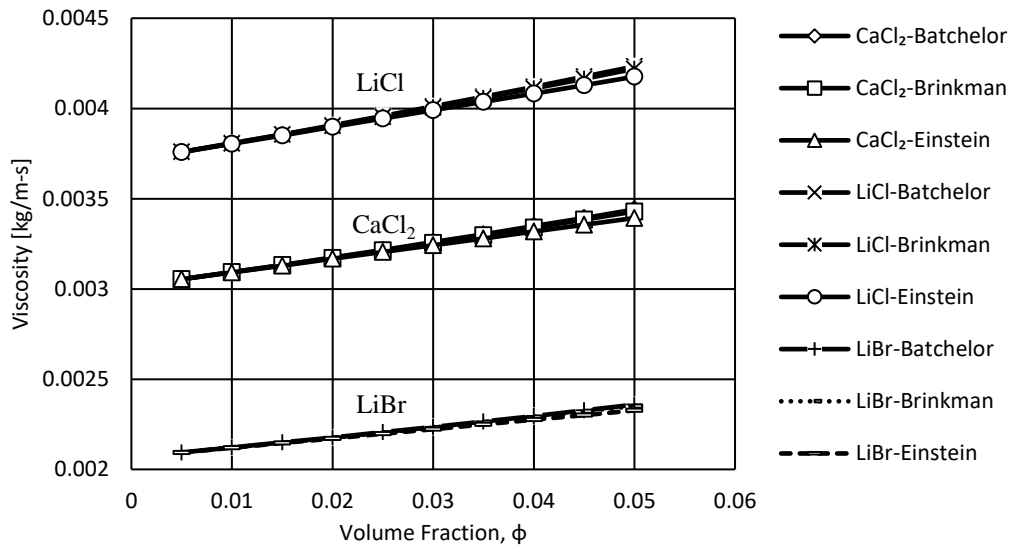


Figure 4.10: Variation of viscosity of LiCl, LiBr and CaCl₂ liquid desiccant with increasing volume fraction of nanoparticles using different viscosity models at 35°C and 30% concentration and 45% concentration for LiBr

Figure 4.10 also illustrates that LiCl results in the highest values of viscosity and LiBr results in the lowest values of viscosity with CaCl₂ also providing low values of viscosity but higher than LiBr. In case of all three liquid desiccants by increasing the volume fraction of nanoparticles an approximate increase of 11-12% is observed.

Figures 4.11 and 4.12 illustrate the variation of viscosity for all three liquid desiccants due to increasing the concentration. In Figure 4.11 it can be seen that for all models increasing the concentration results in a massive increase in viscosity, for CaCl_2 it is almost 224% increase and for LiCl it shows an approximate increase of 212%. In Figure 4.12 LiBr shows a comparatively lower increase in viscosity of approximately 85%. From these results it can be concluded that liquid desiccant at low concentration is ideal for heat transfer as high viscosity can adversely affect heat transfer characteristics of the liquid desiccant.

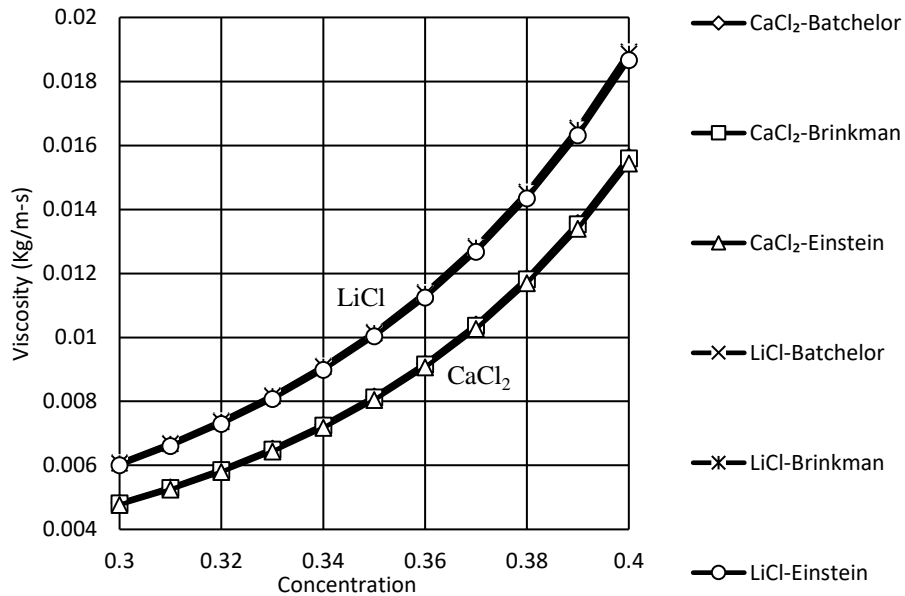


Figure 4.11: Variation of viscosity of CaCl_2 and LiCl with increasing concentration using different viscosity models at 25°C and 5% volume fraction of nanoparticles

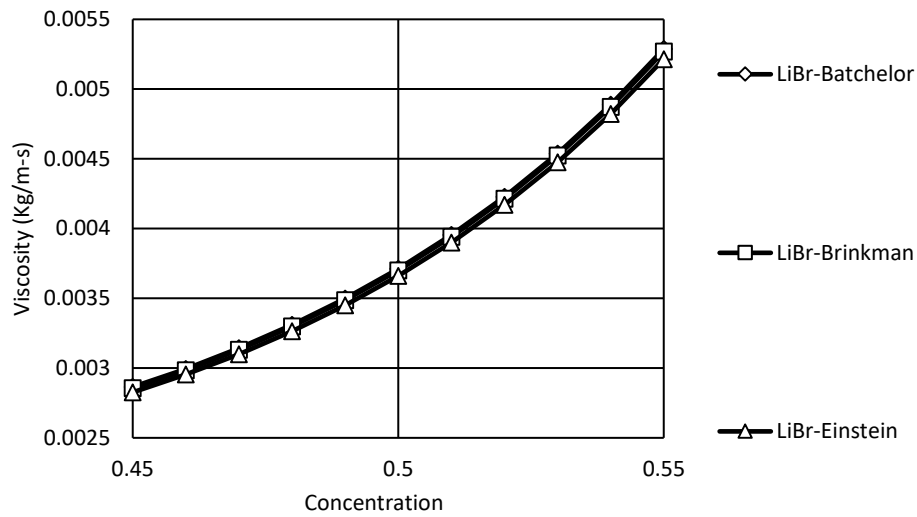


Figure 4.12: Variation of viscosity of LiBr with increasing concentration using different viscosity models at 25°C and 5% volume fraction of nanoparticles

Figures 4.13 and 4.14 show the effect of temperature on viscosity of liquid desiccant. Increasing temperature results in decrease of viscosity of liquid desiccant. For LiCl increasing temperature results in a 55% decrease approximately and for CaCl₂ results in 53% decrease. In case of LiBr the decrease is less significant approximately 18% although the temperature range is also shorter. Hence, high temperature is preferred in order to improve the heat transfer characteristics as both thermal conductivity increases and viscosity decreases at high temperature.

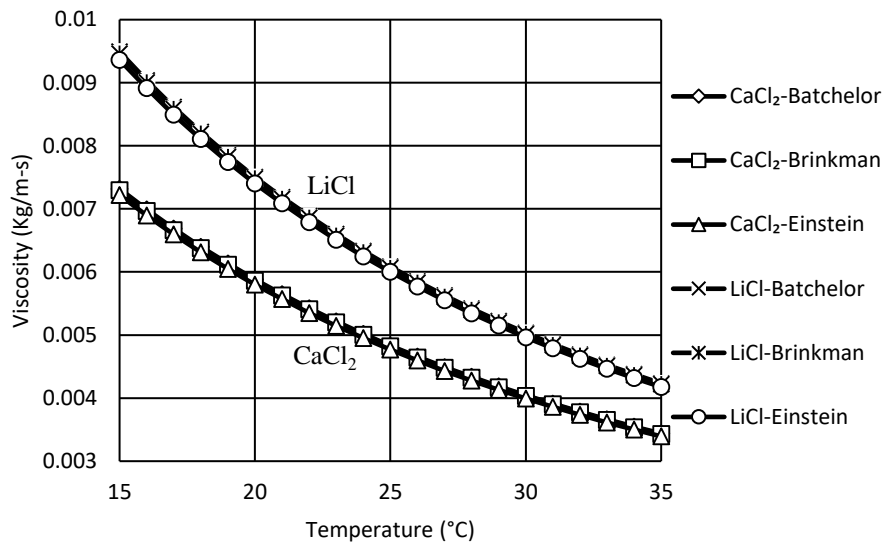


Figure 4.13: Variation of viscosity of CaCl₂ and LiCl with increasing temperature using different viscosity models at 30% concentration and 5% volume fraction of nanoparticles

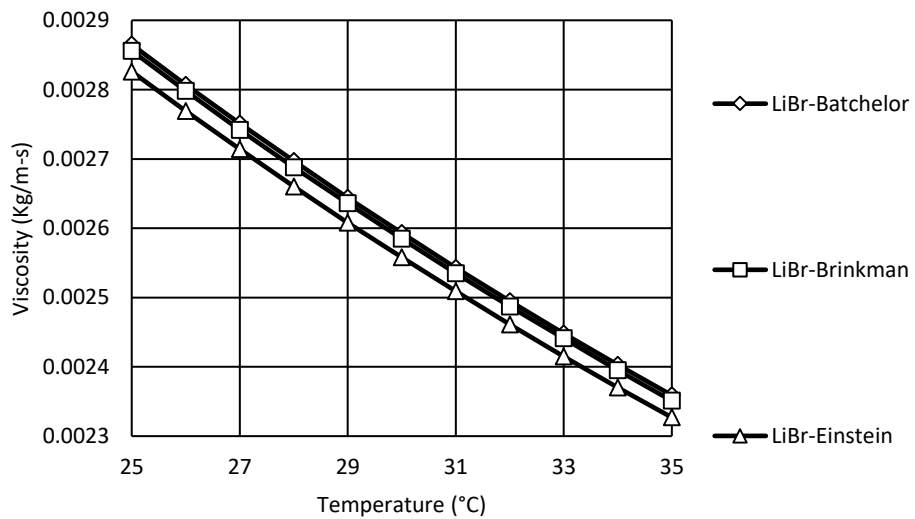


Figure 4.14: Variation of viscosity of LiBr with increasing temperature using different viscosity models at 45% concentration and 5% volume fraction of nanoparticles

CHAPTER 5

NUMERICAL ANALYSIS OF FALLING FILM DEHUMIDIFIER WITH NANOPARTICLES

The equations of momentum and mass for air and desiccant are solved analytically to determine the pressure drop, film thickness and the air and desiccant velocity profiles. By applying appropriate boundary conditions to the energy, concentration and diffusion equations, the energy balance and mass balance at the interface are obtained. Numerical analysis is then carried out for the falling film dehumidifier for counter flow and parallel flow configurations.

By using finite volume method the governing energy, concentration and diffusion equations are solved to obtain the humidity ratio, temperature, and concentration distributions respectively. The control volume approach is used to discretize the governing equations and the finite volume equations are obtained. The average Sherwood number and average Nusselt number at the interface illustrate the mass and heat transfer characteristics of the falling film dehumidifier.

It is essential to obtain the thermophysical properties of liquid desiccant and air to execute the numerical analysis. These properties for air and base fluid are obtained from the thermodynamic database available in EES. In order to get the properties of nanofluids the equations mentioned in the study previously are used. The nanofluid thermal conductivity was determined by the Yu and Choi model and the nanofluid viscosity was derived from Batchelor model. It is essential to define the inlet conditions for the air and liquid desiccant

such as mass flow rate of desiccant, concentration of desiccant, humidity ratio, air temperature, desiccant temperature and Reynolds number of air.

Three different liquid desiccants will be investigated in this study: calcium chloride, lithium chloride and lithium bromide. To each of these desiccants three different nanoparticles copper, aluminum oxide and titanium oxide will be added and the nanoparticle volume fraction will be changed from 1% to 5%.

5.1 Validation of the results for parallel flow channel

The initial research was performed to validate the process used in this research. Parallel flow channel with calcium chloride liquid desiccant was investigated by Rahamah et al. [9].

Taking the nominal values of the various parameters mentioned above numerical simulation was carried out for parallel flow dehumidifier with calcium chloride liquid desiccant without nanoparticles to validate the result accuracy. Rahamah et al. [9] results were plotted and compared with the results of this analysis. The desiccant temperature at the inlet was specified 25°C and the air temperature at the inlet was specified at 35°C.

CaCl₂ liquid desiccant was considered at 40% concentration and the inlet humidity ratio was 0.02 kg_w/kg_{da}.

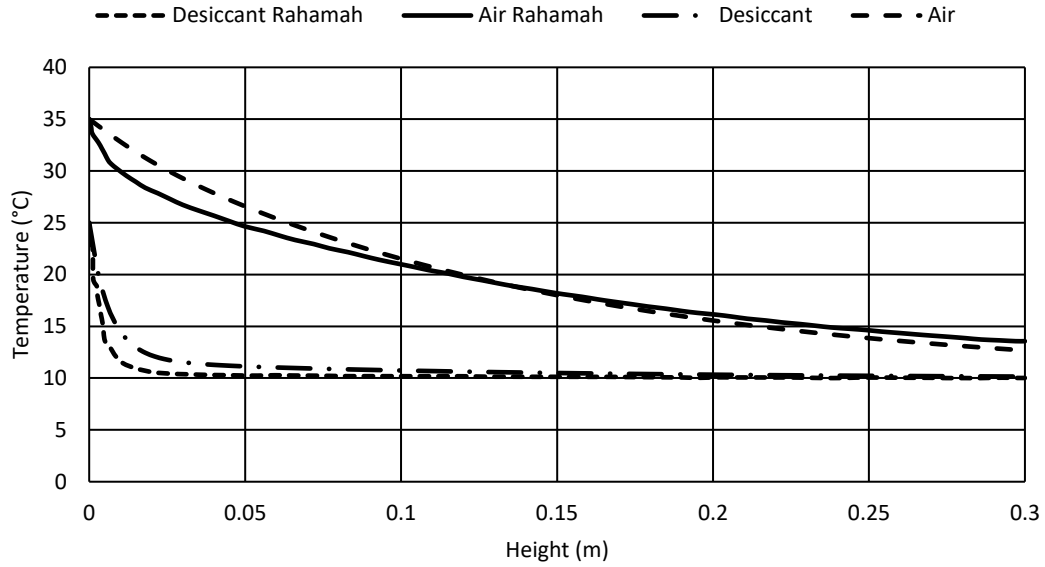


Figure 5.1: Temperature distribution of liquid desiccant and air along the wall height at $T_d=25^\circ\text{C}$, $T_a=35^\circ\text{C}$ and $Z=40\%$

The three different parameters that were compared was the temperature distribution, water concentration and humidity ratio distribution in liquid desiccant. Figure 5.1 illustrates the temperature distribution of liquid desiccant and air along wall height. Temperature results indicated at each point along the x-axis is the velocity weighted average of the temperature values across the thickness of the air flow. Air temperature decreases from 35°C to approximately 13°C and the desiccant temperature decreases from 25°C to approximately 10°C . The figure illustrates that distribution of temperature obtained in this study agrees with the results obtained by Rahamah et al. [9].

There is slight variation in the two distributions and the difference can be explained by a few reasons. This study considers the heat transfer by conduction in the axial direction of flow which is ignored by the study in the literature. Upon further investigation neglecting

the heat transfer by conduction in the axial direction for this validation, it was observed that the difference between the temperature distribution patterns remained the same approximately albeit with slightly lower temperature values. Hence, the conclusion was drawn that the difference in temperature distributions were not due to considering the axial affects as neglecting it did not have a significant effect on the temperature distribution pattern. Several other reasons were considered due to which the variation could have occurred such as the properties of the fluid utilized in our study, the software that was used to run the simulation for the parallel flow channel, and also the methodology to determine the average temperature of the air and liquid desiccant channels. Another reason is that at the interface the convection and diffusion terms calculated in this study were the average of air and desiccant flows.

Figure 5.2 illustrates the decrease in the humidity ratio across the height of the channel from 0.02 kg_w/kg_{da} to approximately 0.005 kg_w/kg_{da} for both the studies.

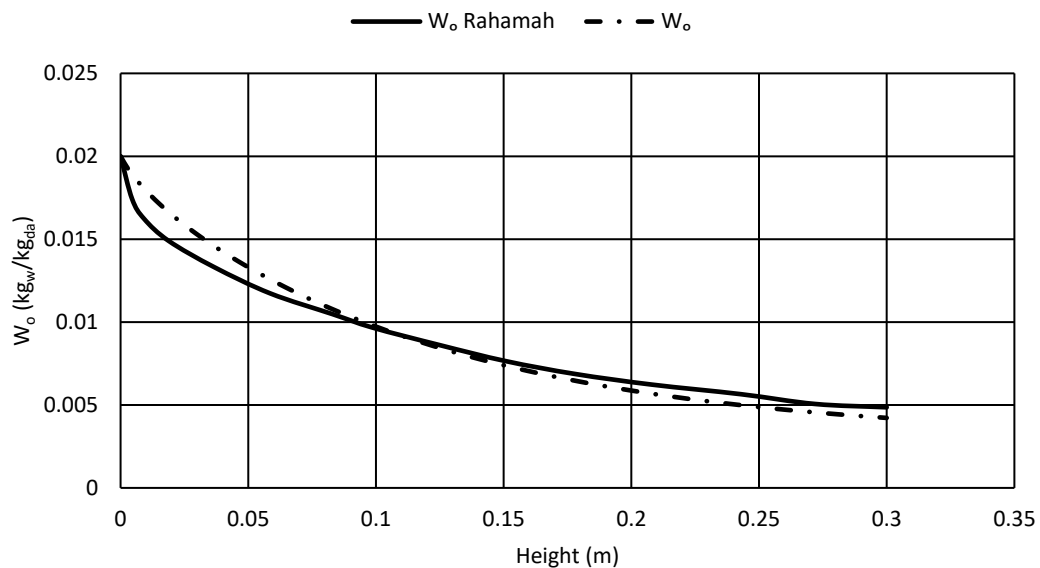


Figure 5.2: Humidity ratio of air along the wall height at $T_d=25^{\circ}\text{C}$, $T_a=35^{\circ}\text{C}$ and $Z=40\%$

From the above results it can be observed that hot air coming in contact with the liquid desiccant is dehumidified and cooled and due to dehumidification of air, water concentration in the liquid desiccant increases. Figure 5.3 illustrates liquid desiccant dilution, which shows that the water concentration increases from 0.6 to 0.613 for both the studies.

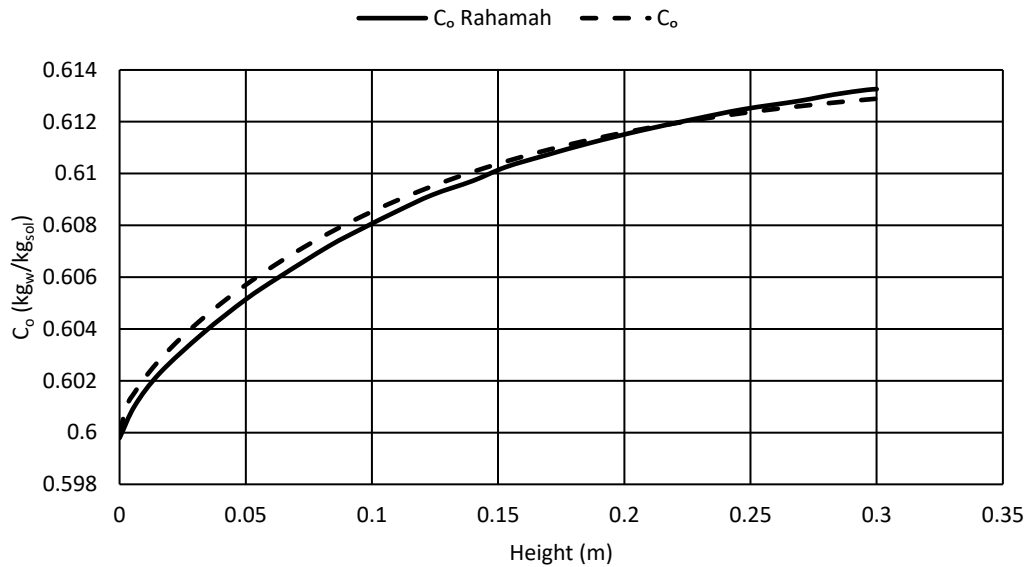


Figure 5.3: Concentration of water in desiccant solution along the wall height at $T_a=25^\circ\text{C}$, $T_a=35^\circ\text{C}$ and $Z=40\%$

In this analysis the grid utilized was divided into 40 cells in the transverse direction and into 100 cells in the axial direction. A grid independence test was carried out to investigate the effect of the grid size on the average Nusselt number and outlet temperature. The size of the grid was halved to 20 cells in the transverse direction and the Nusselt number increased by 2% and outlet temperature increased by 1.9%. Consequently the size of the grid was doubled to 80 cells in the transverse direction and the Nusselt number decreased by 0.95% and outlet temperature decreased by 0.9%. Hence, it can be concluded that

increasing the grid size results in more better and accurate results. Although as the grid size is increased more the variation is insignificant and hence, grid size of 40 cells in transverse direction is used for this analysis.

5.2 Effect of varying various parameters on outlet conditions and heat and mass transfer characteristics

An essential part of this research is to examine the effect of varying the various pertinent inlet conditions as well as other parameters, and study their impact on the cooling and dehumidification as well as the mass and heat transfer characteristics. Cooling of air is indicated by outlet temperature. Similarly, air dehumidification can be indicated by the exit humidity ratio. The mass and heat transfer characteristics are analyzed from the average Sherwood number and Nusselt number at the interface.

For this study only parallel flow dehumidifier is investigated. The liquid desiccant selected for this parametric analysis is calcium chloride and the nanoparticle selected is copper. The different parameters that will be varied include the channel height, Air Reynolds number, mass flow rate and concentration of desiccant, humidity ratio, air and desiccant temperature and volume fraction of nanoparticles. Nominal values have been selected for these various parameters and the results are illustrated in terms of percentage change to give a better comprehension of the effect of these parameters.

Table 5.1: Design and operating parameters: Basic value and the range of variation of each parameter for air dehumidification

Parameters	Units	Basic Value	Range
Desiccant Concentration, C_d	kg _{salt} /kg _{sol}	0.3	0.3-0.4
Channel Height, H	m	0.3	0.3-0.7
Mass flow rate, \dot{m}_d	kg/m s	0.007	0.004-0.01
Volume fraction, ϕ		0.05	0-0.05
Air Reynolds number, Re_a		1350	950-2150
Air temperature, T_a	°C	35	25-40
Desiccant Temperature, T_d	°C	25	20-30
Inlet Humidity ratio, W_i	kg _w /kg _{da}	0.02	0.015-0.025

Table 5.1 illustrates the basic values of all the input parameters and the range of these parameters. These were obtained from the studies carried out by Rahamah et al. [9]. The parameters varied will be represented on the x-axis and on the y-axis, the percentage change of the outlet temperature, outlet humidity ratio, average Nusselt number and average Sherwood number will be illustrated. The percentage change will be measured with respect to the values obtained at the nominal value.

5.2.1 Effect of varying air Reynolds number

The first parameter that was varied was Reynolds number of air from 950 to 2150 and the results are illustrated in Figure 5.4. The figure indicates that there is a significant effect on mass and heat transfer characteristics and exit conditions due to the Reynolds number. The increase in Reynolds number from 950 to 2150 leads to the increase in mass and heat transfer characteristics. Hence, Sherwood number and Nusselt number also increase with increase in Sherwood number approximately 64% and increase in Nusselt number approximately 62%. In addition, the exit temperature and exit humidity ratio increases by approximately 38% and 46% respectively. At high Reynolds number of air there is less

interaction time between air and desiccant solution and hence there is a decrease in mass and heat transfer in falling film dehumidifier leading to higher air temperature and higher humidity ratio. The conclusion reached is that at low Reynolds number better cooling and dehumidification is achieved but the rate of mass and heat transfer is also lower.

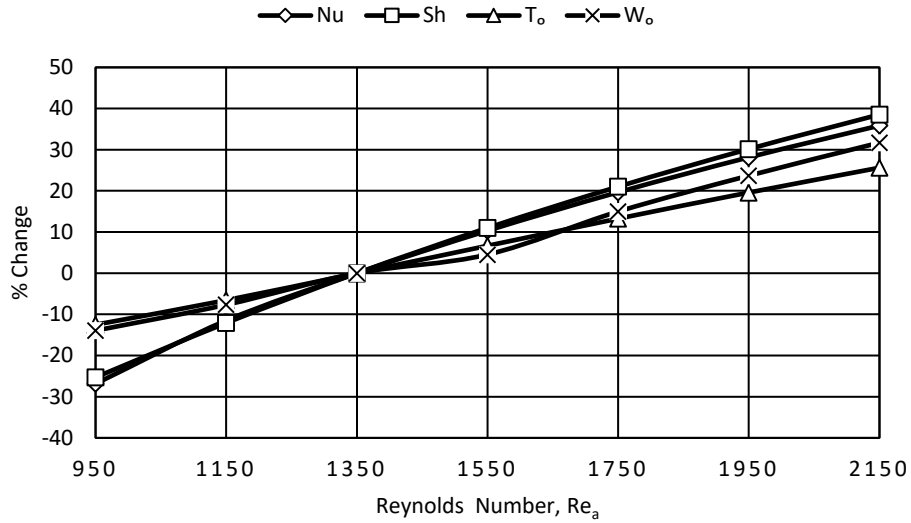


Figure 5.4: Effect of varying Reynolds number of air

5.2.2 Effect of varying desiccant mass flow rate

The desiccant mass flow rate is increased from 0.004 kg/s to 0.01 kg/s and the effects are shown in Figure 5.5. Nusselt number increases by approximately 1.5% signifying the heat transfer rate increment. The outlet temperature decreases by approximately 0.3%. Hence, higher mass flow rates leads to improved rate of heat transfer and cooling. There is also an increase in average Sherwood number by approximately 0.5% and a decrease in outlet humidity ratio by approximately 1%. Hence, better dehumidification of air occurs at a higher rate as the mass flow rate increases.

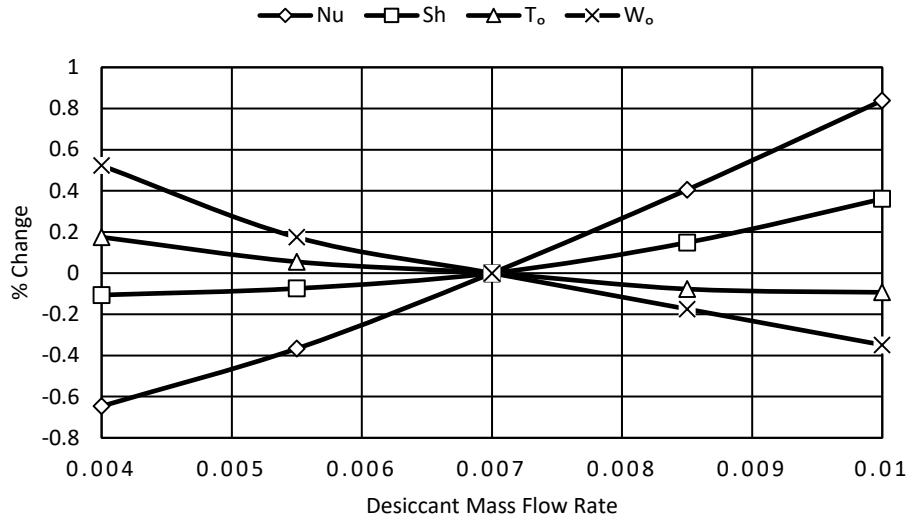


Figure 5.5: Effect of varying mass flow rate of desiccant

5.2.3 Effect of varying height of the channel

The channel height is varied from 0.3 meters to 0.7 meters and the impact on the outlet conditions and the mass and heat transfer characteristics are shown in Figure 5.6. The humidity ratio and temperature decreases by approximately 20%. The average Nusselt number and average Sherwood number decreases by 80% approximately as the channel height increases. The decrease in Nusselt number and Sherwood number is based on equations (3.41) and (3.42), which defines that both Nusselt number and Sherwood number are inversely proportional to the height of the channel and the increase in channel height leads to the decrease in these numbers. Hence, it can be concluded that although increasing channel height leads to better dehumidification and cooling, mass and heat transfer rate is significantly decreased. At lower values of channel height, the decrease in outlet conditions is more significant.

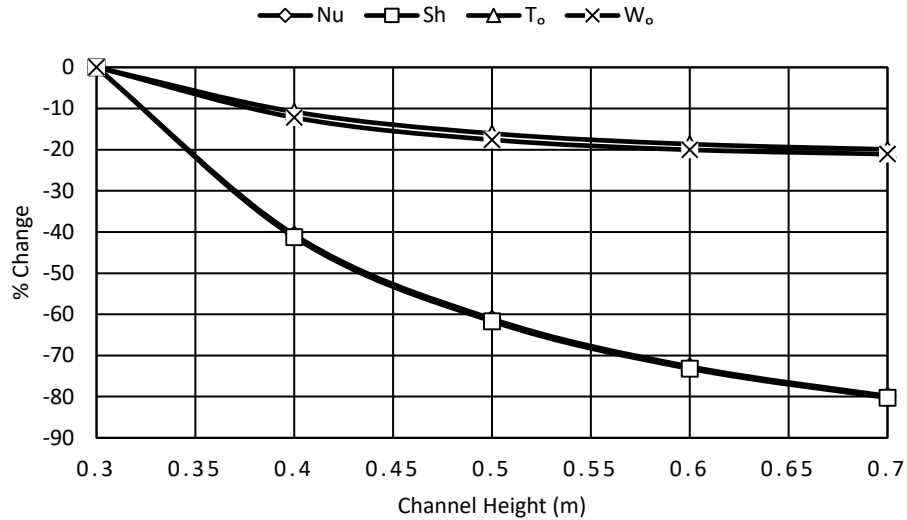


Figure 5.6: Effect of varying height of the channel

5.2.4 Effect of varying desiccant concentration

Figure 5.7 illustrates the variation due to changing the concentration of the salt in the desiccant solution from 30% to 40%. The Sherwood number and Nusselt number decreases as the concentration increases by approximately 3.5% and 2% respectively implying the rate of heat and mass transfer decreases. The outlet temperature decreases by approximately 1% so cooling is improved due to increasing salt concentration. There is a significant decrease in outlet humidity ratio approximately 13% hence dehumidification is significantly improved. The higher the concentration of the salt the better is the dehumidification process but increasing the salt concentration increases the chance of crystallization. Hence, higher values of salt concentration cannot be used for dehumidification of air with the highest value being limited by the crystallization point of the salt.

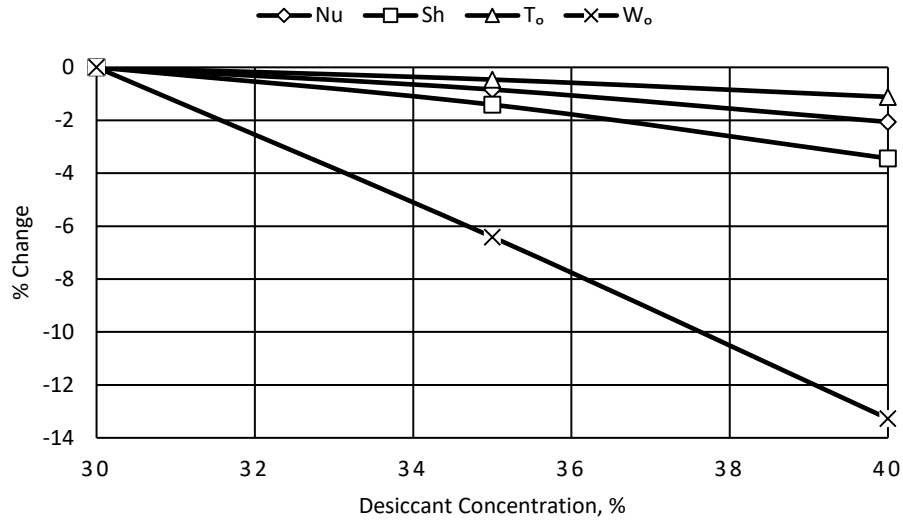


Figure 5.7: Effect of varying desiccant concentration

5.2.5 Effect of varying desiccant temperature

Figure 5.8 illustrates the effect of varying the liquid desiccant temperature from 20°C to 30°C. Increasing desiccant temperature increases the outlet temperature and humidity ratio by 0.4% and 0.5% respectively. As desiccant temperature increases lower dehumidification and cooling occurs, although decrease is less significant. The Sherwood number and Nusselt number increases by approximately 2%. The rate of mass and heat transfer is improved at higher desiccant temperatures. Hence, slightly higher temperature of desiccant is preferred for the falling film dehumidifier.

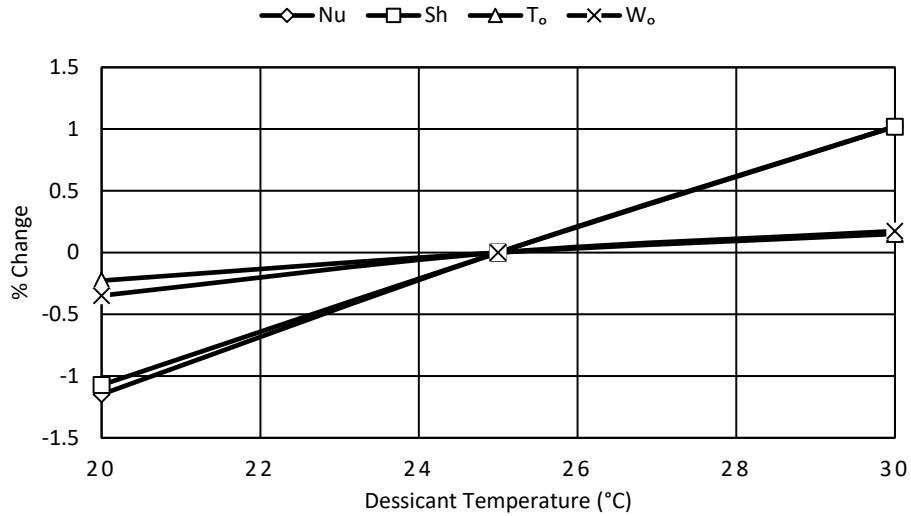


Figure 5.8: Effect of varying desiccant temperature

5.2.6 Effect of varying temperature of air

Air temperature is varied from 25°C to 40°C and its effects are illustrated in Figure 5.9. Varying the temperature of air has an inconsequential effect on the mass transfer rate and humidity ratio. There is a slight increase in average Sherwood number approximately 0.6% and a slight humidity ratio increase approximately 0.3%. Hence, although lower dehumidification occurs the rate increases.

Increasing the temperature of air results in decrease in Nusselt number of approximately 3%. Outlet temperature increases by approximately 12%. Therefore, at higher temperatures although heat transfer rate decreases and the outlet temperature is higher but the cooling of air with respect to temperature difference is higher. This can be illustrated by the fact that air at 40°C is cooled to 13°C indicating a temperature difference of 27° C compared to air at 25°C which is cooled to 11.6° C indicating a much lower temperature difference of 13.4°C.

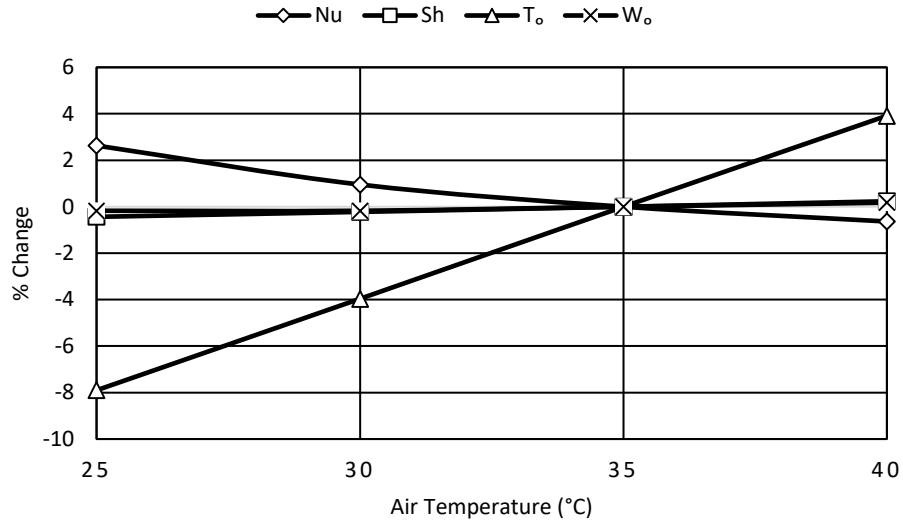


Figure 5.9: Effect of varying air temperature

5.2.7 Effect of varying nanoparticles volume fraction

The effect of varying nanoparticles volume fraction is illustrated in Figure 5.10. The nanoparticles volume fraction is increased from 0% to 5%. In this scenario, the liquid desiccant is calcium chloride with copper nanoparticles for parallel flow channel. The temperature at the outlet decreases by approximately 0.5% and humidity ratio decreases by 0.2%. Hence, better cooling and dehumidification occurs in this case.

However, the rate of mass and heat transfer decreases. The average Nusselt number decreases by approximately 0.9% and the average Sherwood number decreases by approximately 0.25%. Hence although rate of heat transfer decreases, there is an improvement in the cooling of air. This is because the Nusselt number does not include the latent heat transfer due to the change of phase from water vapor in humid air to water in desiccant solution. Nusselt number deals with only the sensible heat transfer. Hence, the addition of nanoparticles improves the dehumidification process resulting in higher number

of water vapor molecules changing phase to liquid water and the heat transfer involved with higher latent heat of condensation results in improving the cooling process of air.

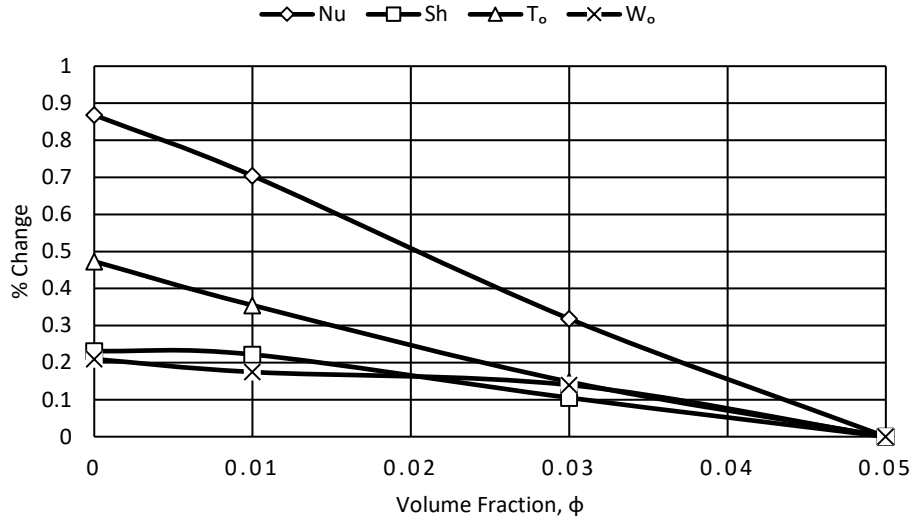


Figure 5.10: Effect of varying volume fraction of nanoparticles

5.2.8 Effect of varying humidity ratio of air

The humidity ratio of air is varied from 0.015 kg_w/kg_{da} to 0.025 kg_w/kg_{da} and its effects are illustrated in Figure 5.11. Varying the humidity ratio of air has a negligible effect on the heat transfer rate and air temperature. There is a slight increment in average Nusselt number and air temperature approximately 0.7% as the humidity ratio is increased. Hence, although less cooling occurs the rate increases.

Increasing the humidity ratio of air results in decrease in Sherwood number of approximately 2% and an increase in outlet humidity ratio of approximately 14%. Therefore, at higher inlet humidity ratio although the rate of mass transfer decreases and the outlet humidity ratio is higher but the dehumidification of air with respect to difference

in humidity ratio is higher. This can be illustrated by the fact that air at 0.025 humidity ratio is dehumidified to 0.00613 kg_w/kg_{da} indicating a difference of 0.01887 kg_w/kg_{da} compared to air at 0.015 humidity ratio which is dehumidified to 0.00535 kg_w/kg_{da} indicating a much lower difference of 0.00965 kg_w/kg_{da}.

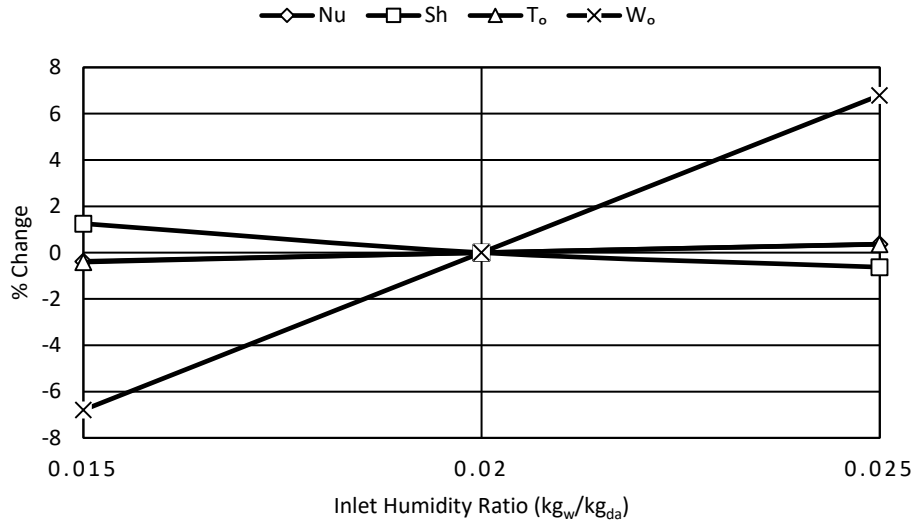


Figure 5.11: Effect of varying the humidity ratio of air

5.3 Sensitivity Analysis

Sensitivity analysis is done in order to analyze which of the varying inlet parameters has the most significant effect on the humidity ratio, air temperature and mass and heat transfer characteristics.

There are four outputs that have been primarily investigated in this study which are the outlet air temperature, outlet air humidity ratio, average Nusselt number at the interface and average Sherwood number at the interface. On each of these four output parameters the sensitivity analysis was carried out individually to study the impact of eight different input parameters. The eight input parameters are the channel height, air Reynolds number, mass flow rate and concentration of desiccant, humidity ratio, air and desiccant temperature and volume fraction of nanoparticles.

With each input parameter a range of values were assigned. To study the impact of one input parameter the value of that parameter was varied while keeping the other input parameters fixed at their nominal values. The nominal values are the same as the parametric analysis as mentioned in Table 5.1. Following this parallel flow simulation was carried out for each of the values of the particular input parameter according to its range and the output values were recorded. For example, Reynolds number of air was varied from 950 to 2150 and at seven values across this range the simulations were carried out individually and the output values of temperature, humidity ratio, average Nusselt number and average Sherwood number were recorded. These output values were then plotted in terms of percentage change to give a better comprehension of the effect of these parameters. The percentage change was measured with respect to the output parameter at the nominal value.

For example, the nominal value of Reynolds number was fixed at 1350 and in case of the average Nusselt number, the percentage difference of Nusselt number at other values of Reynolds number with that of the Nusselt number at 1350 Reynolds number was calculated and these values were illustrated in the y-axis of the sensitivity analysis. Similarly individual simulations were carried out for the remaining seven input parameters across their particular range and their output results were recorded and illustrated in the sensitivity analysis in terms of percentage change. In this way, the sensitivity analysis for this study was carried out.

5.3.1 Sensitivity analysis for average Nusselt number

Sensitivity analysis for average Nusselt number was carried out with Figure 5.12 indicating the parameters that have a significant effect and also the parameters that have a comparatively inconsequential effect on Nusselt number.

The two parameters that have a very pronounced effect on Nusselt number are height of the channel and Reynolds number of air. Increasing the height of the channel results in decrease in Nusselt number of approximately 80%. As the Reynolds number of air is increased, average Nusselt number increases by approximately 60%. Hence, it is very important to control these two parameters to improve the rate of heat transfer of the dehumidifier. Among the other parameters that have a comparatively lower impact on heat transfer rate variation, it is essential to control air inlet temperature which results in a 3.2% variation, concentration of desiccant which indicates a 2% variation and temperature of desiccant which indicates a 2.2% variation.

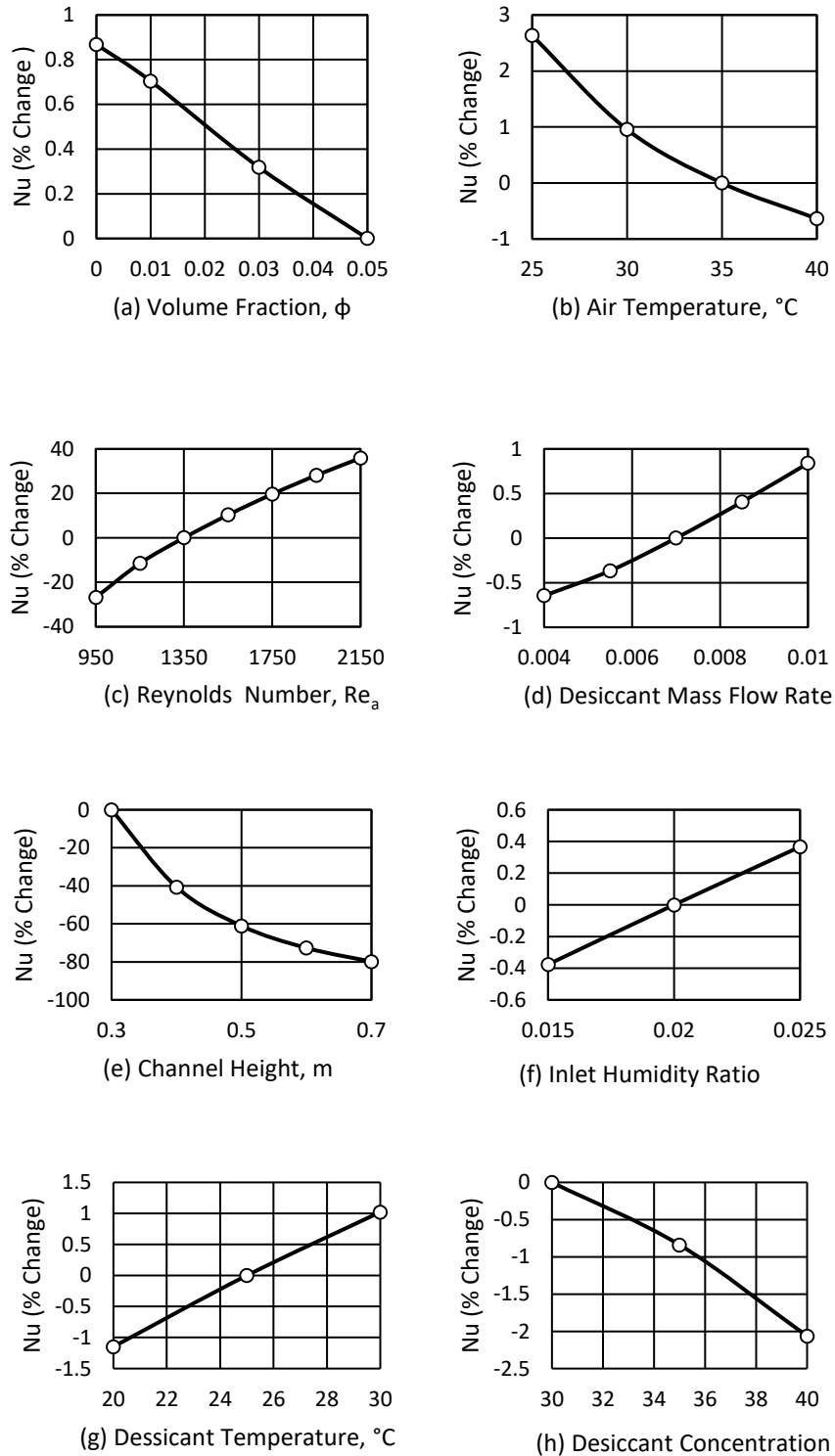


Figure 5.12: Sensitivity analysis of average Nusselt number (a) Volume fraction (b) Air temperature (c) Reynolds number (d) Mass flow rate (e) Channel height (f) Inlet humidity ratio (g) Desiccant temperature (h) Concentration

5.3.2 Sensitivity analysis for average Sherwood number

Sensitivity analysis for average Sherwood number was carried out with Figure 5.13 indicating the parameters that have comparatively inconsequential effect as well as the parameters, which have a considerable effect on the Sherwood number.

Similar to the Average Nusselt number analysis the two parameters that have a very considerable effect on Sherwood number are Height of the channel and air Reynolds number. Increasing the channel height results in decrease in Sherwood number of approximately 80%. Average Sherwood number increases by approximately 64% due to increase in air Reynolds number. Hence, it is very important to control these two parameters to improve the dehumidifier mass transfer rate. Among the other parameters that have a comparatively lower impact on mass transfer rate variation, it is important to control air humidity ratio which results in a 1.9% variation, concentration of desiccant which indicates a 3.5% variation and temperature of desiccant which indicates a 2.1% variation.

5.3.3 Sensitivity analysis for outlet Air temperature

Sensitivity analysis for outlet air temperature was carried out with Figure 5.14 indicating the parameters that have comparatively lower effect on air temperature at the outlet and also the parameters having a considerable effect on outlet air temperature.

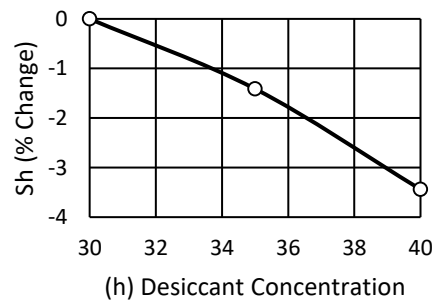
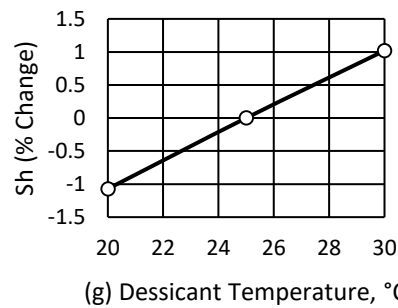
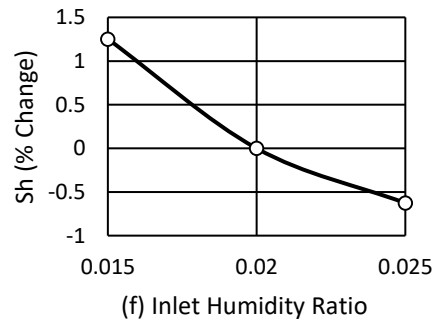
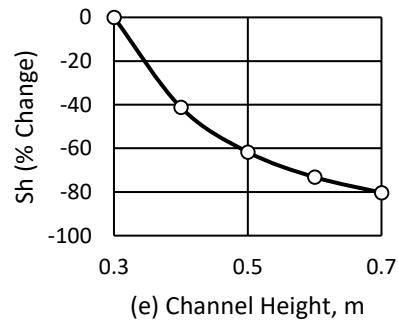
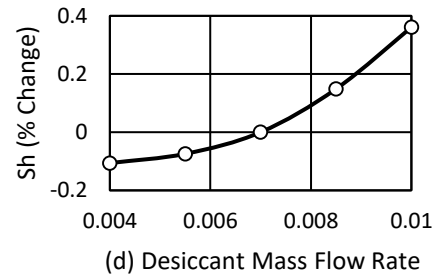
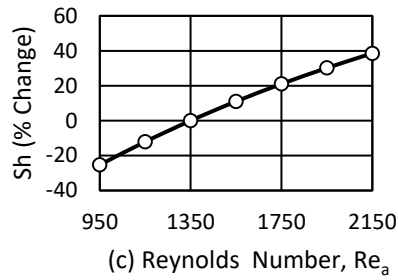
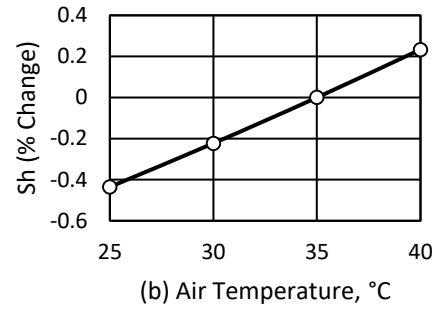
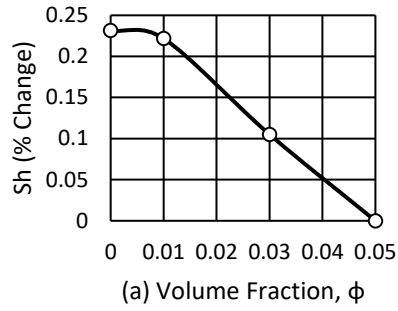


Figure 5.13: Sensitivity analysis of average Sherwood number (a) Volume fraction (b) Air temperature (c) Reynolds number (d) Mass flow rate (e) Channel height (f) Inlet humidity ratio (g) Desiccant temperature (h) Concentration

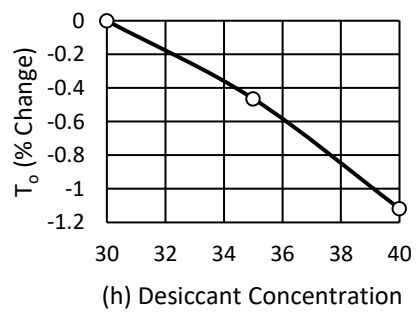
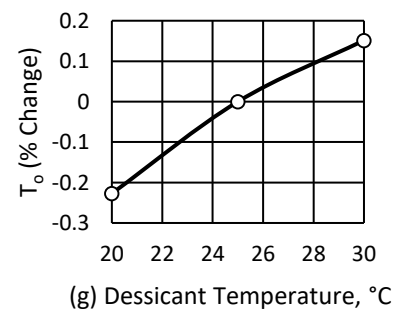
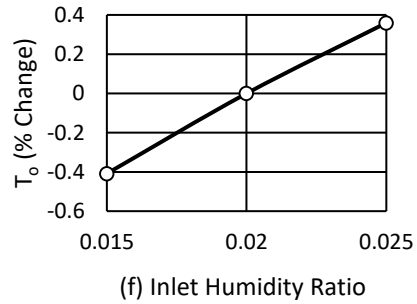
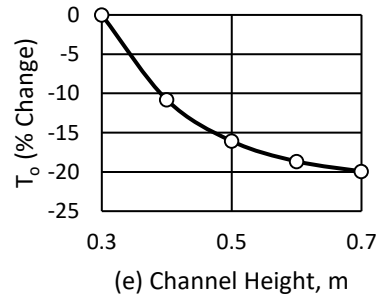
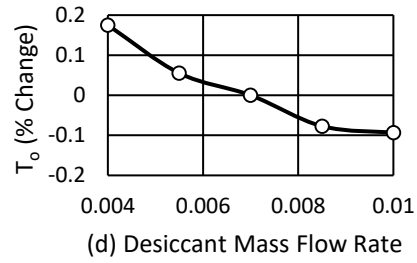
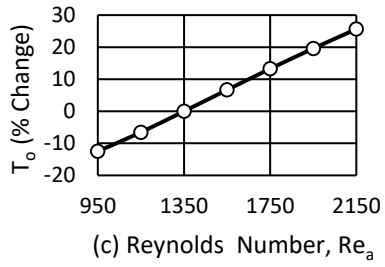
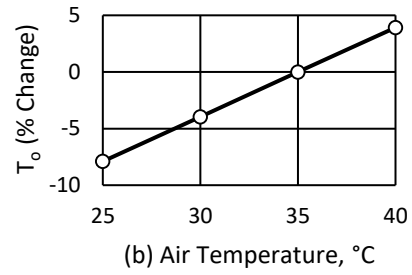
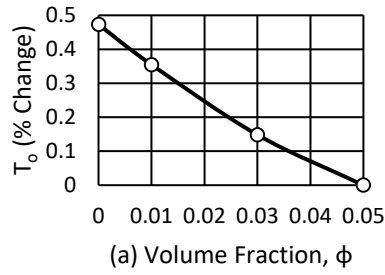


Figure 5.14: Sensitivity analysis of outlet air temperature (a) Volume fraction (b) Air temperature (c) Reynolds number (d) Mass flow rate (e) Channel height (f) Inlet humidity ratio (g) Desiccant temperature (h) Concentration

In this analysis, three parameters have a considerable impact on temperature of air at the outlet. These are channel height, Reynolds number of air and inlet air temperature. Increasing the height of the channel results in air temperature decreasing by approximately 20%. An increase in the Reynolds number of air results in outlet air temperature increasing by approximately 37%. As the air temperature at inlet increases, air temperature at outlet increases by approximately 12%. Hence, it is very important to control these three parameters to enhance the cooling output of dehumidifier. Among other parameters that have a comparatively lower impact on outlet air temperature, it is important to control inlet humidity ratio which results in a 0.8% variation, concentration of desiccant which indicates a 1.2% variation and volume fraction of nanoparticles which indicates a 0.5% variation.

5.3.4 Sensitivity analysis for outlet Humidity ratio

Sensitivity analysis for outlet humidity ratio was carried out with Figure 5.15 indicating the parameters that have comparatively lower impact as well as the parameters, having a considerable effect on the outlet humidity ratio.

In this analysis, the four parameters that have a very significant effect on exit humidity ratio are Height of the channel, concentration of the desiccant, Reynolds number of air and humidity ratio. Increasing channel height leads to decrease in outlet humidity ratio of approximately 20%. An increase in air Reynolds number results in outlet humidity ratio increasing by approximately 46%. An increase in humidity ratio at inlet leads to an increment in outlet humidity ratio of approximately 13.6%.

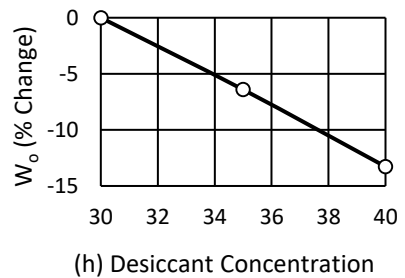
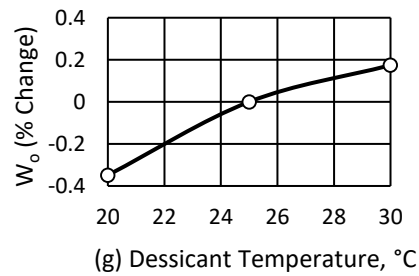
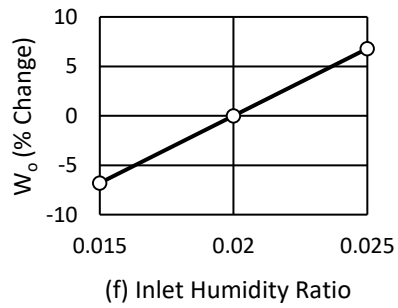
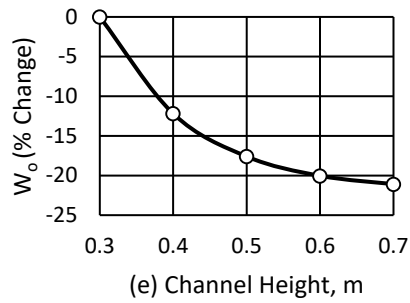
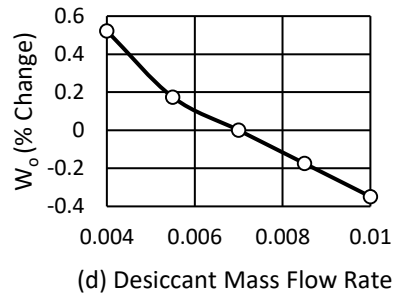
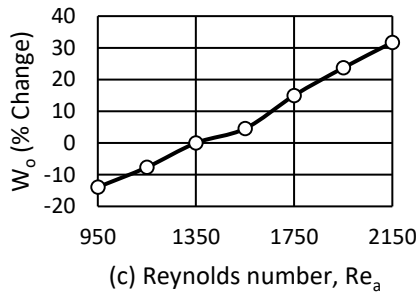
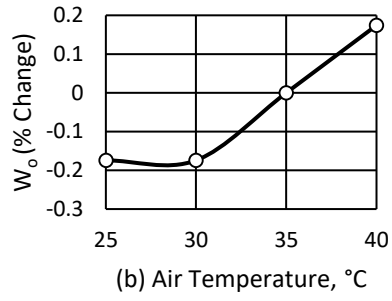
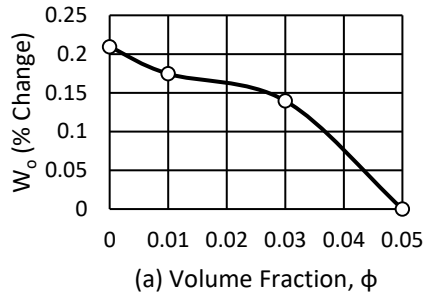


Figure 5.15: Sensitivity analysis of outlet humidity ratio (a) Volume fraction (b) Air temperature (c) Reynolds number (d) Mass flow rate (e) Channel height (f) Inlet humidity ratio (g) Desiccant temperature (h) Concentration

An increase in the concentration of the desiccant results in decrease in outlet humidity ratio of approximately 13%. Hence, it is very important to control these four parameters to enhance the dehumidification of falling film dehumidifier.

5.3.5 Sensitivity analysis results by uncertainty propagation method

Sensitivity analysis can also be carried out by using the uncertainty propagation method specified in EES. Sensitivity analysis has been carried out in order to analyze and identify which of the varying inlet parameters are significantly affecting the output parameters. The equations required to carry out this analysis is specified in EES and are mentioned below. The independent variables can be specified by X. The variation in the independent variable can be specified by the following equation.

$$X = X_{nom} + U_X \quad (5.1)$$

In the above equation, X_{nom} represent nominal values of X and U_X represents the uncertainty in X. The dependent output variable is a function of X and can be represented by Y(X). Hence, the uncertainty in Y due to the uncertainty in X can be represented as:

$$U_Y = \frac{\partial Y}{\partial X} U_X \quad (5.2)$$

For a multivariable function $Y=Y(X_1, X_2, X_3, \dots, X_N)$ the uncertainty in Y due to uncertainties in X is given by the following equation:

$$U_Y = \left[\sum_{i=1}^N \left(\frac{\partial Y}{\partial X_i} U_{X_i} \right)^2 \right]^{0.5} \quad (5.3)$$

The partial derivatives in the above expression illustrate the sensitivity of Y due to the variation in a particular independent variable X_i . The percentage uncertainty or percentage contribution of a particular independent variable is given by the following equation:

$$\% \text{ Uncertainty} = \frac{\left[\frac{\partial Y}{\partial X_i} U_{X_i} \right]^2}{U_Y^2} \quad (5.4)$$

The analysis was carried out by using the above mentioned equations to determine the partial derivatives for each independent variable, the uncertainty in Y and % Uncertainty for each independent variable. The nominal values of the various inlet parameters were obtained from the studies carried out by Rahamah et al. [9] and they have been specified in Table 5.1 illustrated previously. These nominal values were varied by 1% in positive and negative direction and for these new values, numerical simulation was carried out to obtain the output data at each of these input values. The results for each of the outputs average Nusselt number, average Sherwood number, outlet air temperature and outlet humidity ratio are illustrated in the tables below.

Sensitivity Analysis for average Nusselt number (Nu) by uncertainty propagation is illustrated in Table 5.2. The independent variables are varied by 1% in both directions and using the above equations the total uncertainty U_Y was obtained along with the percentage contribution of each independent variable. Nusselt number is most sensitive to channel height, which has an 85.11 % contribution followed by air Reynolds number having a 14.68% contribution. The other independent parameters have insignificant contribution to the uncertainty in Nusselt number as illustrated in the table results.

Table 5.2: Sensitivity Analysis of average Nusselt number by uncertainty propagation

Independent Variables (X)	Nom- inal ± 1%	Uncer- tainty 1%	$\frac{\partial Nu}{\partial X}$	Nu at Nom- inal	U _Y	% Uncer- tainty
Desiccant Concentration (C _d)	30	0.3	-0.01	10.368	0.198	0.04
Channel Height (H)	0.3	0.003	-61	10.368	0.198	85.11
Desiccant mass flow rate (ṁ _d)	0.007	0.00007	24.3	10.368	0.198	0.007
Volume Fraction (φ)	0.05	0.0005	-1.5	10.368	0.198	0.0014
Air Reynolds number (Re _a)	1350	13.5	0.006	10.368	0.198	14.68
Air Temperature (T _a)	35	0.35	-0.016	10.368	0.198	0.077
Desiccant Temperature (T _d)	25	0.25	0.02	10.368	0.198	0.075
Inlet humidity ratio (W _i)	0.02	0.0002	7.5	10.368	0.198	0.006

Sensitivity Analysis for average Sherwood number (Sh) by uncertainty propagation is illustrated in Table 5.3. Similar to average Nusselt number, average Sherwood number is most sensitive to channel height, which has an 84.4 % contribution followed by air Reynolds number having a 15.44% contribution. The other independent parameters have insignificant contribution to the uncertainty in Sherwood number as illustrated in the table results.

Table 5.3: Sensitivity Analysis of average Sherwood number by uncertainty propagation

Independent Variables (X)	Nom- inal ± 1%	Uncer- tainty 1%	$\frac{\partial Sh}{\partial X}$	Sh at Nom- inal	U _Y	% Uncer- tainty
Desiccant Concentration (C _d)	30	0.3	-0.015	9.42	0.184	0.06
Channel Height (H)	0.3	0.003	-56.5	9.42	0.184	84.4
Desiccant mass flow rate (ṁ _d)	0.007	0.00007	5.7	9.42	0.184	0.0004
Volume Fraction (φ)	0.05	0.0005	-0.4	9.42	0.184	0.001
Air Reynolds number (Re _a)	1350	13.5	0.005	9.42	0.184	15.44
Air Temperature (T _a)	35	0.35	0.004	9.42	0.184	0.006
Desiccant Temperature (T _d)	25	0.25	0.02	9.42	0.184	0.06
Inlet humidity ratio (W _i)	0.02	0.0002	-18	9.42	0.184	0.04

Sensitivity Analysis for outlet air temperature (T_o) by uncertainty propagation is illustrated in Table 5.4. Outlet air temperature is most sensitive to air Reynolds number (42.6% contribution) followed by channel height having a 41.8% contribution. The inlet air temperature also has a significant effect with a 15.5% contribution.

Sensitivity Analysis for outlet humidity ratio (W_o) by uncertainty propagation is illustrated in Table 5.5. Outlet humidity ratio is most sensitive to air Reynolds number (40.73% contribution) followed by channel height (36.76% contribution). The desiccant concentration and inlet humidity ratio also has a significant effect with a 13.86% and 8.62% contribution to outlet humidity ratio respectively.

Overall, we can conclude that the falling film parallel flow dehumidifier is very sensitive to channel height and air Reynolds number as variation in these input parameters result in the maximum variation of all the output parameters.

Table 5.4: Sensitivity Analysis of outlet air temperature by uncertainty propagation

Independent Variables (X)	Nom- inal $\pm 1\%$	Uncer- tainty 1%	$\frac{\partial T_o}{\partial X}$	T_o at Nom- inal	U_Y	% Uncer- tainty
Desiccant Concentration (C_d)	30	0.3	-0.001	12.685	0.087	0.002
Channel Height (H)	0.3	0.003	-18.82	12.685	0.087	41.8
Desiccant mass flow rate (\dot{m}_d)	0.007	0.00007	-28.6	12.685	0.087	0.05
Volume Fraction (ϕ)	0.05	0.0005	-0.5	12.685	0.087	0.0008
Air Reynolds number (Re_a)	1350	13.5	0.004	12.685	0.087	42.6
Air Temperature (T_a)	35	0.35	0.1	12.685	0.087	15.5
Desiccant Temperature (T_d)	25	0.25	0.002	12.685	0.087	0.003
Inlet humidity ratio (W_i)	0.02	0.0002	7.5	12.685	0.087	0.03

Table 5.5: Sensitivity Analysis of outlet air temperature by uncertainty propagation

Independent Variables (X)	Nom- inal $\pm 1\%$	Uncer- tainty 1%	$\frac{\partial W_o}{\partial X}$	W _o at Nom- inal	U _Y	% Uncer- tainty
Desiccant Concentration (C _d)	30	0.3	-6E-05	0.00574	4.7E-05	13.86
Channel Height (H)	0.3	0.003	-0.009	0.00574	4.7E-05	36.76
Desiccant mass flow rate (\dot{m}_d)	0.007	0.00007	-0.008	0.00574	4.7E-05	0.02
Volume Fraction (ϕ)	0.05	0.0005	-4E-05	0.00574	4.7E-05	1.8E-05
Air Reynolds number (Re _a)	1350	13.5	2.2E-06	0.00574	4.7E-05	40.73
Air Temperature (T _a)	35	0.35	1.3E-06	0.00574	4.7E-05	0.01
Desiccant Temperature (T _d)	25	0.25	6E-07	0.00574	4.7E-05	0.001
Inlet humidity ratio (W _i)	0.02	0.0002	0.07	0.00574	4.7E-05	8.62

CHAPTER 6

COMPARATIVE NUMERICAL ANALYSIS OF PARALLEL AND COUNTER FLOW FALLING FILM DEHUMIDIFIERS FOR DIFFERENT LIQUID DESICCANTS WITH DIFFERENT NANOPARTICLES

It is essential to investigate and compare the different flow configurations to improve the heat and mass transfer characteristics for falling film dehumidifier and studies were done previously to analyze this scenario. However, focus of the previous studies had been on a particular liquid desiccant solutions and one study investigated the presence of copper nanoparticles in the solution only.

This research will focus on investigating the effects on mass transfer and transfer attributes for three different liquid desiccant solutions. To each of these three liquid desiccants three different nanoparticles are added. The nanoparticles volume fraction is varied from 1% to 5%. The analysis is carried out for both counter flow configuration and parallel flow configuration. For improving performance of a variety of dehumidifiers many studies have been carried out, but very less research has been carried out for the case that has been proposed in this research.

The three different liquid desiccant solutions selected for this study are calcium chloride (CaCl_2), lithium bromide (LiBr) and lithium chloride (LiCl). The concentration of salt in

CaCl₂ and LiCl liquid desiccant is fixed at 30% to avert the risk of crystallization at higher concentrations. Working range of concentration for LiBr solution is 45% to 55% hence nominal value of 50% was fixed for LiBr solution.

The three different nanoparticles selected for this study as mentioned previously are titanium oxide (TiO₂), aluminium oxide (Al₂O₃) and copper (Cu). For this research, volume fraction of these nanoparticles is varied from 1% to 5% to study the effect of increasing the volume fraction on transfer characteristics of mass and heat as well as dehumidification and cooling process.

Thermodynamic properties of these liquid desiccant nanofluid solutions are obtained by expressions mentioned in the literature. For the various inlet conditions, and height of the channel wall, the nominal values as mentioned in the parametric analysis is selected for this study to produce the best possible output.

Depending on the combination of liquid desiccant and nanoparticle, the two parameters that are affected are the desiccant film thickness and the maximum velocity at the centreline of the channel.

The numerical simulation was then carried out for each combination of liquid desiccant and nanoparticle with specified volume fraction and for each simulation four output results were recorded. These are the velocity weighted average temperature at the outlet, velocity weighted average humidity ratio, Nusselt number and Sherwood number at interface.

The comparative results are split in three sections, the first section illustrates the results for parallel flow configuration, the second section illustrates the results for counter flow configuration and the third sections illustrates the comparison between parallel and counter

flow. The effect of nanoparticles on both flow configurations for three different liquid desiccants were investigated and from the results the difference between them was analyzed. Conclusions were drawn on the best combination of liquid desiccant and nanoparticle for both flow configurations.

6.1 Comparative numerical analysis of parallel flow falling film dehumidifiers for three different liquid desiccants with three different nanoparticles

The analysis for parallel flow falling film dehumidifier is split into three sections and each section deals with a particular liquid desiccant.

6.1.1 Calcium chloride (CaCl₂) liquid desiccant (PF)

In this section the calcium chloride liquid desiccant at 30% concentration is analyzed. The effect of different nanoparticles with varying volume fraction in CaCl₂ liquid desiccant on the outlet air temperature is indicated in Figure 6.1

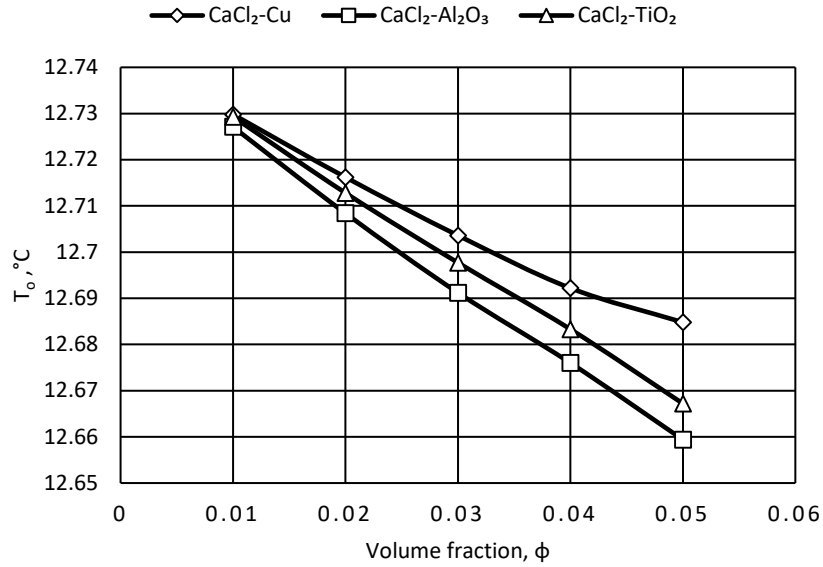


Figure 6.1: Effect of different nanoparticles with varying volume fraction in CaCl₂ liquid desiccant on outlet air temperature (PF)

As volume fraction of nanoparticles increases from 1% to 5% outlet temperature decreases indicating the cooling of air also increases. The temperature decrease is the lowest with Cu nanoparticles showing a decrease of 0.35% and the highest with Al₂O₃ nanoparticles of approximately 0.53%. For TiO₂ the decrease is approximately 0.49%. The results with TiO₂ is almost similar to Al₂O₃ and the utilization of both these nanoparticle result in better cooling of hot air than using Cu nanoparticle.

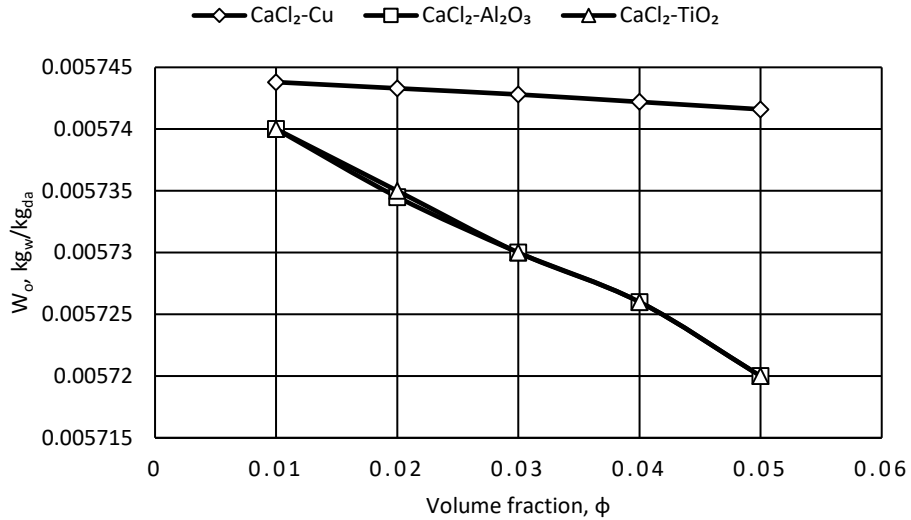


Figure 6.2: Effect of different nanoparticles with varying volume fraction in CaCl₂ liquid desiccant on outlet humidity ratio (PF)

The effect of different nanoparticles in CaCl₂ liquid desiccant with varying volume fraction on the outlet humidity ratio is illustrated in Figure 6.2. The figure indicates that as nanoparticles volume fraction increase from 1% to 5%, outlet humidity ratio decreases indicating the dehumidification of air also increases. The decrease in air humidity ratio is the lowest with Cu nanoparticles showing a decrease of 0.04% and for both Al₂O₃ and TiO₂ the decrease is the same approximately 0.35%. Hence TiO₂ and Al₂O₃ results in better dehumidification of humid air than using Cu nanoparticle.

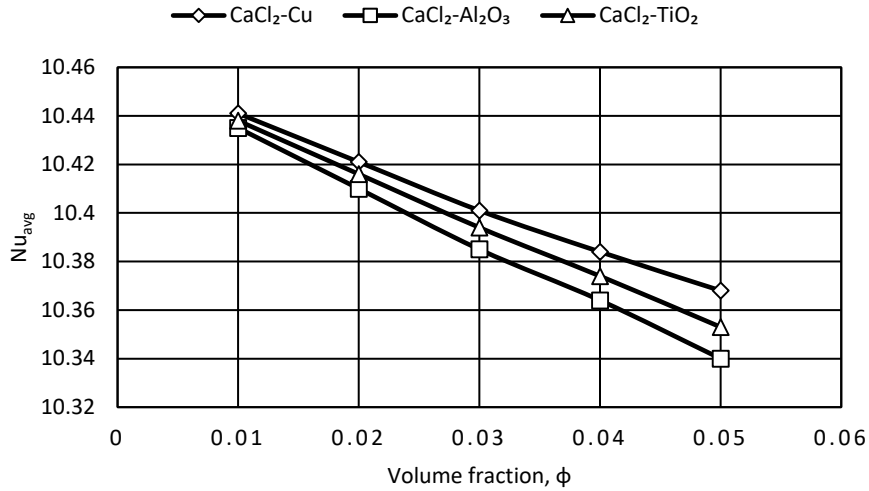


Figure 6.3: Effect of different nanoparticles with varying volume fraction in CaCl₂ liquid desiccant on Nusselt number. (PF)

The effect of different nanoparticles with varying volume fraction in CaCl₂ liquid desiccant on Nusselt number at interface is illustrated in Figure 6.3. The figure indicates that as nanoparticles volume fraction increase from 0.01 to 0.05 the average Nusselt number decreases. The decrease is the lowest with Cu nanoparticles showing a decrease of 0.69% and the highest with Al₂O₃ nanoparticles of approximately 0.91%. For TiO₂ the decrease is approximately 0.81%. Hence, heat transfer rate is the highest while utilizing copper nanoparticles. However, the contradictory result that can be observed is that Nusselt number decreases but the cooling is improved indicating that more heat transfer occurs. The conclusion made for this scenario is that Nusselt number does not account for latent heat and only accounts for sensible heat. Hence, latent heat transfer due to changing of phase from water vapor to water increases with increasing volume fraction. This contributes to lower temperature of air at the outlet of the channel.

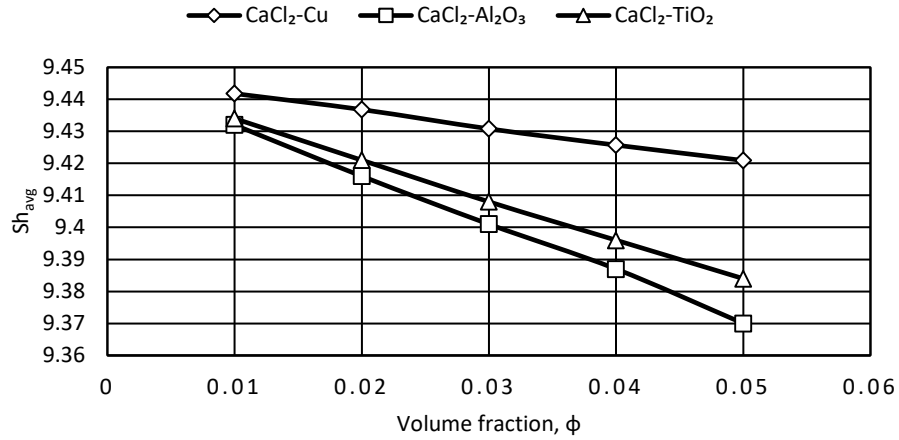


Figure 6.4: Effect of different nanoparticles with varying volume fraction in CaCl₂ liquid desiccant on average Sherwood number at the interface (PF)

In CaCl₂ liquid desiccant, the impact of different nanoparticles with varying volume fraction on average Sherwood number at the interface is illustrated in Figure 6.4. The figure indicates that as nanoparticles volume fraction increase from 1% to 5% average Sherwood number decreases. The decrease is the lowest with Cu nanoparticles showing a decrease of 0.22% and the highest with Al₂O₃ nanoparticles of approximately 0.66%. For TiO₂ the decrease is approximately 0.53%. Hence, the rate of mass transfer is the highest while using copper nanoparticles.

For parallel flow configuration, utilizing CaCl₂ liquid desiccant Al₂O₃ at 5% is concluded to be the most suitable nanoparticle for producing maximum dehumidification and cooling although the rates of heat and mass transfer are slightly lower compared to other nanoparticles.

6.1.2 Lithium chloride (LiCl) liquid desiccant (PF)

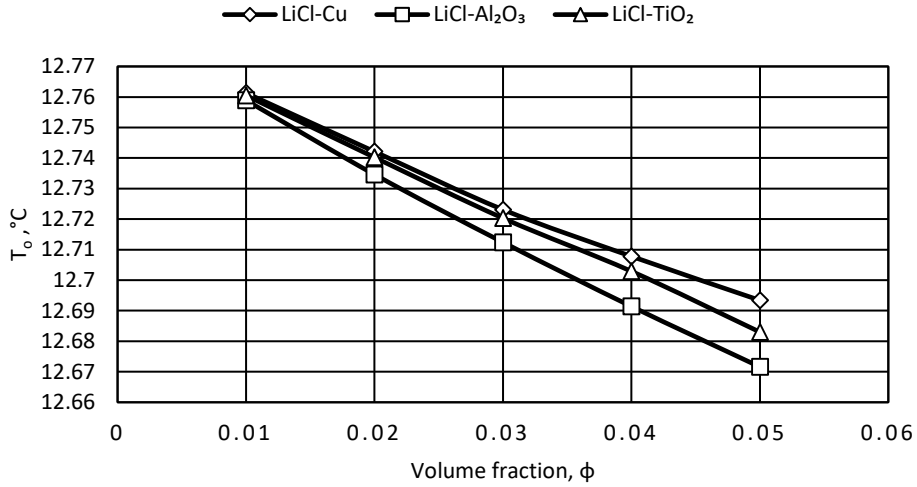


Figure 6.5 : Effect of different nanoparticles with varying volume fraction in LiCl liquid desiccant on outlet air temperature (PF)

The lithium chloride liquid desiccant solution at 30% concentration is analyzed. The impact of different nanoparticles with different volume fraction in LiCl liquid desiccant on the outlet air temperature is illustrated in Figure 6.5. The figure indicates that as volume fraction of nanoparticles increase from 1% to 5% outlet temperature decreases indicating the cooling of air also increases. The temperature decrease is the lowest with Cu nanoparticles showing a decrease of 0.53% and the highest with Al_2O_3 nanoparticles of approximately 0.684%. For TiO_2 the decrease is approximately 0.61%. The results with TiO_2 is almost similar to Al_2O_3 and the utilization of both these nanoparticle result in better cooling of hot air than using Cu nanoparticle. Comparing the LiCl liquid desiccant with the $CaCl_2$ liquid desiccant with respect to outlet temperature, LiCl liquid desiccant results in higher outlet air temperature indicating that less cooling occurs due to using LiCl.

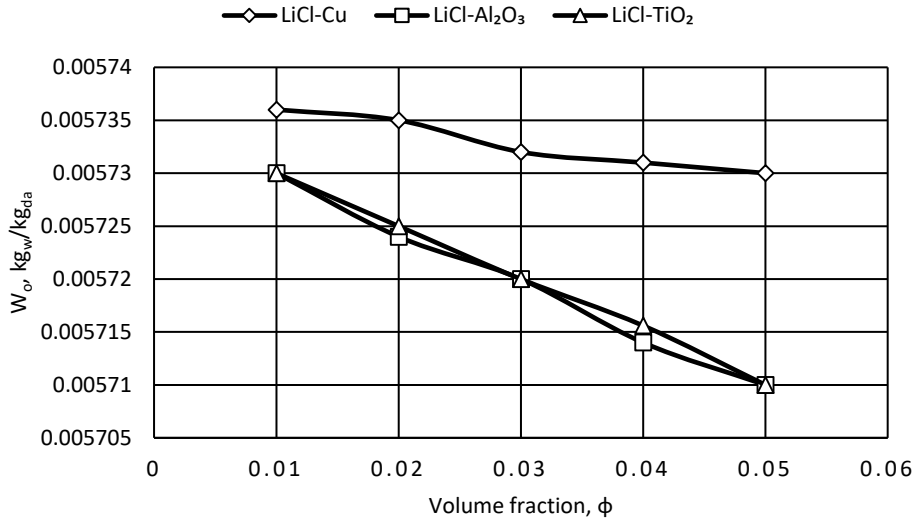


Figure 6.6: Effect of different nanoparticles with varying volume fraction in LiCl liquid desiccant on outlet humidity ratio (PF)

The effect of different nanoparticles in LiCl liquid desiccant with varying volume fraction on the outlet humidity ratio is illustrated in Figure 6.6. The figure indicates that as nanoparticles volume fraction increases the outlet humidity ratio decreases indicating the dehumidification of air also increases. The decrease in air humidity ratio is the lowest with Cu nanoparticles showing a decrease of 0.1% and for both Al₂O₃ and TiO₂ the decrease is the same approximately 0.35%. Hence TiO₂ and Al₂O₃ results in better dehumidification of humid air than using Cu nanoparticle. Comparing the LiCl liquid desiccant with the CaCl₂ liquid desiccant with respect to outlet humidity ratio, LiCl liquid desiccant results in lower outlet humidity ratio indicating that higher dehumidification occurs due to using LiCl.

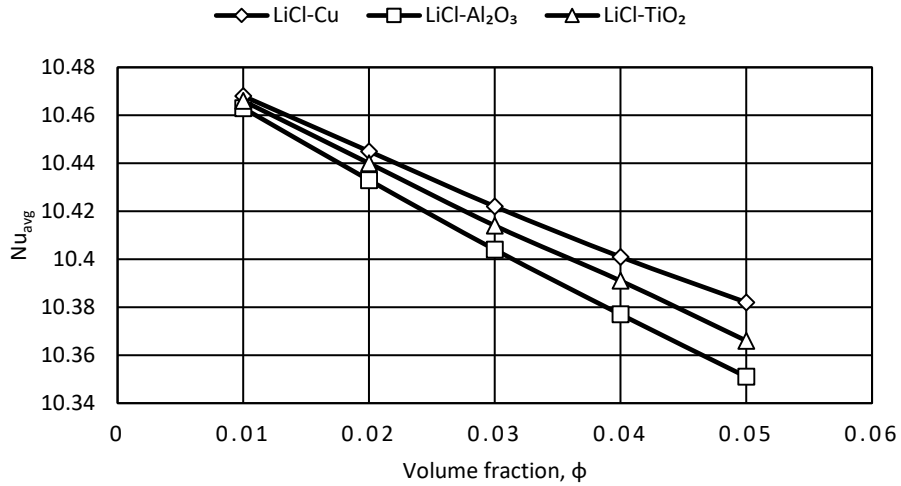


Figure 6.7: Effect of different nanoparticles with varying volume fraction in LiCl liquid desiccant on Nusselt number (PF).

The effect of different nanoparticles with varying volume fraction in LiCl liquid desiccant on Nusselt number at interface is illustrated in Figure 6.7. The figure indicates that as nanoparticles volume fraction increases the average Nusselt number decreases. The decrease is the lowest with Cu nanoparticles showing a decrease of 0.82% and the highest with Al₂O₃ nanoparticles of approximately 1.07%. For TiO₂ the decrease is approximately 0.95%. Hence, the rate of heat transfer is the highest while using copper nanoparticles. Compared to CaCl₂ liquid desiccant LiCl has a higher rate of heat transfer.

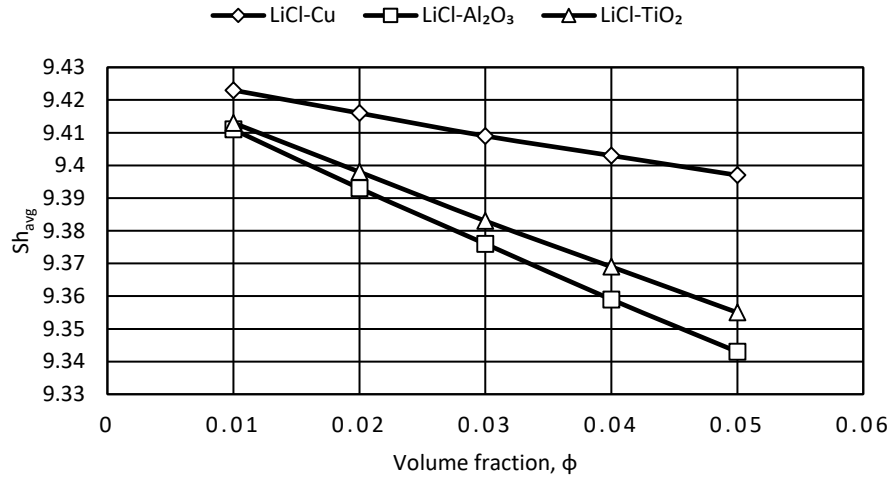


Figure 6.8: Effect of different nanoparticles with varying volume fraction in LiCl liquid desiccant on average Sherwood number at the interface (PF)

In LiCl liquid desiccant, the effect of different nanoparticles with varying volume fraction on the average Sherwood number at the interface is illustrated in Figure 6.8. The figure indicates that as nanoparticles volume fraction increases the average Sherwood number decreases. The decrease is the lowest with Cu nanoparticles showing a decrease of 0.28% and the highest with Al₂O₃ nanoparticles of approximately 0.72%. For TiO₂ the decrease is approximately 0.62%. Hence, the rate of mass transfer is the highest while using copper nanoparticles. Compared to CaCl₂ liquid desiccant LiCl has a lower rate of mass transfer.

For parallel flow configuration, utilizing LiCl liquid desiccant Al₂O₃ at 5% is concluded to be the most suitable nanoparticle for producing maximum cooling and dehumidification although the rates of mass and heat transfer are slightly lower compared to other nanoparticles. It is also suitable to use TiO₂ nanoparticles as it produces relatively similar albeit slightly lower cooling and dehumidification of hot humid air and has slightly higher

heat and mass transfer rates. Comparison between CaCl_2 liquid desiccant and LiCl liquid desiccant indicates that better cooling of air occurs due to utilizing CaCl_2 and better dehumidification occurs due to LiCl .

6.1.3 Lithium bromide (LiBr) liquid desiccant (PF)

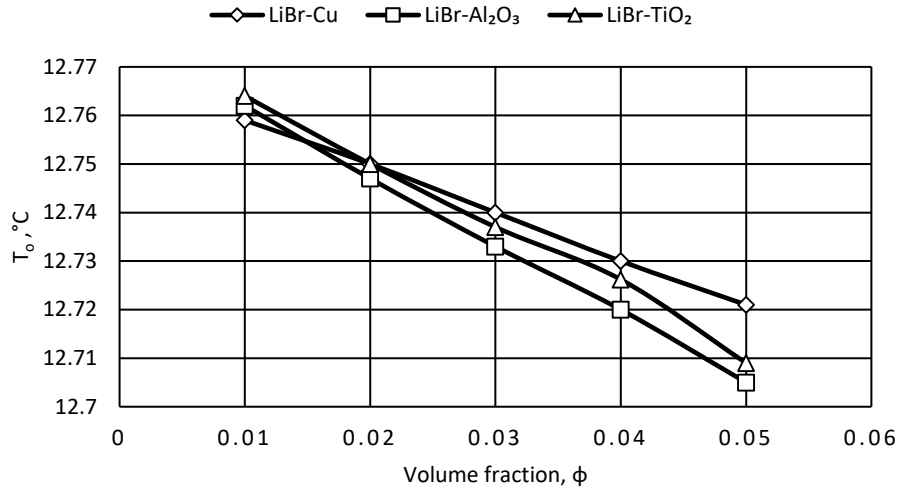


Figure 6.9: Effect of different nanoparticles with varying volume fraction in LiBr liquid desiccant on outlet air temperature (PF)

Lithium bromide liquid desiccant solution at 50% concentration is investigated in this section. Higher concentration of lithium bromide is selected, as working range of lithium bromide solution is 45% to 55%. The effect of different nanoparticles with varying volume fraction in LiBr liquid desiccant on the outlet air temperature is illustrated in Figure 6.9. The figure indicates that as volume fraction of nanoparticles increases, temperature decreases indicating the cooling of air also increases. The temperature decrease is the lowest with Cu nanoparticles showing a decrease of 0.3% and the highest with Al_2O_3 nanoparticles of approximately 0.45%. For TiO_2 the decrease is approximately 0.43%. The

results with TiO_2 is almost similar to Al_2O_3 and the utilization of both these nanoparticle result in better cooling of hot air than using Cu nanoparticle. Comparing the three liquid desiccant with respect to outlet temperature of air, CaCl_2 results in lowest outlet temperature indicating that most cooling occurs, and LiBr results in highest outlet temperature indicating that least cooling occurs and the difference in cooling is approximately 0.3%.

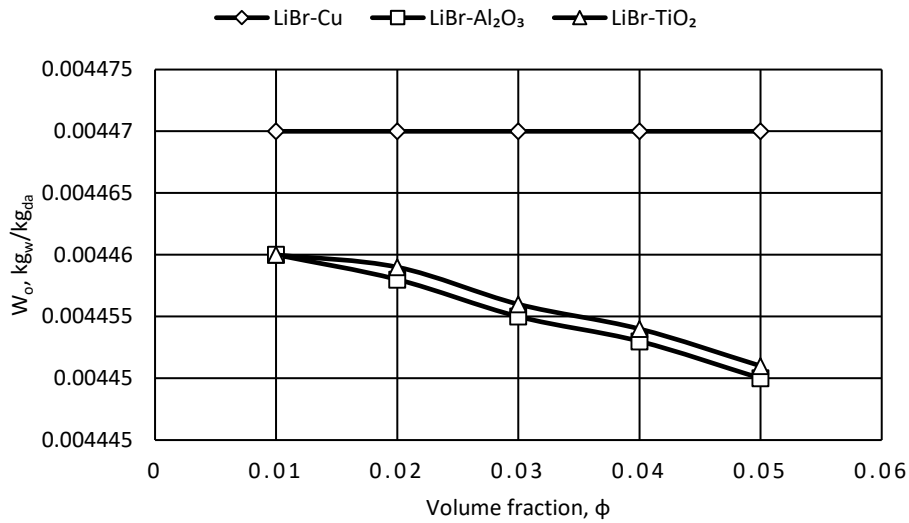


Figure 6.10: Effect of different nanoparticles with varying volume fraction in LiBr liquid desiccant on outlet humidity ratio (PF)

The effect of different nanoparticles in LiBr liquid desiccant with varying volume fraction on the outlet humidity ratio is illustrated in Figure 6.10. The figure indicates that as nanoparticles volume fraction increases the outlet humidity ratio decreases indicating the dehumidification of air also increases. Decrease in air humidity ratio is negligible with Cu nanoparticles. For Al_2O_3 the decrease is the most approximately 0.23% and for TiO_2 the decrease is approximately 0.2%. Hence TiO_2 and Al_2O_3 results in better dehumidification

of humid air than using Cu nanoparticle. The outlet humidity ratio with using LiBr liquid desiccant is much lower compared to both CaCl_2 and LiCl liquid desiccant indicating that much better dehumidification occurs with using LiBr. The outlet humidity ratio with using LiBr is approximately 22% lower than both the other desiccants.

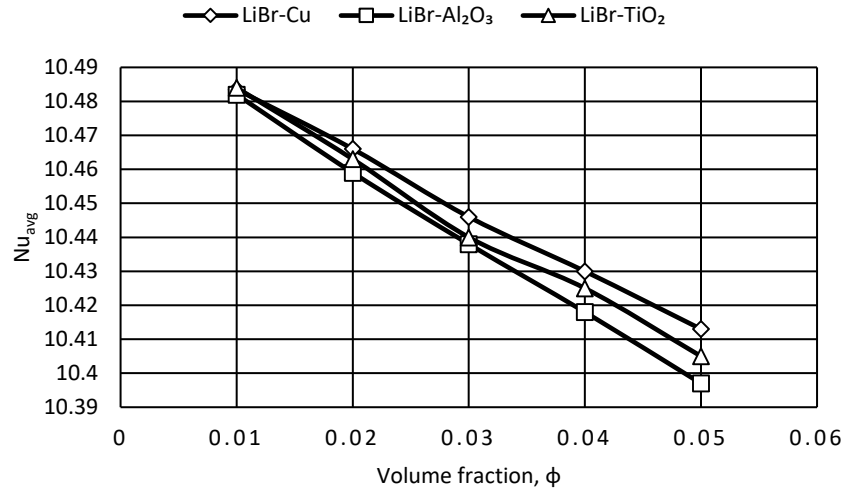


Figure 6.11: Effect of different nanoparticles with varying volume fraction in LiBr liquid desiccant on Nusselt number. (PF)

The effect of different nanoparticles with varying volume fraction in LiBr liquid desiccant on Nusselt number at interface is illustrated in Figure 6.11. Figure indicates that as nanoparticles volume fraction increases, Nusselt number decreases. Decrease is lowest with Cu nanoparticles showing a decrease of 0.67% and the highest with Al_2O_3 nanoparticles of approximately 0.82%. For TiO_2 the decrease is approximately 0.75%. Hence, the rate of heat transfer is the highest while using copper nanoparticles. Comparing the three liquid desiccants indicates that LiBr has the highest heat transfer rate approximately 0.45% higher than CaCl_2 liquid desiccant.

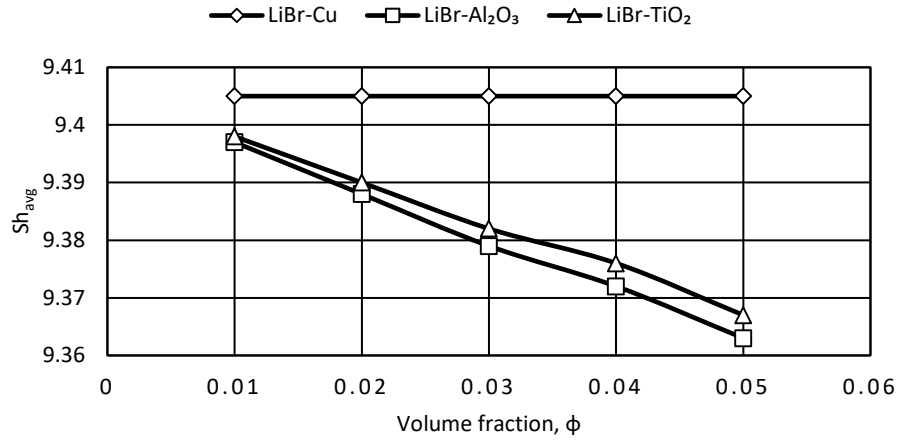


Figure 6.12: Effect of different nanoparticles with varying volume fraction in LiBr liquid desiccant on average Sherwood number at the interface (PF)

In LiBr liquid desiccant, the effect of different nanoparticles with varying volume fraction on the average Sherwood number at the interface is illustrated in Figure 6.12. The figure indicates that as nanoparticles volume fraction increases, average Sherwood number decreases. The decrease is negligible with Cu nanoparticles and the highest with Al_2O_3 nanoparticles of approximately 0.36%. For TiO_2 the decrease is approximately 0.33%. Hence, the rate of mass transfer is the highest while using copper nanoparticles.

For parallel flow configuration, utilizing LiBr liquid desiccant Al_2O_3 at 5% is concluded to be the most suitable nanoparticle for producing maximum dehumidification and cooling although rates of heat and mass transfer are slightly lower compared to other nanoparticles. It is also suitable to use TiO_2 nanoparticles as it produces relatively similar albeit slightly lower cooling and dehumidification of hot humid air and has slightly higher rates of heat and mass transfer.

Comparison between three liquid desiccants for parallel flow indicate that utilizing CaCl_2 liquid desiccant most cooling occurs and the difference in cooling is approximately 0.3% compared to LiBr. However, the best dehumidification occurs with using LiBr with humidity ratio for LiBr is approximately 22% lower than other desiccants. The analysis indicates that LiBr desiccant is better for producing better cooling and dehumidification compared to the other desiccants. Hence, for parallel flow it can be concluded that the combination of LiBr liquid desiccant with 5% volume fraction of Al_2O_3 nanoparticle is the ideal choice for producing the highest cooling and dehumidification.

6.2 Comparative numerical analysis of counter flow falling film dehumidifiers for three different liquid desiccants with three different nanoparticles

The analysis for counter flow falling film dehumidifier is split into three sections with each section discussing a particular liquid desiccant. After the numerical analysis of counter flow falling film dehumidifier was carried out the results indicated, that outlet temperature and air humidity ratio was higher compared to parallel flow configuration. In addition, Sherwood number and Nusselt number at interface is lower in counter flow configuration. Since direction of flow of air is opposite to the liquid desiccant, at the exit conditions mass transfer and heat transfer occurs in the opposite direction due to higher temperature and concentration at desiccant inlet. Hence, this slightly reduces average mass transfer and heat transfer rate. The outlet humidity ratio and temperature is also slightly higher.

6.2.1 Calcium chloride (CaCl_2) liquid desiccant (CF)

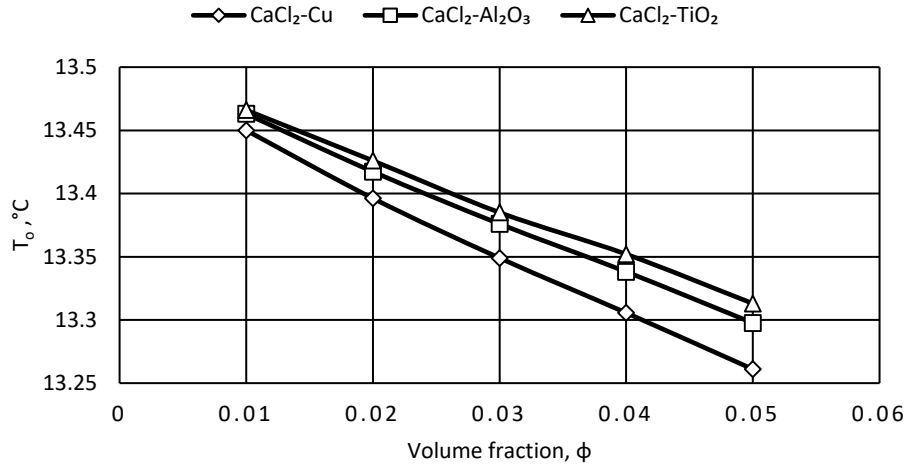


Figure 6.13: Effect of different nanoparticles with varying volume fraction in CaCl_2 liquid desiccant on outlet air temperature (CF)

In this section the calcium chloride liquid desiccant at 30% concentration is analyzed. The effect of different nanoparticles with varying volume fraction in CaCl_2 liquid desiccant on the outlet air temperature is indicated in Figure 6.13. The figure illustrates that as nanoparticles volume fraction increases the temperature at outlet decreases indicating the cooling of air also increases. The temperature decrease is the highest with Cu nanoparticles showing a decrease of 1.4% and the lowest with TiO_2 nanoparticles of approximately 1.14%. For Al_2O_3 the decrease is approximately 1.23%. The results with TiO_2 is almost similar to Al_2O_3 and from the analysis, it can be concluded that utilization of Cu nanoparticles result in the best cooling of air.

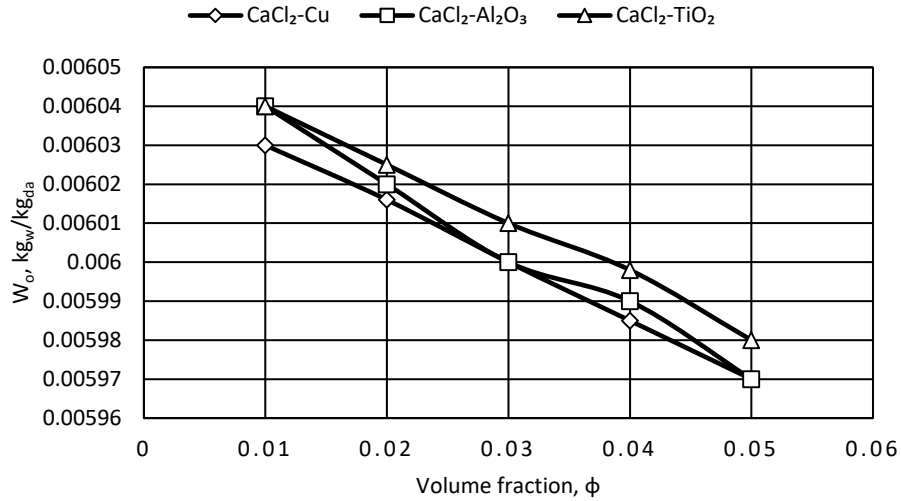


Figure 6.14: Effect of different nanoparticles with varying volume fraction in CaCl₂ liquid desiccant on outlet humidity ratio (CF)

The effect of different nanoparticles in CaCl₂ liquid desiccant with varying volume fraction on the outlet humidity ratio is illustrated in Figure 6.14. The figure indicates that as nanoparticles volume fraction increases the outlet humidity ratio decreases indicating the dehumidification of air also increases. Air humidity ratio decrease with Cu nanoparticles is around 1.005% and for Al₂O₃ the decrease is the highest approximately 1.16% and the lowest with TiO₂ approximately 0.99%. The outlet humidity ratio is the same for both Al₂O₃ and Cu nanoparticle hence both of them provide better dehumidification of humid air compared to TiO₂ nanoparticle.

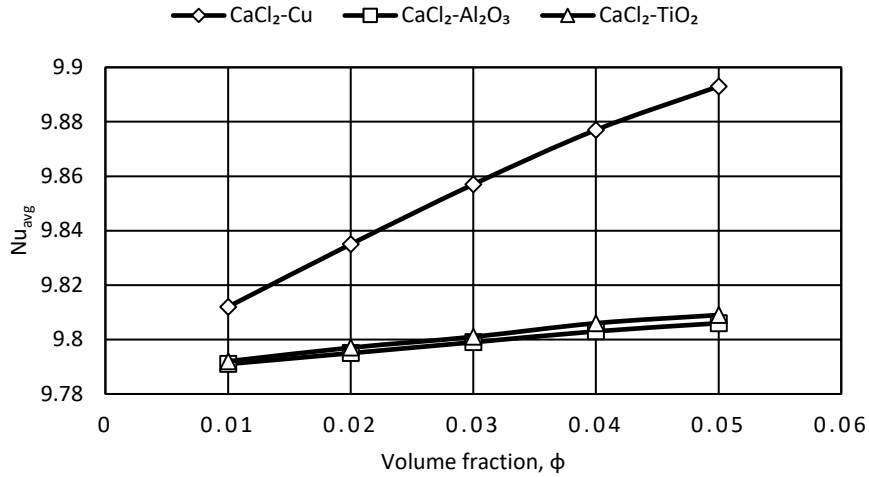


Figure 6.15: Effect of different nanoparticles with varying volume fraction in CaCl_2 liquid desiccant on Nusselt number. (CF)

The effect of different nanoparticles with varying volume fraction in CaCl_2 liquid desiccant on Nusselt number at interface is illustrated in Figure 6.15. The figure indicates that as nanoparticles volume fraction increases Nusselt number becomes higher. The increment is the highest with Cu nanoparticles showing an increase of 0.83% and the lowest with Al_2O_3 nanoparticles of approximately 0.15%. For TiO_2 the increase is approximately 0.17%. The rate of heat transfer is the highest while using copper nanoparticles compared to the other two nanoparticles. Hence, for counter flow channel as the nanoparticles volume fraction increase rate of heat transfer also increases with a decrease in outlet air temperature. Therefore, the cooling is improved as well as the rate of cooling.

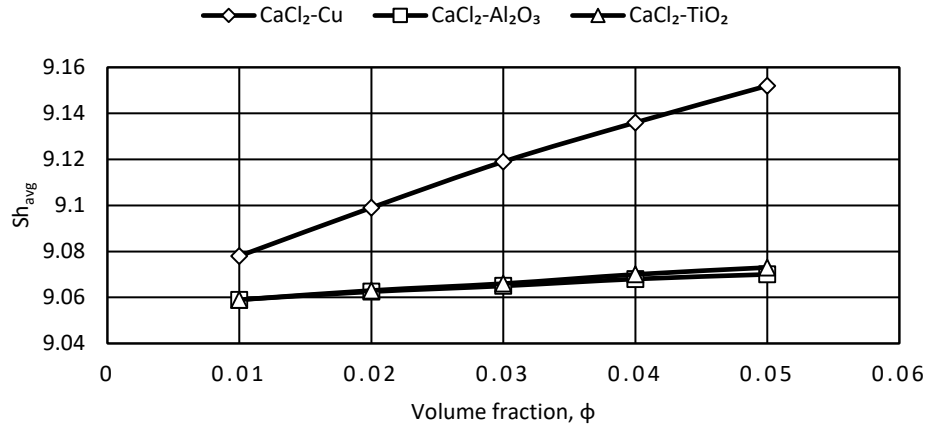


Figure 6.16: Effect of different nanoparticles with varying volume fraction in CaCl₂ liquid desiccant on average Sherwood number at the interface (CF)

In CaCl₂ liquid desiccant, the effect of different nanoparticles with varying volume fraction on the average Sherwood number at the interface is illustrated in Figure 6.16. The figure indicates that as nanoparticles volume fraction increases the average Sherwood number increases. The increase is the highest with Cu nanoparticles showing an increase of 0.82% and the lowest with Al₂O₃ nanoparticles of approximately 0.12%. For TiO₂ the increase is approximately 0.15%. The rate of mass transfer is the highest while using copper nanoparticles.

For counter flow configuration utilizing CaCl₂ liquid desiccant Cu nanoparticle at 5% volume fraction is concluded to be the most suitable nanoparticle for producing maximum cooling and dehumidification due to having higher heat and mass transfer rates and lower humidity ratio and temperature at outlet.

6.2.2 Lithium chloride (LiCl) liquid desiccant (CF)

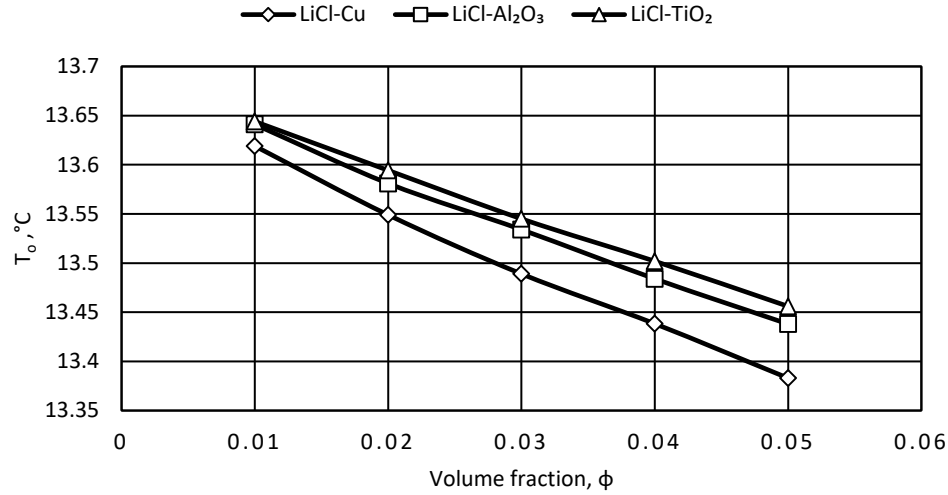


Figure 6.17: Effect of different nanoparticles with varying volume fraction in LiCl liquid desiccant on outlet air temperature (CF)

The lithium chloride liquid desiccant solution at 30% concentration is analyzed. The impact of different nanoparticles with different volume fraction in LiCl liquid desiccant on the outlet air temperature is illustrated in Figure 6.17. The figure indicates that as nanoparticles volume fraction increases the temperature becomes less indicating the cooling of air also increases. The temperature decrease is the highest with Cu nanoparticles showing a decrease of 1.73% and the lowest with TiO_2 nanoparticles of approximately 1.38%. For Al_2O_3 the decrease is approximately 1.49%. The results with TiO_2 is almost similar to Al_2O_3 and from the analysis it can be concluded that utilization of Cu nanoparticles result in best cooling.

Comparing LiCl liquid desiccant with the CaCl_2 liquid desiccant with respect to outlet temperature, LiCl liquid desiccant results in higher outlet air temperature by approximately 1% indicating that less cooling occurs due to using LiCl.

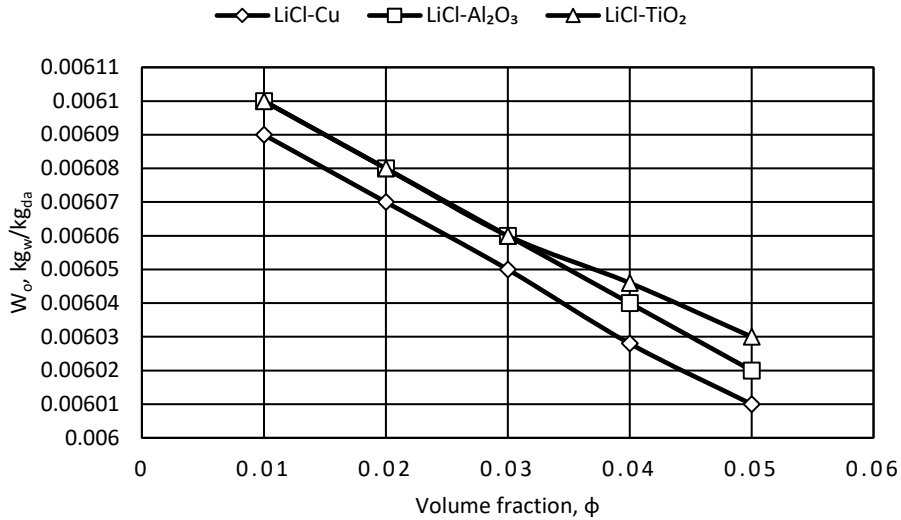


Figure 6.18: Effect of different nanoparticles with varying volume fraction in LiCl liquid desiccant on outlet humidity ratio (CF)

The effect of different nanoparticles in LiCl liquid desiccant with varying volume fraction on the outlet humidity ratio is illustrated in Figure 6.18. The figure indicates that as nanoparticles volume fraction increase, outlet humidity ratio decreases indicating the dehumidification of air also increases. The decrease in humidity ratio of air with Cu nanoparticles is the highest around 1.313% and for Al₂O₃ the decrease is almost similar approximately 1.311% and the lowest with TiO₂ approximately 1.15%. The outlet humidity ratio is the lowest for Cu nanoparticle hence it provides better dehumidification of humid air compared to both Al₂O₃ and TiO₂ nanoparticle.

Comparing the LiCl liquid desiccant with the CaCl₂ liquid desiccant with respect to outlet humidity ratio, LiCl liquid desiccant results in higher outlet humidity ratio indicating that higher dehumidification occurs due to using CaCl₂.

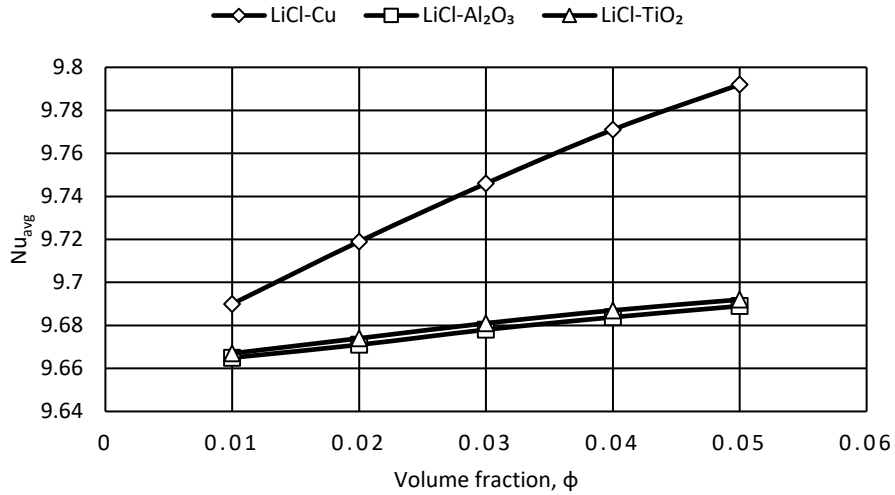


Figure 6.19: Effect of different nanoparticles with varying volume fraction in LiCl liquid desiccant on Nusselt number (CF).

The effect of different nanoparticles with varying volume fraction in LiCl liquid desiccant on Nusselt number at interface is illustrated in Figure 6.19. The figure indicates that as nanoparticles volume fraction increases the Nusselt number becomes higher.

The increment is the highest with Cu nanoparticles showing an increase of 1.05% and the lowest with Al₂O₃ nanoparticles of approximately 0.25%. For TiO₂ the increase is approximately 0.26%. The rate of heat transfer is the highest while using copper nanoparticles compared to the other two nanoparticles. Hence, for counter flow channel as the nanoparticles volume fraction increase, heat transfer rate also increases and outlet air temperature decreases. Therefore, the cooling is improved as well as the rate of cooling. Compared to CaCl₂ liquid desiccant LiCl has a lower rate of heat transfer.

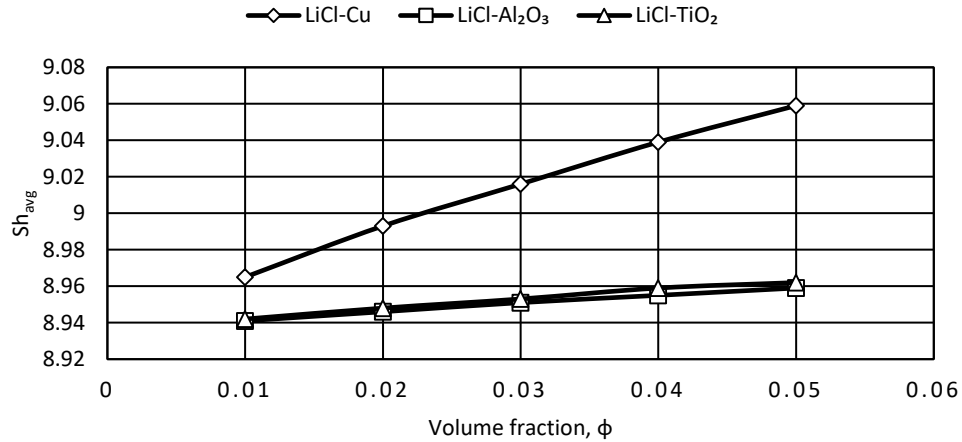


Figure 6.20: Effect of different nanoparticles with varying volume fraction in LiCl liquid desiccant on average Sherwood number at the interface (CF)

In LiCl liquid desiccant, the effect of different nanoparticles with varying volume fraction on the average Sherwood number at the interface is illustrated in Figure 6.20. The figure indicates that as nanoparticles volume fraction increases, average Sherwood number increases. The increase is the highest with Cu nanoparticles showing an increase of 1.04% and the lowest with Al₂O₃ nanoparticles of approximately 0.2%. For TiO₂ the increase is approximately 0.22%. The rate of mass transfer is the highest while using copper nanoparticles. Compared to CaCl₂ liquid desiccant LiCl has a lower rate of mass transfer.

For counter flow configuration utilizing LiCl liquid desiccant Cu nanoparticle at 5% volume fraction is concluded to be the most suitable nanoparticle for producing maximum cooling and dehumidification due to having higher rates of heat transfer and mass transfer and humidity ratio and temperature. The comparison between CaCl₂ liquid desiccant and LiCl liquid desiccant indicates that better cooling and better dehumidification of air at higher rates of heat and mass transfer occurs due to utilizing CaCl₂ liquid desiccant.

6.2.3 Lithium bromide (LiBr) liquid desiccant (CF)

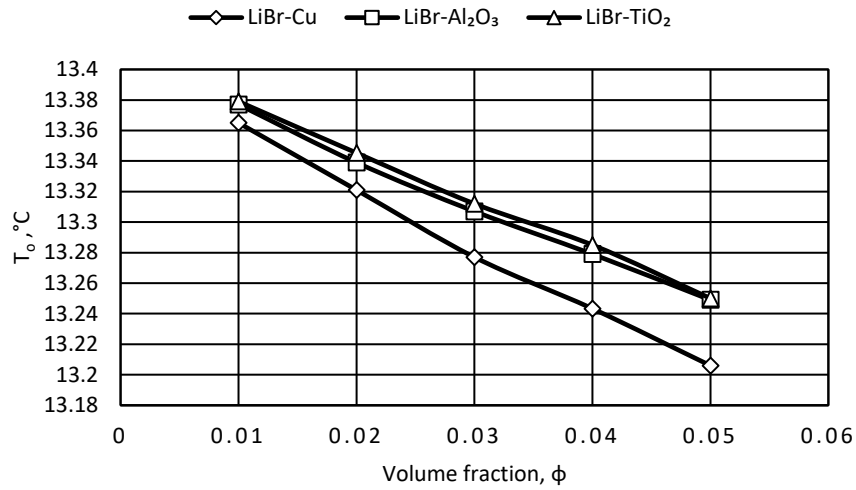


Figure 6.21: Effect of different nanoparticles with varying volume fraction in LiBr liquid desiccant on outlet air temperature (CF)

Lithium bromide liquid desiccant solution at 50% concentration is investigated in this section. Higher concentration of lithium bromide is selected, as working range of lithium bromide solution is 45% to 55%. The effect of different nanoparticles with varying volume fraction in LiBr liquid desiccant on the outlet air temperature is illustrated in Figure 6.21. The figure indicates that as volume fraction of nanoparticles increases the temperature decreases indicating the cooling of air also increases. The temperature decrease is the highest with Cu nanoparticles showing a decrease of 1.19% and the lowest with TiO_2 nanoparticles of approximately 0.96%. For Al_2O_3 the decrease is approximately 0.95%. The results with TiO_2 is almost similar to Al_2O_3 and from the analysis, it can be concluded that utilization of Cu nanoparticles result in best cooling.

Comparing three liquid desiccant considering air temperature at outlet, utilizing LiBr liquid desiccant results in lowest outlet temperature indicating that most cooling occurs, and compared with LiCl, which has the highest outlet temperature the difference in cooling is approximately 1.3%.

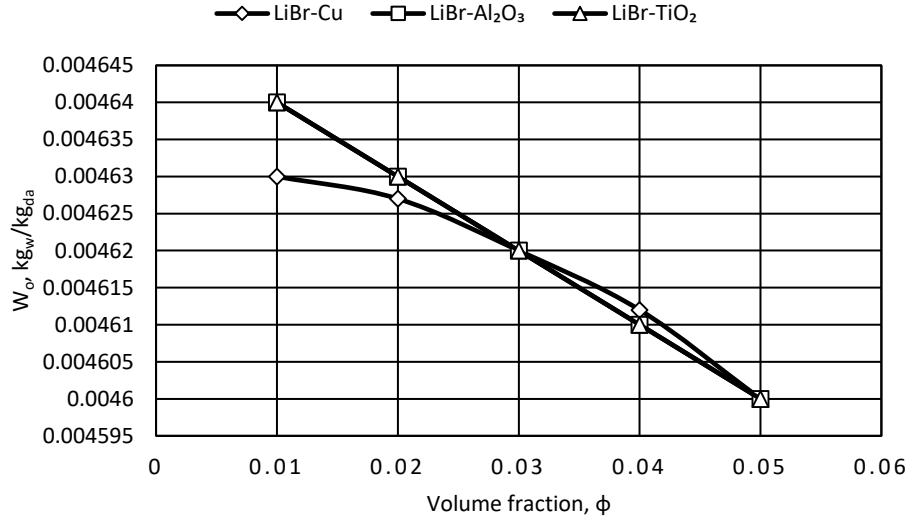


Figure 6.22: Effect of different nanoparticles with varying volume fraction in LiBr liquid desiccant on outlet humidity ratio (CF)

The effect of different nanoparticles in LiBr liquid desiccant with varying volume fraction on the outlet humidity ratio is illustrated in Figure 6.22. The figure indicates that as nanoparticles volume fraction increases, outlet humidity ratio decreases indicating the dehumidification of air also increases.

The decrease in humidity ratio of air with Cu nanoparticles is the lowest around 0.65% and for Al₂O₃ and TiO₂ the decrease is similar approximately 0.86%. The outlet humidity ratio is the same however for all three nanoparticles.

The outlet humidity ratio with using LiBr liquid desiccant is much lower compared to both CaCl_2 and LiCl liquid desiccant indicating that much better dehumidification occurs with using LiBr liquid desiccant solution. The outlet humidity ratio with using LiBr is approximately 24% lower than both the other desiccants.

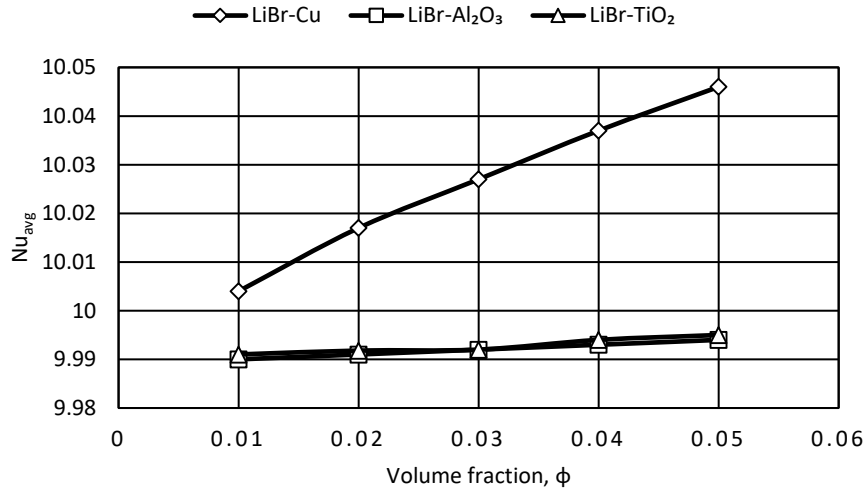


Figure 6.23: Effect of different nanoparticles with varying volume fraction in LiBr liquid desiccant on Nusselt number. (CF)

The effect of different nanoparticles with varying volume fraction in LiBr liquid desiccant on Nusselt number at interface is illustrated in Figure 6.23. The figure indicates that as nanoparticles volume fraction increases the Nusselt number becomes higher.

The increase is the highest with Cu nanoparticles showing an increase of 0.42% and the lowest with both Al_2O_3 and TiO_2 nanoparticles of approximately 0.04%. The rate of heat transfer is the highest while using copper nanoparticles compared to the other two nanoparticles. Hence, for counter flow channel as nanoparticles volume fraction increase the heat transfer rate also increases with outlet air temperature decreasing. Therefore, the

cooling is improved as well as the rate of cooling. Comparing the three liquid desiccants indicates that LiBr has the highest heat transfer rate approximately 2.56% higher than LiCl liquid desiccant.

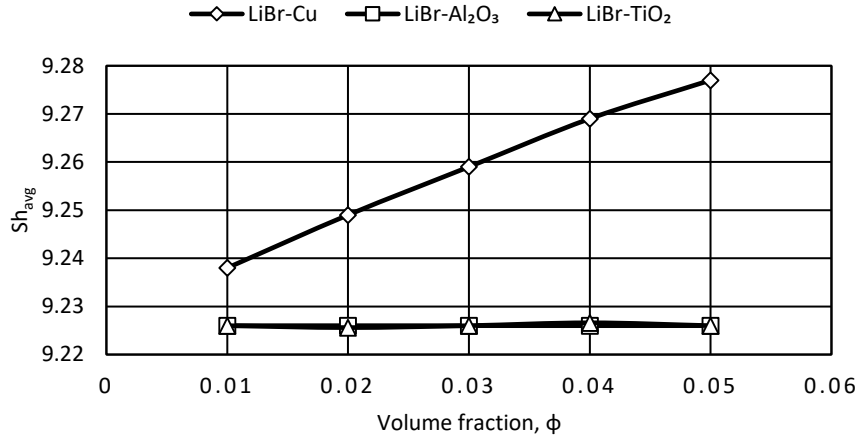


Figure 6.24: Effect of different nanoparticles with varying volume fraction in LiBr liquid desiccant on average Sherwood number at the interface (CF)

In LiBr liquid desiccant, the effect of different nanoparticles with varying volume fraction on the average Sherwood number at the interface is illustrated in Figure 6.24. The figure indicates that as nanoparticles volume fraction increases, average Sherwood number increases.

The increase is the highest with Cu nanoparticles showing an increase of 0.42% and for both Al_2O_3 and TiO_2 nanoparticles, the increase is negligible. Mass transfer rate is the highest while using copper nanoparticles.

For counter flow configuration utilizing LiBr liquid desiccant Cu nanoparticle at 5% volume fraction is concluded to be the most suitable nanoparticle for producing maximum

cooling and dehumidification due to having higher rates of heat transfer and mass transfer and humidity ratio and temperature.

The comparison between the three liquid desiccants for counter flow falling film liquid desiccant dehumidifier indicate that utilizing LiBr liquid desiccant most cooling occurs and the difference in cooling is approximately 1.3% compared to LiCl. The best dehumidification also occurs with using LiBr liquid desiccant. Humidity ratio for LiBr is approximately 24% lower than both desiccants. LiBr also has higher rates of mass and heat transfer by 2.4% and 2.5% respectively compare to LiCl liquid desiccant. Hence, for counter flow it can be concluded that the combination of LiBr liquid desiccant with 5% volume fraction of Cu nanoparticle is the ideal choice for producing the highest cooling and dehumidification at highest heat and mass transfer rates.

6.3 Comparative numerical analysis of parallel and counter flow falling film dehumidifiers for CaCl₂ liquid desiccant with copper nanoparticles

It is essential to compare the performance of parallel and counter flow falling film dehumidifier with regards to cooling and dehumidification of air and the heat and mass transfer characteristics. The comparison is done for CaCl₂ liquid desiccant to which copper nanoparticle is added and the results are illustrated.

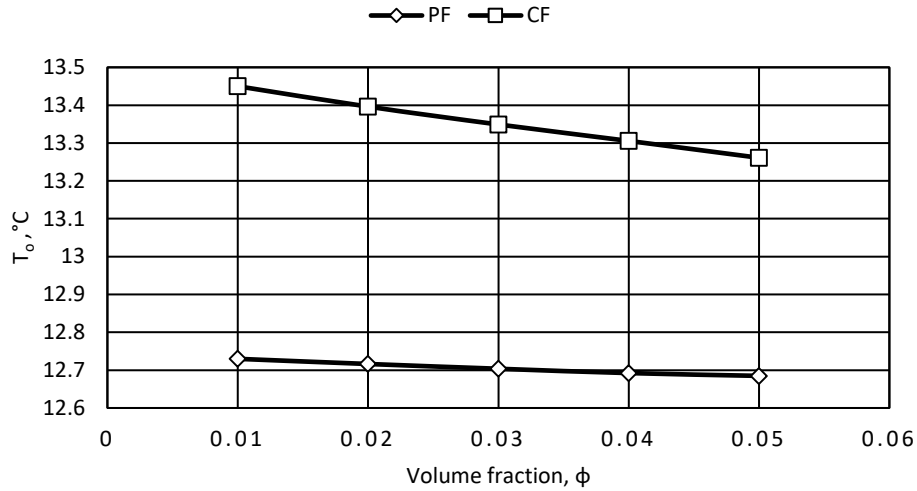


Figure 6.25: Effect of increasing volume fraction of copper nanoparticle in CaCl_2 liquid desiccant on outlet air temperature for both parallel and counter flow.

The effect of increasing the volume fraction of copper nanoparticles in CaCl_2 liquid desiccant on outlet air temperature for both parallel and counter flow is illustrated in Figure 6.25. The outlet air temperature is approximately 5.65% higher for counter flow channel compared to parallel flow at 1% volume fraction indicating that better cooling of air occurs in parallel flow channel. The reason behind counter flow channel having a higher outlet air temperature is attributed to the fact that the outlet air will receive heating instead of cooling at the very end of the channel due to the high inlet desiccant temperature resulting in heat transfer occurring in the opposite direction in that region.

However, as the volume fraction of nanoparticle increases the outlet temperature decreases by 0.35% for parallel flow channel and 1.4% for counter flow channel. This indicates that addition of nanoparticles has a more significant effect on cooling in counter flow channel.

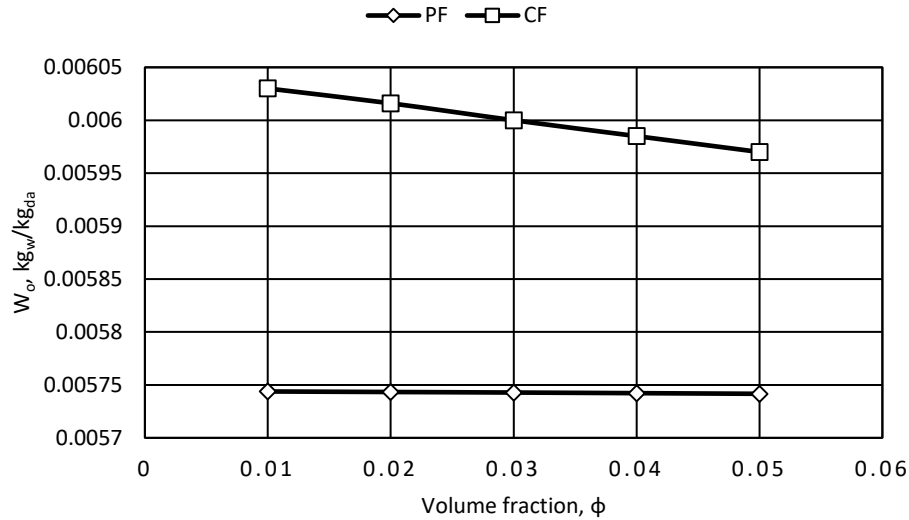


Figure 6.26: Effect of increasing volume fraction of copper nanoparticle in CaCl_2 liquid desiccant on outlet humidity ratio for both parallel and counter flow.

The effect of increasing the volume fraction of copper nanoparticles in CaCl_2 liquid desiccant on outlet humidity ratio for both parallel and counter flow is illustrated in Figure 6.26. The outlet humidity ratio of air is approximately 5% higher for counter flow channel compared to parallel flow at 1% volume fraction indicating that better dehumidification of air occurs in parallel flow channel. The reason behind counter flow channel having a higher outlet humidity ratio is due to the fact that at the end of the channel due to the high inlet desiccant concentration, mass transfer occurs in the opposite direction.

However, as the volume fraction of nanoparticle increases the outlet humidity decreases by 0.04% for parallel flow channel and 1.005% for counter flow channel. This indicates that addition of nanoparticles has a more significant effect on dehumidification in counter flow channel. The decrease in parallel flow channel with copper nanoparticle is

insignificant compared to the counter flow channel, although with other nanoparticles the decrease in humidity ratio is slightly higher but still comparatively much less.

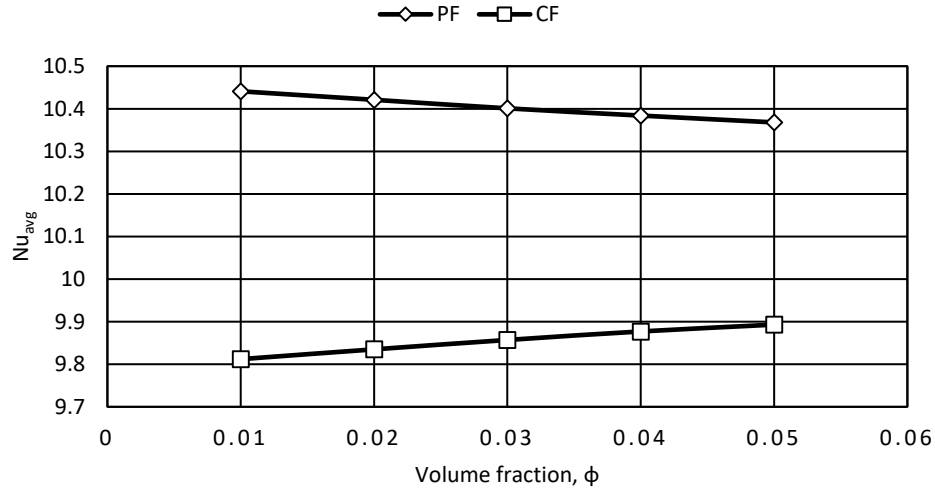


Figure 6.27: Effect of increasing volume fraction of copper nanoparticle in $CaCl_2$ liquid desiccant on Nusselt number for both parallel and counter flow

The effect of increasing the volume fraction of copper nanoparticles in $CaCl_2$ liquid desiccant on average Nusselt number for both parallel and counter flow is illustrated in Figure 6.27. The Nusselt number is approximately 6.4% higher for parallel flow channel compared to the counter flow at 1% volume fraction indicating that in parallel flow channel the heat transfer rate is higher. This is because in counter flow channel, heat transfer occurs in the opposite direction at the end of the channel thus reducing the overall heat transfer rate.

However, as the volume fraction of nanoparticle increases the Nusselt number increases by 0.83% for counter flow channel but decreases by 0.69% for parallel flow channel. Hence, it is observed that heat transfer rate is improved in counter flow channel due to the

addition of nanoparticles but the opposite happens in parallel flow where the heat transfer rate decreases. Thus, it is concluded that addition of nanoparticles have a negative effect on the heat transfer rate for parallel flow channel, but although the heat transfer rate decreases the cooling is improved. The explanation for this phenomenon is that Nusselt number does not account for latent heat and only accounts for sensible heat. Hence, latent heat transfer due to changing of phase from water vapor to water increases with increasing volume fraction. This contributes to lower temperature of air at the outlet of the channel.

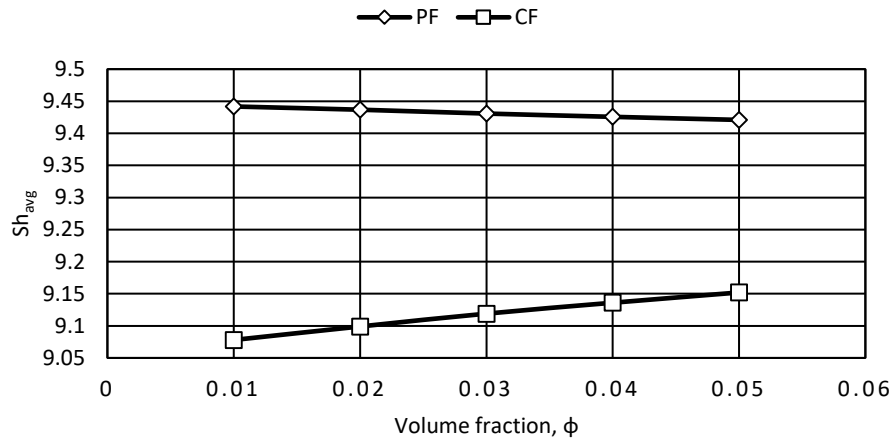


Figure 6.28: Effect of increasing volume fraction of copper nanoparticle in $CaCl_2$ liquid desiccant on Sherwood number for both parallel and counter flow

The effect of increasing the volume fraction of copper nanoparticles in $CaCl_2$ liquid desiccant on average Sherwood number for both parallel and counter flow is illustrated in Figure 6.28. The Sherwood number is approximately 4% higher for parallel flow channel compared to the counter flow at 1% volume fraction indicating that in parallel flow channel the mass transfer rate is higher. This is because in counter flow channel, mass transfer

occurs in the opposite direction at the end of the channel thus reducing the overall mass transfer rate.

However, as the volume fraction of nanoparticle increases the Sherwood number increases by 0.82% for counter flow channel but decreases by 0.22% for parallel flow channel. Hence, it is observed that mass transfer rate is improved in counter flow channel due to the addition of nanoparticles but the opposite happens in parallel flow where the mass transfer rate decreases. Thus, it is concluded that addition of nanoparticles have a negative effect on the mass transfer rate for parallel flow channel, but although the mass transfer rate decreases, the dehumidification is improved.

CHAPTER 7

CONCLUSIONS AND RECOMMENDATIONS

In this investigation the liquid desiccant based falling film dehumidifier with nanoparticles have been studied, for improvement of the mass transfer and heat transfer characteristics and to improve the cooling and dehumidification process. Different liquid desiccants have been investigated by addition of different nanoparticles. Two flow configurations for falling film dehumidifier have been primarily investigated; counter flow and parallel flow configuration. Numerical analysis was done to determine the mass and heat transfer characteristics. At the outlet conditions humidity ratio and temperature was determined.

The summary of the results from the thermophysical property analysis indicated that for all models increasing the volume fraction of nanoparticles caused a significant increase in thermal conductivity and also an increase in the viscosity of the liquid desiccant. The Yu and Choi model was concluded to be most suitable for predicting the values of thermal conductivity as it illustrates the highest increase and this is justified by the experimental results by Eastman et al. [28] who concluded that experimental results indicated much higher values than those predicted by the theoretical models. The reason for this difference is due to several factors such as size of the nanoparticle, the effect of Brownian motion of nanoparticles and the aggregation of nanoparticles. For this reason further research needs to be carried out to obtain a more accurate model.

The Batchelor model is concluded to be most suitable in determining the viscosity of nanofluids as Brownian motion is considered in that model. CaCl_2 has been concluded to be the most suitable liquid desiccant for enhancing heat transfer characteristics due to its

high thermal conductivity and moderate viscosity. Although if higher concentration of liquid desiccant is required LiBr is the ideal choice as it gives the lowest values of viscosity and although has lower thermal conductivity values, higher volume fraction of nanoparticles can be used as variation in viscosity is much less compared to the other two liquid desiccant.

The conclusions drawn from the parametric analysis of the falling film dehumidifier with nanoparticles were:

- As Reynolds number of air increases from 950 to 2150, cooling and dehumidification is decreased by 38% and 46% respectively, although Sherwood number and Nusselt number increases by 62% and 64% respectively.
- As the desiccant mass flow rate increases from 0.004 kg/s to 0.01 kg/s cooling and dehumidification of air increases by 0.3% and 1% respectively. The heat and mass transfer rate also improves by 1.5% and 0.5% respectively.
- Increasing channel height leads from 0.3 to 0.7 meters leads to better dehumidification and cooling by 20%, but the rate of transfer of heat and mass is significantly decreased by approximately 80%.
- The concentration of the salt in the liquid desiccant is increased from 30% to 40% leading to an improvement in cooling and dehumidification by 1% and 13% respectively, but the mass and heat transfer rate is reduced by 3.5% and 2% respectively. Hence, the dehumidification process is significantly improved but increasing the salt concentration increases the chance of crystallization.

- Heat and mass transfer rate is improved by 2% as desiccant temperature is increased from 20°C to 30° C. However, cooling and dehumidification is decreased by 0.5% approximately.
- The heat transfer rate decreases by 3% as inlet air temperature is increased from 25°C to 40°C and the cooling is decreased by 12%. The mass transfer rate and dehumidification decrease by 0.6% and 0.3% respectively.
- The rate of mass transfer decreases by 2% as inlet humidity ratio is increased from 0.015 kg_w/kg_{da} to 0.025 kg_w/kg_{da} and the dehumidification is decreased by 14%. The heat transfer rate and cooling decrease by 0.7% approximately.
- Cooling and dehumidification improves by 0.5% and 0.2% respectively as nanoparticles volume fraction is increased from 0% to 5%. The heat and mass transfer rate however, decreases by 0.9% and 0.25% respectively. This decrease in heat and mass transfer rate is specific to parallel flow only.

The results of sensitivity analysis indicated that height of the channel and Reynolds number of air had considerable impact on average Nusselt number, average Sherwood number temperature and humidity ratio at the outlet. Inlet air temperature also has a considerable impact on outlet air temperature. For outlet humidity ratio, inlet humidity ratio and concentration of the desiccant has a significant effect. These parameters should be controlled for maximum performance output of dehumidifier.

This study investigates the effects on mass transfer and heat transfer characteristics for three different liquid desiccant solutions. To each of these three liquid desiccants three different nanoparticles were added. The nanoparticles volume fraction was increased from 1% to 5%.

The analysis was carried out for both counter flow configuration and parallel flow configuration. The comparative results indicated that outlet temperature and outlet air humidity ratio was higher compared to the parallel flow configuration. In addition, the Sherwood number and Nusselt number at the interface is lower in counter flow configuration.

The parallel flow falling film dehumidifier was investigated and the conclusions drawn from the analysis were as follows:

- As nanoparticles volume fraction was increased the outlet temperature and outlet humidity ratio decreased resulting in better cooling and dehumidification although the mass transfer rate and heat transfer rate also decreased.
- The results with TiO_2 is almost similar to Al_2O_3 and the utilization of both these nanoparticle result in better cooling and better dehumidification of hot and humid air than using Cu nanoparticle. For CaCl_2 liquid desiccant cooling is improved by approximately 0.5% utilizing TiO_2 and Al_2O_3 and 0.35% for Cu nanoparticle. Dehumidification is improved by approximately 0.35% utilizing TiO_2 and Al_2O_3 and 0.04% for Cu nanoparticle. The heat transfer rate decreases by 0.69% for Cu and the most with Al_2O_3 approximately 0.91%. The mass transfer rate decreases by 0.22% for Cu and the most with Al_2O_3 approximately 0.66%.
- For parallel flow configuration, utilizing all three liquid desiccants Al_2O_3 nanoparticle at 5% volume fraction is concluded to be the most suitable nanoparticle for producing maximum dehumidification and cooling although rates of heat transfer and mass transfer are slightly lower compared to other nanoparticles. It is also suitable to use TiO_2 nanoparticles as it produces relatively

similar albeit slightly lower cooling and dehumidification of hot humid air and also has slightly higher Sherwood number and Nusselt number.

- The comparison between CaCl_2 liquid desiccant and LiCl liquid desiccant indicates that better cooling of air occurs due to utilizing CaCl_2 by 0.06% and better dehumidification occurs due to LiCl liquid desiccant by 0.17%.
- The comparison between the three liquid desiccants for parallel flow indicate that utilizing CaCl_2 liquid desiccant most cooling occurs and the difference in cooling is approximately 0.3% compared to LiBr . However, the best dehumidification occurs with using LiBr liquid desiccant. The outlet humidity ratio for LiBr is approximately 22% lower than both the other desiccants. The conclusion reached is that LiBr desiccant is better for producing better cooling and dehumidification compared to the other desiccants.

The counter flow falling film dehumidifier was investigated and the conclusions drawn from the analysis were as follows:

- As the nanoparticles volume fraction were increased the outlet temperature and outlet humidity ratio decreased resulting in better dehumidification and cooling and the heat and mass transfer rates also increased.
- Utilization of Cu nanoparticle result in better cooling of hot and humid air at higher mass transfer and heat transfer rates compared to the other two nanoparticles. Al_2O_3 however results in better dehumidification. For CaCl_2 liquid desiccant cooling is improved the most using Cu nanoparticle by approximately 1.4% and the least with TiO_2 by approximately 1.14%. Dehumidification is improved the most using Al_2O_3 nanoparticle by approximately 1.16% and the least with TiO_2 by approximately

0.99%. The heat transfer rate increases the most for Cu by 0.83% and the least with Al_2O_3 approximately 0.15%. The mass transfer rate increases the most for Cu by 0.82% and the least with Al_2O_3 approximately 0.12%.

- For counter flow configuration utilizing all three liquid desiccants Cu nanoparticle at 5% volume fraction is concluded to be the most suitable nanoparticle for producing maximum cooling and dehumidification due to having higher rates of mass and heat transfer and lower humidity ratio and temperature at the outlet.
- The comparison between CaCl_2 liquid desiccant and LiCl liquid desiccant indicates that better cooling and better dehumidification of air by 0.92% and 0.67% respectively, at higher rates of heat and mass transfer by 1.03% approximately occurs due to utilizing CaCl_2 liquid desiccant.
- The comparison between the three liquid desiccants for counter flow falling film liquid desiccant dehumidifier indicate that utilizing LiBr liquid desiccant most cooling occurs and the difference in cooling is approximately 1.3% compared to LiCl . The best dehumidification also occurs with using LiBr liquid desiccant. The outlet humidity ratio for LiBr is approximately 24% lower than both the other desiccants. LiBr also has higher rates of mass and heat transfer by 2.4% and 2.5% respectively compared to LiCl liquid desiccant.

The overall conclusions drawn from this study are that utilizing parallel flow configuration for falling film liquid desiccant dehumidifier with the addition of nanoparticles, leads to better cooling and dehumidification of hot and humid air at higher rates of heat and mass transfer. The best liquid desiccant for carrying out cooling and dehumidification is lithium bromide and the best nanoparticle is copper. However, addition of nanoparticles and

increasing their volume fraction has a more significant effect in counter flow channels as decrease in air temperature and air humidity ratio is higher as volume fraction increases compared to parallel flow. In addition, the rate of heat and mass transfer increases as volume fraction of nanoparticles increases in counter flow channel compared to parallel flow where the rate of heat and mass transfer decreases due to the increase in volume fraction of nanoparticles.

Hence, from this investigation it is recommended that nanoparticles should be added for enhancing cooling, dehumidification, and increasing the heat and mass transfer rate for counter flow falling film dehumidifiers. For parallel flow configuration also the cooling and dehumidification is improved but it is less significant compared to counter flow and the rate of heat and mass transfer also decreases hence further experimental studies is required to investigate the feasibility of adding nanoparticles to parallel flow channel.

As there has been no previous experimental study done in this field it is also recommended to carry out such studies to validate the results of this study. The models used in this study for determining the thermo-physical properties are theoretical models but from experimental studies it has been proved that adding nanoparticles has a much higher impact on the properties compared to values given by the theoretical models. Hence, experimental studies can help investigate whether nanoparticles have a much more significant impact on improving the performance of falling film dehumidifiers compared to the results in this study. Experimental studies will also help resolve issues such as whether agglomeration of nanoparticles will affect the heat transfer rate of falling film dehumidifiers, and also investigate whether desiccants may have a possibility to adversely affect the nanoparticles as they are aggressive materials.

References

- [1] Dai, Y. ., Wang, R. ., Zhang, H. ., and Yu, J. ., 2001, “Use of Liquid Desiccant Cooling to Improve the Performance of Vapor Compression Air Conditioning,” *Appl. Therm. Eng.*, **21**(12), pp. 1185–1202.
- [2] Loff, G. O., 1955, “House Heating and Cooling with Solar Energy,” *Solar Energy Research*, Univ. of Wisconsin, Madison.
- [3] Rahamah, A., 1997, “Heat and Mass Transfer between Air and a Falling Film of Desiccant Solution in a Fin-Tube Arrangement,” M.S. Thesis, Kuwait University, Kuwait.
- [4] Pesaran, A. A., 1993, “A Review of Des Dehumidification Nt Ogy,” *Growth* (Lakeland), (October 1994).
- [5] Al-Farayedhi, A. A., Gandhidasan, P., and Al-Mutairi, M. A., 2002, “Evaluation of Heat and Mass Transfer Coefficients in a Gauze-Type Structured Packing Air Dehumidifier Operating with Liquid Desiccant,” *Int. J. Refrig.*, **25**(3), pp. 330–339.
- [6] Mesquita, L. C. S., Harrison, S. J., and Thomey, D., 2006, “Modeling of Heat and Mass Transfer in Parallel Plate Liquid-Desiccant Dehumidifiers,” *Sol. Energy*, **80**(11), pp. 1475–1482.
- [7] Sheridan, J. C., and Mitchell, J. W., 1985, “A Hybrid Solar Desiccant Cooling System,” *Sol. Energy*, **34**(2), pp. 187–193.
- [8] Howell, J. R., and Peterson, J. L., 1986, “Preliminary Performance Evaluation of a Hybrid Vapor-Compression/Liquid Desiccant Air Conditioning System.,” *American Society of Mechanical Engineers (Paper)*.
- [9] Rahamah, A., Elsayed, M. M., and Al-Najem, N. M., 1998, “A Numerical Solution for Cooling and Dehumidification of Air by a Falling Desiccant Film in Parallel Flow,” *Renew. Energy*, **13**(3), pp. 305–322.
- [10] Ali, A., Vafai, K., and Khaled, A. R. A., 2003, “Comparative Study between Parallel and Counter Flow Configurations between Air and Falling Desiccant in the Presence of Nanoparticle Suspensions,” *Int. J. Energy Res.*, **27**(8), pp. 725–745.
- [11] Ali, A., and Vafai, K., 2004, “An Investigation of Heat and Mass Transfer between Air and Desiccant Film in an Inclined Parallel and Counter Flow Channels,” *Int. J. Heat Mass Transf.*, **47**(8–9), pp. 1745–1760.
- [12] Park, M. S., Howell, J. R., Vliet, G. C., and Peterson, J., 1994, “Numerical and

- Experimental Results for Coupled Heat and Mass Transfer between a Desiccant Film and Air in Cross-Flow Cebu,” *Int. J. Heat Mass Transf.*, **37**, pp. 395–402.
- [13] Saman, W. Y., and Alizadeh, S., 2001, “Modelling and Performance Analysis of a Cross-Flow Type Plate Heat Exchanger for Dehumidification/Cooling,” *Sol. Energy*, **70**(4), pp. 361–372.
- [14] Liu, X. H., Jiang, Y., and Qu, K. Y., 2007, “Heat and Mass Transfer Model of Cross Flow Liquid Desiccant Air Dehumidifier/Regenerator,” *Energy Convers. Manag.*, **48**(2), pp. 546–554.
- [15] Ali, A., Vafai, K., and Khaled, A. R. A., 2004, “Analysis of Heat and Mass Transfer between Air and Falling Film in a Cross Flow Configuration,” *Int. J. Heat Mass Transf.*, **47**(4), pp. 743–755.
- [16] Escher, W., Brunschwiler, T., Shalkevich, N., Shalkevich, A., Burgi, T., Michel, B., and Poulikakos, D., 2011, “On the Cooling of Electronics With Nanofluids,” *J. Heat Transfer*, **133**(5), p. 051401.
- [17] Mahian, O., Kianifar, A., Kalogirou, S. A., Pop, I., and Wongwises, S., 2013, “A Review of the Applications of Nanofluids in Solar Energy,” *Int. J. Heat Mass Transf.*, **57**(2), pp. 582–594.
- [18] Natarajan, E., and Sathish, R., 2009, “Role of Nanofluids in Solar Water Heater,” *Int. J. Adv. Manuf. Technol.*, pp. 3–7.
- [19] Li, Y., Zhou, J., Tung, S., Schneider, E., and Xi, S., 2009, “A Review on Development of Nanofluid Preparation and Characterization,” *Powder Technol.*, **196**(2), pp. 89–101.
- [20] Lee, J. H., 2014, “A Review of Thermal Conductivity Data,” *Heat Transf. Eng.*, **36**(13), pp. 1085–1110.
- [21] Ghadimi, A., Saidur, R., and Metselaar, H. S. C., 2011, “A Review of Nanofluid Stability Properties and Characterization in Stationary Conditions,” *Int. J. Heat Mass Transf.*, **54**(17–18), pp. 4051–4068.
- [22] Ramesh, G., and Prabhu, N. K., 2011, “NRL2011 Review of Thermo-Physical Properties, Wetting and Heat Transfer Characteristics of Nanofluids and Their Applicability in Industrial Quench Heat Treatment.Pdf,” pp. 1–15.
- [23] S. U. S. Choi and J. A. Eastman, 1995, “Thermal Conductivity of Fluids With.Pdf,” *Am. Soc. Mech. Eng.*, pp. 99–105.
- [24] Lee, S., Choi, S. U.-S., Li, S., and Eastman, J. A., 1999, “Measuring Thermal Conductivity of Fluids Containing Oxide Nanoparticles,” *J. Heat Transfer*, **121**(2),

p. 280.

- [25] Xuan, Y., and Li, Q., 2000, "Heat Transfer Enhancement of Nanofluids," *Int. J. Heat Fluid Fluid Flow*, **21**, pp. 58–64.
- [26] Xuan, Y., and Roetzel, W., 2000, "Conceptions for Heat Transfer Correlation of Nanofluids," *Int. J. Heat Mass Transf.*, **43**(19), pp. 3701–3707.
- [27] Thomas, S., and Panicker Sobhan, C. B., 2011, "A Review of Experimental Investigations on Thermal Phenomena in Nanofluids," *Nanoscale Res. Lett.*, **6**, pp. 1–21.
- [28] Eastman, J. A., Choi, S. U. S., Li, S., Yu, W., and Thompson, L. J., 2001, "Anomalously Increased Effective Thermal Conductivities of Ethylene Glycol-Based Nanofluids Containing Copper Nanoparticles," *Appl. Phys. Lett.*, **78**(6), pp. 718–720.
- [29] Garg, J., Poudel, B., Chiesa, M., Gordon, J. B., Ma, J. J., Wang, J. B., Ren, Z. F., Kang, Y. T., Ohtani, H., Nanda, J., McKinley, G. H., and Chen, G., 2008, "Enhanced Thermal Conductivity and Viscosity of Copper Nanoparticles in Ethylene Glycol Nanofluid," *J. Appl. Phys.*, **103**(7), p. 74301.
- [30] Murshed, S. M. S., Leong, K. C., and Yang, C., 2005, "Enhanced Thermal Conductivity of TiO₂- Water Based Nanofluids," *Int. J. Therm. Sci.*, **44**(4), pp. 367–373.
- [31] Murshed, S. M. S., Leong, K. C., and Yang, C., 2008, "Investigations of Thermal Conductivity and Viscosity of Nanofluids," *Int. J. Therm. Sci.*, **47**(5), pp. 560–568.
- [32] Nguyen, C. T., Desgranges, F., Galanis, N., Roy, G., Maré, T., Boucher, S., and Angue Mintsa, H., 2008, "Viscosity Data for Al₂O₃-Water Nanofluid-Hysteresis: Is Heat Transfer Enhancement Using Nanofluids Reliable?," *Int. J. Therm. Sci.*, **47**(2), pp. 103–111.
- [33] Hamilton, R. L., 1962, "Thermal Conductivity of Heterogeneous Two-Component Systems," *Ind. Eng. Chem. Fundam.*, **1**(3), pp. 187–191.
- [34] Hui, P. M., Zhang, X., Markworth, A. J., and Stroud, D., 1999, "Thermal Conductivity of Graded Composites: Numerical Simulations and an Effective Medium Approximation," *J. Mater. Sci.*, **34**(22), pp. 5497–5503.
- [35] Yu, W., and Choi, S. U. S., 2003, "The Role of Interfacial Layers in the Enhanced Thermal Conductivity of Nanofluids: A Renovated Maxwell Model," *J. Nanoparticle Res.*, **5**(1–2), pp. 167–171.
- [36] Einstein, A., 1906, "Eine Neue Bestimmung Der Molekuldimensionen.Pdf," *Ann.*

Phys., **19**(2), pp. 289–306.

- [37] Brinkman, H. C., 1952, “The Viscosity of Concentrated Suspensions and Solutions,” J. Chem. Phys., **20**(4), pp. 571–571.
- [38] Batchelor, G. K., 1977, “The Effect of Brownian Motion on the Bulk Stress in a Suspension of Spherical Particles,” J. Fluid Mech., **83**(1), pp. 97–117.
- [39] Conde, M. R., 2004, “Properties of Aqueous Solutions of Lithium and Calcium Chlorides: Formulations for Use in Air Conditioning Equipment Design,” Int. J. Therm. Sci., **43**(4), pp. 367–382.

Vitae

Name: : Qazi Talal

Nationality: : Bangladeshi

Date of Birth: :5/15/1991

Email: : qazitalal476@gmail.com

Address: : Jhumjhumpur, Kotwali, Jessore, Bangladesh. P.O. 7401

Academic Background: M.S in Mechanical Engineering (May, 2018)
King Fahd University of Petroleum and Minerals

B.Sc. in Mechanical Engineering (Oct, 2013)
Islamic University of Technology

Publications:

1. Q. Talal, P. Gandhidasan, H. Bahaidarah, “Enhancing the Heat Transfer Characteristics of Liquid Desiccants with Nanoparticles” 2nd Thermal and Fluids Engineering Conference (TFEC), April 2-5, 2017, Las Vegas, Nevada, USA.